Mise en forme et caractérisation de nano-fibres fonctionnalisées par chimie click pour l'ingénierie tissulaire

Anica Lancuski

UNIVERSITÉ DE GRENOBLE

THESIS

To obtain the degree of

DOCTOR OF UNIVERSITY OF GRENOBLE

Specialty: **2MGE : matériaux, mécanique, génie civil, électrochimie**

Arrêté ministériel : 7 août 2006

Presented by

Anica LANCUŠKI

Thesis directed by **Frédéric BOSSARD** and
Co-directed by **Sébastien FORT**

Prepared in the **Laboratoire Rhéologie et Procédés** and **Centre de Recherches sur les Macromolécules Végétales (CERMAV)**
In the Doctoral School **Ingénierie-Matériaux, Mécanique, Energétique, Environnement, Procédés, Production (I-MEP2)**

Processing and Characterization of Click-Functionalized Electrospun Nano-Fibers toward Tissue Engineering Applications

Thesis defended publically on **«20.12.2013»**,
In front of the esteemed jury comprised of:

M. François BOUÉ DR, INRA Agro Paris Tech	President
M. Guy SCHLATTER Prof., Université de Strasbourg	Reviewer
M. Eric DROCKENMULLER Prof., Université Lyon 1	Reviewer
Ms. Catherine PICART Prof., INP Grenoble	Examiner
M. Arkadii ARINSTEIN Prof., Israel Institute of Technology	Examiner
M. Frédéric BOSSARD Prof., Université Joseph Fourier	Director
M. Sébastien FORT CR, CERMAV-CNRS	Co-director

Grenoble INP

TABLE OF CONTENTS

Aknowledgements

I would like to express my special appreciation and thanks to my supervisor Prof. Frédéric Bossard and to my cosupervisor Dr. Sébastien Fort for all their professional and moral support during my PhD studies – they had guided me throughout three intensive years of both theoretical and experimental work and had thaught me how to do an extensive research while concising it to a few sentences.

I would like to thank to my jury committee: Prof. Eric Drockenmuller and Prof. Guy Schlatter for approving my PhD work, and, together with Dr. François Boué, Prof. Arkadii Arinstein, Prof. Catherine Picart and my supervisors: Prof. Frédéric Bossard and Dr. Sébastien Fort, for aknowledging me a degree of Doctor of University of Grenoble.

I would like to thank my home-laboratory: Laboratoire Rhéologie et Procédés and its former director, Dr. Albert Magnin, as well as its present director, Dr. Nadia el Kissi, for welcoming me in their fascilities. Also, I had spent an important and fruitful period in CERMAV – Centre de Recherches sur les Macromolécules Végétales – owing to its director, Dr. Redouane Borsali, what I am truly thankful for.

The PhD thesis study exposed in this manuscript would not have been possible without many collegues: researchers, engineers and technicians that have participated in this work, and I give them my most sincere thanks. My special thanks to Dr. Yahya Rharbi and Dr. François Boué for introducing me into small angle neutron scattering technique and for their aboundant help in data measurement, analysis and interpretation. I would also like to thank to: Stéphanie Boullanger, Amandine Durrand-Terrasson, Hélène Galliard, Rachel Martin, Stéphanie Pradau, Didier Blésès, Frédéric Hugenell, Mohamed Karrouch, Dr. Otsuka Issei, Dr. Bernard Priem and Dr. Christophe Travelet for their assistance and helpful instructions.

I aknowledge the financial support given by MNERT for PhD grant and Institute Carnot Polynat as well as Grenoble Institute of Technology and University of Grenoble for allowing my PhD studies and University Joseph Fourier for giving me the teaching opportunities.

I would like to thank my family – my parents, Milivoj and Dragica, and my sister, Jelena – for their neverending and inspiring support throughout my education: mama, tata, Jelena, ovom prilikom vam se i zvanično zahvaljujem na vašoj nesebičnoj i sveprisutnoj podršci tokom svih ovih godina mog školovanja; najlepše i najponiznije vam hvala, ostajem vaš večiti dužnik. I give my humble thanks to my life-companion, Clément, for his unconditional support and help to overcome the most difficult moments of my PhD studies. And finally, I would like to thank to my friends, those amazing peope I met during my studies, at home in Serbia, in Finland, in Netherlands and in France. Thank you all for your inspiring words and deeds, jokes and serious discussions we shared throughout these years.

Abbreviations

AFD – average fiber diameter

AFM – atomic-force microscopy

ATR-FTIR – attenuated total reflectance FTIR

CF – fluorocarbon

CO-PCL – castor oil-poly(*ε*-caprolactone)

CuAAc – copper(I)-catalyzed azide-alkine cycloaddition

DCE – dichloroethane

DCM – dichloromethane

DLS – dynamic light scattering

DMF – *N*,*N*-dimethylformamide

DMSO – dimethylsulfoxide

DNA – deoxyribonucleic acid

dPS – perdeuterated polystyrene

ECM – extracellular matrix

ELLA – enzyme-linked lectin assay

FDA – Food and Drug Administration

FESEM – field-emission gun scanning electron microscopy

f-hPS – fibers electrospun from hydrogenated polystyrene

f-hPS/dPS – fibers electrospun from a blend (1:1) of hydrogenated and perdeuterated polystyrene

FITC – fluorescein isothiocyanate

f-PCL$_{45}$-X – fibers electrospun from a polymer solution containing X wt. % of PCL$_{45}$

f-PCL$_{80}$ – poly(*ε*-caprolactone) fibers

f-PCLx-FITCs– surface-functionalized f-PCL-N_3-X fibers with FITC-alkyne fluorophore, X= 20, 40 and 60 wt. % of PCL-N_3

f-PCLx-Gals – surface-functionalized f-PCL-N_3-X fibers with propargyl-β-D-galactose, X= 20, 40 and 60 wt. % of PCL-N_3

f-PCL-Gal-X – fibers containing X=20 and 40 wt. % of PCL-Gal and (100-X) wt. % of non-derivative poly(ε-caprolactone)

f-PCLx-Mans – surface-functionalized f-PCL-N_3-X fibers with propargyl-α-D-mannose, X= 20, 40 and 60 wt. % of PCL-N_3

f-PCL-N_3-X – fibers containing X=20, 40 and 60 wt. % of PCL-N_3 and (100-X) wt. % of non-derivative poly(ε-caprolactone)

f-PS – fibers electrospun from polystyrene

FTIR – Fourier transformation infra-red

GPC – gel-permeation chromatography

HEMA – poly(2-hydroxyethyl metacrylate)

HFP – hexafluoropropanol

HNK – human natural killer epitope

hPS – hydrogenated polystyrene

HRP-ConA – horseradish peroxidase conjugated Concanavalin A

HRP-PNA – horseradish peroxidase conjugated *Arachis hypogaea*

HSA – hydroxystearic acid

MALDI-TOF MS – matrix-assisted laser desorption/ionization time-of-flight mass spectroscopy

MeOH – methanol

M_n – number-average molecular weight

M_w – weight-average molecular weight

MWD – molecular weight distribution

NGF – nerve-growth factor

NGP – nerve-growth precursor

NIPAM – *N*-isopropylacrylamide

NMR – nuclear magnetic resonance

NSC – nerve stem cells

PBS – phosphate-buffer saline

PCL – poly(*ε*-caprolactone)

PCL$_2$ – *α,ω*-diol-poly(*ε*-caprolactone) M_n 2 000 g mol^{-1}

PCL$_{45}$ – poly(*ε*-caprolactone) M_n 45 000 g mol^{-1}

PCL$_{80}$ – poly(*ε*-caprolactone) M_n 80 000 g mol^{-1}

PCL$_2$-Gal – *α,ω*-galactoside-poly(*ε*-caprolactone)

PCL$_2$-N$_3$ – *α,ω*-azido-poly(*ε*-caprolactone)

PCL$_2$-OTs – *α,ω-p*-toluenesulfonyl-poly(*ε*-caprolactone)

PDO – poly(dyoxanone)

PEG – poly(ethylene glycol)

PEI – poly(ethylene imide)

PEO – poly(ethylene oxide)

PET – poly(ethylene terephtalate)

PGA – poly(glycolic acid)

PGMA – poly(glycidyl methacrylate)

PLA – poly(lactic acid)

PLEY – co-polypeptide of L-glutamic acid and L-tyrosine

PLO – poly(L-ornithine)

PMMA – poly(methylmethacrylate)

PNIPAM – poly(*N*-isopropylacrylamide)

PPh$_3$ – triphenylphosphine

PPpfMA – poly(pentafluorophenyl methacrylate)

PS – polystyrene

PSBMA – poly(sulfobetaine methacrylate)

PSU – polysulfone

PTFE – poly(tetrafluoroethylene)

PU – polyurethane

PVA – poly(vinyl alcohol)

PVBC – poly(4-vinyl-benzyl chloride)

PVDF – poly(vinylidene fluoride)

PVP – poly(vinylpyrrolidone)

RAFT – reversible addition-fragmentation chain-transfer polymerization

RH – relative humidity

ROP – ring-opening polymerization

SANS – small angle neutron scattering

SAXS – small angle X-ray scattering

SEM – scanning electron microscopy

TEA – triethylamine

TEM – transmission electron microscopy

TFA – trifluoroacetic acid

TFE – trifluoroethanol

THF – tetrahydrofuran

USANS – ultra-small angle neutron scattering

UV-Vis – ultraviolet-visible light

WCA – water contact angle

XRD – X-ray diffraction

Contributions

The work done during the 3-year PhD research was well valorized and presented during different events (national and international conferences and doctoral school meetings) and in a different manner (journal publications, oral presentations or posters).

Journal publications

1) **A. Lancuški**, S. Fort, F. Bossard, "Electrospun Azido-PCL Nanofibers for Enhanced Surface Functionalization by Click Chemistry", *ACS App. Mater. Interfaces*, 2012, 4, 6499-6504
2) **A. Lancuški**, S. Fort, F. Bossard, "Carbohydrate-Decorated PCL Fibers for Specific Protein Adhesion", *Biomacromolecules*, 2013, *14*, 1877-1884
3) **A. Lancuški**, F. Bossard, Y. Rharbi, F. Boué, "SANS study of monodispersed PS electrospun fibers", in preparation

Oral presentations

1) **A. Lancuški**, S. Fort, F. Bossard, "Functionalized Bio-polymeric Fibers Processed by Electrospinning for Neuroscience Applications", Conference – Interface vivant/matériaux nanostructurés 2011, Clermont-Ferrand, France
2) **A. Lancuški**, S. Fort, F. Bossard, "Clickable PCL Nanofibers - Processing and Applications", Conference – Electrospinning, Principles, Possibilities and Practice 2012, London, United Kingdom
3) F. Bossard, **A. Lancuški**, Y. Rharbi, F. Boué, "Dynamique de relaxation de chaînes de Polystyrène dans des nano-fibres obtenues par electrospinning", 47ème Congrès du GFR 2012 – Pau, France

4) **A. Lancuški**, F. Bossard, Y. Rharbi, F. Boué, "SANS Investigation of the Chain Conformation in Electrospun Polystyrene Nanofibers", Alpine Rheology Meeting 2013, Les Gets, France
5) **A. Lancuški**, F. Bossard, Y. Rharbi, F. Boué, "SANS Study of Chain Conformation and Relaxation Kinetics of Electrospun Polystyrene Fibers", Conference – Electrospinning, Principles, Possibilities and Practice 2013, London, United Kingdom

Poster presentations

1) **A. Lancuški**, S. Fort, F. Bossard, "Mise en forme de nanofibres de bio-polymères fonctionnels par electrospinning pour des applications en neurosciences", Journée des doctorants 2011, Ecole Doctorale I-MEP^2, Université de Grenoble, France
2) **A. Lancuški**, S. Fort, F. Bossard, "Electrospun Azido-PCL Nanofibers for Enhanced Surface Functionalization by Click Chemistry", 41ème congrès du Groupe Français des Polymères GFP 2012, Grenoble, France

Introduction

Introduction

Constant development of materials science and engineering in service of nanotechnology has marked the beginning of 21st century. Nanotechnology enables producing materials with nanometer scale with advantage of being smaller, lighter, and cheaper, with superior physicochemical and mechanical properties than their bulk equivalents. Nowadays, there are many techniques of nano-fiber fabrication, like drawing, template synthesis, phase separation, or electrospinning. Among them, electrospinning was evidenced as the most promising method in terms of cost, simplicity and versatility of the process. Electrospun nonwoven scaffolds, with a porous structure and a high surface-to-volume ratio, extraordinary resemble to the connective cell tissue (extracellular matrix). Nano-fibrous structure of electrospun scaffolds mimics the size scale of the fibrous proteins (fibrils) found in the extracellular matrix. Moreover, 3D nature of the nonwoven structure could allow cells to infiltrate the matrix and proliferate, making these scaffolds ideal for tissue engineering applications. Superior mechanical properties compared to the bulk, high surface-to-volume ratio, and high inter-connected porosity have made electrospun nano-fibers equally present in drug delivery, as filtration membranes, batteries and fuel cells, hi-tech clothes, and in many other areas of academic and industrial research. Electrospinning process is also wide-spread in industry all over the world under the names of: Electrospunra, Singapore; eSpin, USA; NaBond, Hong Kong; NanoSpun Technologies, Israel; Cella Energy, United Kingdom; etc.

If one considers applying electrospun fibers in medicine, high criteria concerning biocompatibility and biodegradation are imposed. Passive biocompatibility and “do-no-harm” requirements previously considered as acceptable are no longer in option. Nowadays, advanced materials with bioactive and biomimetic properties are required. However often, one material cannot meet all the expected specificities, and one should turn toward optimal

modification methods. One of such methods is a chemical functionalization through click chemistry coupling. Ever since it has been discovered, copper-catalyzed azide-alkyne cycloaddition (CuAAC), popularly called click chemistry, holds an important place in the chemistry synthesis. Click chemistry could be performed at ambient temperatures, in both aqueous and organic solvents, as well as in homogeneous and heterogeneous phase. Click chemistry is a high yielding synthesis method and without side products, which makes it attractive candidate for chemical functionalization.

The research project, presented in this manuscript, is directed toward processing of functionalized fibrous materials from commercially available biopolymers by the technique of electrospinning, and involving click chemistry as a functionalization method. We made use of poly(ε-caprolactone) (PCL), a synthetic polyester, because of its favorable mechanical properties, biocompatible and biodegradable morphology, it is easy to manipulate with in the electrospinning process and it is commercially available. We were particularly interested in processing and optimization of PCL-based ultra-fine fibers for tissue engineering. The aim was to make *one-type* electrospun PCL nano-fibers available for *many* areas of interest through click chemistry and its ability of introducing any desired functionality.

The work accomplished in the course of the PhD thesis has been carried out in collaboration between *Laboratoire Rhéologie et Procédés* and *Centre de Recherches sur les Macromolécules Végétales (CERMAV)*. Gathered knowledge of fluid rheology and processing on one hand, and natural organic chemistry on the other, was molded over three-year research study into functionalized PCL fibers for applications targeting tissue engineering. Additional experience of small angle neutron scattering technique on electrospun polystyrene (PS) fibers was generously afforded by *Laboratoire Léon Brillouin*, CEA Saclay. This technique provided us with better understanding of fiber processing phenomena during the electrospinning by

observing and analyzing polymer chain conformation and thermal relaxation in the electrospun fibers.

This manuscript begins with the bibliographic study of up-to-date research dealing with the electrospinning technique, its possibilities, and practice in drawing polymeric structures into fibrous nonwovens aiming for tissue engineering applications. Bibliography continues with SANS technique as a tool for structural investigation of polymeric materials. In the end, the latest developments in the area of biomaterials with accentuation on synthetic polymers and their use in medicine and tissue engineering are exposed.

Chapter two gives a closer view on the electrospinning process through the model of polystyrene fibers using SANS technique. Polymer chain conformation and relaxation dynamics after annealing are discussed.

Chapter three is dealing with processing and functionalization of PCL-based fibers, and their characterization. Two techniques of PCL fiber functionalization were adopted and some others suggested for further investigations. Consequently, physicochemical properties of final products are studied.

The results exposed are assembled and a critical overview, with the future possibilities continuing the research, is offered in the “General Conclusions and Perspectives” fourth chapter.

The closing fifth chapter, “Materials and Methods”, is detailing the compounds used, various syntheses and characterization techniques performed. It highlights the electrospinning process – from solution preparation to optimal processing conditions.

Bibliography

Chapter I – Bibliography

1 Nano-Fiber Formation Techniques

Materials made of nano-fibers have attracted a considerable attention because of their lightness, great specific surface and highly porous morphology. Today, one could find nano-fibrous scaffolds being used in drug delivery, tissue engineering, for medical bandages and sutures, in batteries and fuel cells, as filters, nano-sensors, protective clothes, etc., as illustrated in Scheme I.1.

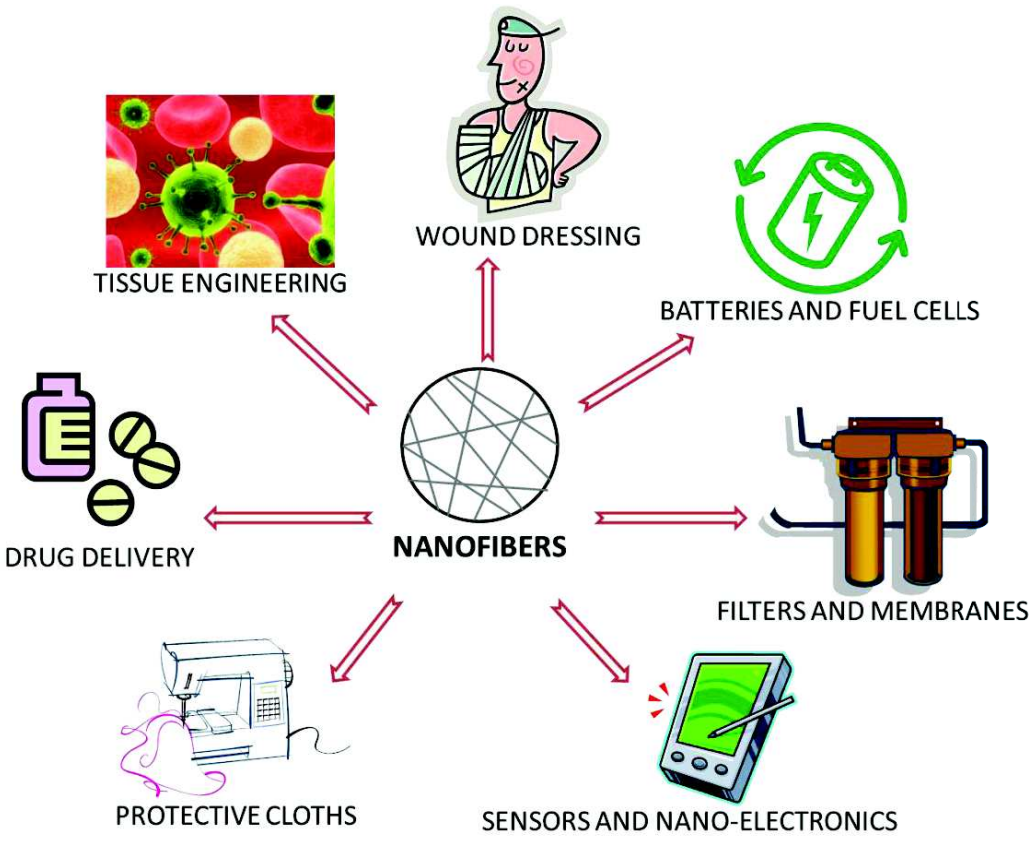

Scheme I.1. Application possibilities of nano-fibrous scaffolds

Several fiber-processing techniques emerged from a tremendous need for nano-fibrous structures, particularly in the field of nanotechnology and tissue engineering. The most important ones are:

- Drawing,
- Template synthesis,
- Temperature-induced phase separation,
- Self-assembly,
- Electrospinning.

A brief description of each processing technique, with a particular focus on electrospinning process, is presented in the following sections.

1.1. Fiber Drawing Technique

Early descriptions of a drawing technique were presented by Taylor 1920 where fiber wires were produced.[1] From a polymer molded into a cylinder preform, having 30 cm length and 40 mm diameter, about 1 km long fibers with a 0.5 mm diameter can be drawn in an oven while heated above the polymer melting temperature (Scheme I.2). Under the pulling force of a circumference drum, one continuous solid fiber is collected at a time. This technique offers a possibility of drawing very long micron fibers, and it is intensively employed for drawing optical fibers. The possible limitations of this technique would be the possibility of drawing only thermoplastic polymers with micron-sized or thicker fiber diameters.

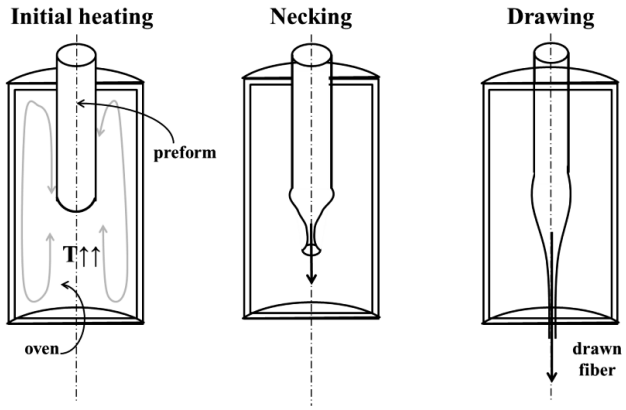

Scheme I.2. Schematic representation of the fiber's drawing technique: 1) initial heating, 2) necking and 3) drawing

Ondarçuhu and Joachim[2] described a nano-fiber drawing technique from a micro-droplet or a micro-pipette of a polymer solution in a continuous manner over precisely defined period of time. Each fiber is pulled at the threshold of solidification. When they used long polymer chains entangled in the solution, fibers with micron diameters could be obtained. When shorter unentangled molecules are used, sub-micron fibers are collected. Even though generating nano-sized fibers, this process is strongly limited by the size of the droplet as well as by the time of solvent evaporation.

1.2. Template Synthesis

Template synthesis is a method for preparing nanostructures (nanotubes or nanowires) by directly synthesizing a desired material within the pores of a porous template-membrane.[3] Common membranes, used for template synthesis, include anodic aluminium oxide and mesoporous silica. Depending of the type of the membrane, pores could be inter-connected or isolated. When anodic alumina membranes are used, solid material is formed inside the isolated pores.[4,5] In the case of mesoporous silica template, nanowires or nanotubes are inter-connected by the porous silica wall. Sol-gel chemistry,[6,7] electrochemistry[8] or *in-situ* polymerization[9] methods could be used for depositing a material inside the pores of such membranes. Finally, nano-fibrils or nano-tubules are formed within each pore of a membrane.

Porter *et al.*[10] adopted a solvent-free nano-templating method to fabricate poly(ε-caprolactone) nanowires in alumina membranes for bone tissue engineering. The idea of using the solvent-free templating is to avoid the toxic organic solvents for medical purposes. In Scheme I.3 is illustrated the nano-wire templating process: sintered PCL puck is placed on nanoporous alumina membrane (Scheme I.3A). At moderately elevated temperatures PCL nanowires are gravimetrically extruded (Scheme I.3B, C). The alumina membrane is then dissolved in NaOH (Scheme I.3D) leaving a nanowire surface (Scheme I.3E).

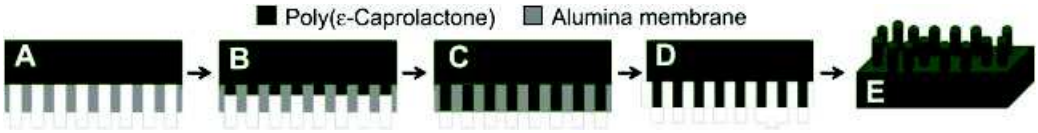

Scheme I.3. Schematic representation of PCL nanowire fabrication: sintered PCL placed on nanoporous alumina membrane (A), gravimetric extrusion of PCL nanowires (B, C), alumina membrane dissolution in NaOH (D) PCL nanowire (E)[10]

Template synthesis generates aligned fibers with well-defined fiber's size and inter-fibrous distance. However, this technique strongly depends on the size of the template adopted. Nevertheless, by carefully choosing the template and polymer for molding, various materials' architectures could be easily attained, serving as a sensitive gravimetric apparatus for detecting ammonia gas[11] or as biodegradable extracellular matrices[12].

1.3. Phase Separation Technique

In thermally-induced phase separation process, a polymer solution is heated in a controlled way to induce a phase separation into two phases: a polymer-rich phase and a polymer-lean phase.[13] After the solvent removal (extraction, evaporation or sublimation), a polymer-rich phase solidifies and forms a polymer foam. By varying the polymer solution properties as well as phase-separation temperature, one could achieve different pore morphologies and fiber-like structures.[14,15]

To produce porous matrices, Asefnejad *et al.*[16] used poly(ε-caprolactone)-based polyurethanes (PU) in dioxane/water solution with a sodium chloride (NaCl) salt for pore creation in phase separation method. Three different types of polyurethanes were prepared by varying the ratio of PCL and 1,4-butanediol/hexamethylenediisocianate/1,4-butanediol copolymer. The pore size of the scaffolds was successfully tuned by using different size of salt particulates. Figure I.1 represents the porous scaffolds they obtained from different polyurethanes (A-C) and after 7 days cell culture of human fibroblasts. It could be noticed that

one could vary the pore size of the scaffold by varying the size of the NaCl particulates (from 50 to 355 µm) present in the polymer bulk. However, for higher porosity, mechanical properties had to be sacrificed, and PUA3 (Figure I.1C), showing the highest compressive strength and modulus, had the lowest porosity.[16]

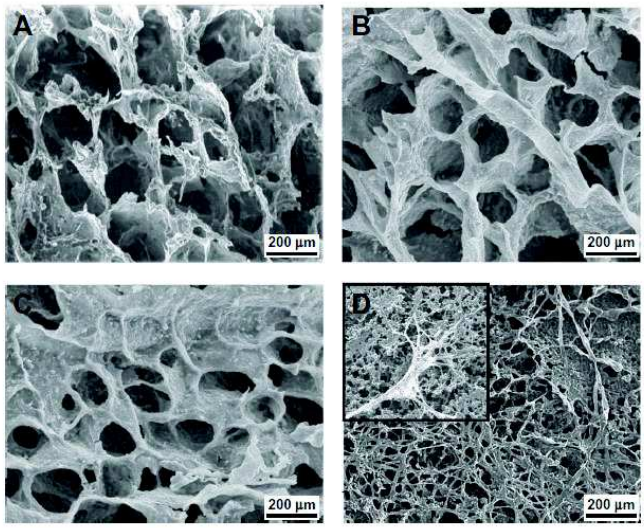

Figure I.1. SEM images of polyurethane scaffolds prepared by phase-separation method: (A) PUA1, (B) PUA2, (C) PUA3 and (D) human fibroblasts on polyurethane scaffold after 7 days culture on PUA3[16]

This method is advantageous because it does not require specific equipment and can be molded into various shapes with the convenience of possible adjustment of pore size of the scaffold. However, phase separation could be prepared with only a limited number of polymers.[17]

1.4. Molecular Self-Assembly Technique

Self-assembly is a spontaneous process by which molecules and nano-sized entities materialize into well-organized fibrous networks and aggregates.[18–20] The self-assembly arrangements are obtained through a number of various non-covalent interactions, such as hydrogen bonds, van der Waals, electrostatic or hydrophobic interactions.

Structure of collagen fibers is a good example of naturally occurring self-assembly process. Procollagen fibrils are secreted by cells and converted into collagen by peptide cleavage (Scheme I.4). Collagen molecules are then self-assembled to collagen fibrils which are further ordered in parallel fashion into collagen fibers with diameter ranging from 50 to 500 nm.[21]

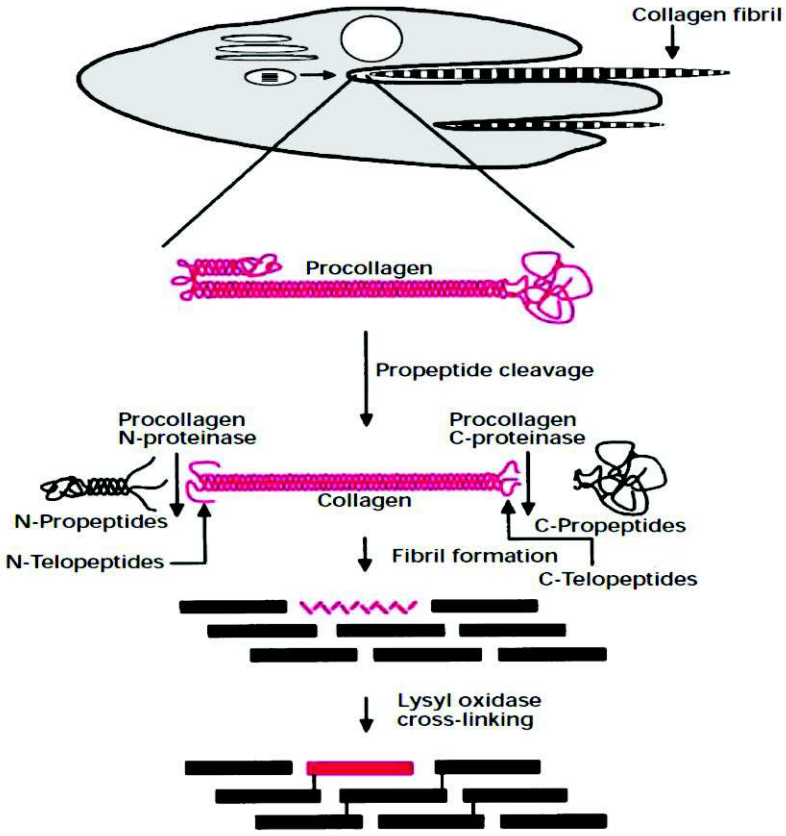

Scheme I.4. Schematic representation of fibrillar collagen synthesis[21]

Shibata *et al.*[22] prepared fiber-reinforced plastic from a mixture of castor-oil-modified poly(ε-caprolactone) resin (CO-PCL) and hydroxystearic acid (HSA) able to form self-assembled supramolecular fibrous networks. CO-PCL was obtained from the ring-opening polymerization of ε-caprolactone in the presence of castor oil. CO-PCL/HSA samples were prepared by blending and molding of CO-PCL and HSA and different samples were prepared by varying the annealing time. In order to obtain the formation of supramolecular HSA

aggregates and fine fibrous structures, repeated annealing of a HSA/CO-PCL composite took place.

Vauthey *et al.*[23] prepared a dense fibrous network using surfactant-like peptides. Four different amphiphilic peptides were obtained by varying the size of hydrophilic head (1 or 2 aspartic acid molecules) and the type of hydrophobic amino acid (alanine, valine or leucine). These peptides were able to self-assemble in water forming nanotubes and nano-vesicles that are further organized into a dense network as represented in Figure I.2.

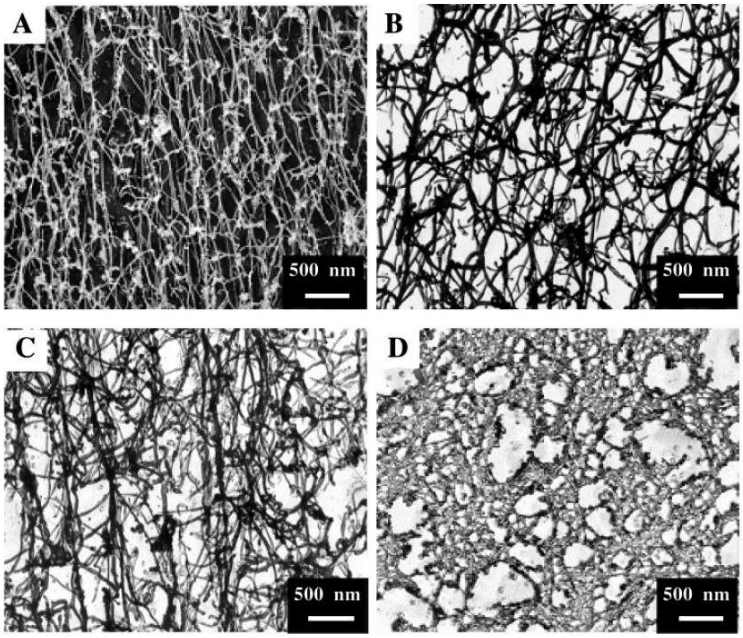

Figure I.2. Quick-squeeze/deep-etch TEM image showing a 3D network structure of four different surfactant peptides (A-D) self-assembled in water[23]

Using self-assembly method, one could obtain rather thin fibers (tens of nanometers), from a large variety of molecules: synthetic polymers as well as natural oligo- and poly-peptides, etc. While fibrous structure could be easily obtained, fiber orientation cannot be controlled and random fibrous network is usually created.

1.5. Electrospinning Technique

Electrospinning is a processing technique for fabrication nano-fibrous nonwoven mats under high electric field. Variety of chemical structures that can be used and simplicity of the setup has made this technique quite popular and easily adopted in nanotechnology and fiber processing. Even though mainly used for research studies, this technique has already found many useful applications in industry as well. Some of the examples are Donaldson Company and Freudenberg which are using electrospun fibers in filtration products, or Cella Energy where electrospun fibers serve as low-cost hydrogen storage.

Electrospinning process uses a high voltage power supply, applied to a polymer solution or a melt, to produce dry polymeric micro- and nano-sized fibers, collected on a metallic collector (Scheme I.5). Electrospinning process has a simple setup, it is rather easy to manipulate with, and it makes high-porosity scaffolds with interconnected pores. Compared to mechanical drawing, electrospinning produces fibers of thinner diameters via contactless procedure; it is less complex than self-assembly and can be used for a wide range of materials unlike phase separation.

First electrospinning-related patent was deposited by John Francis Cooley about *"apparatus for electrically dispersing fluids"*.[24,25] Later followed several patents from Anton Formhals about *"electrically spun artificial fibers"*.[26–28] It is only after these patents that, in 1969, a specific behavior of a water drop under electric field was described by sir G. Taylor.[29] The first use of this phenomenon on polymer solutions under the name of electrospinning was published 1995 by J. Doshi and D. Reneker,[30,31] and ever since the term of electrospinning appeared until now, the interest in this topic has been only expanding.

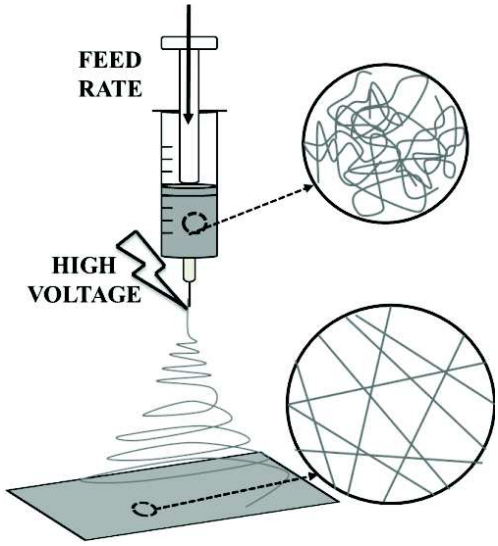

Scheme I.5. Illustration of electrospinning process – from a viscous polymer solution or a melt to solid nano-fibers

The word electrospinning is suggesting a processing behavior of spinning motions under electric field applied (from *electro* and *spinning*), but what exactly electrospinning process is? Once a high voltage is applied to a polymer solution or a melt in flow, a pendant drop, formed at the needle tip, will undergo two electrostatic forces: electrostatic repulsion between the surface charges and Columbic force exerted by the external electric field. Under sufficiently high electric field, electrostatic forces in the charged drop will overcome the surface tension, and a Taylor cone will be formed at the nozzle, ejecting a liquid jet.[29,32] The flying jet will then undergo bending instability and whipping (spinning-like) motions followed by strong elongation and thinning. At the end, under electric (for polymer solutions) and temperature gradient (for polymer melts), flying jet will deposit dry polymeric fibers onto the collector. During the electrospinning process, three stages take place one after another (Scheme I.6):

1. *Stability zone* is formed near the tip of the spinneret; the jet is stable, linear and follows the direction of electric field.

2. It soon enters the *bending instability zone* where jet undergoes whipping motions in the direction perpendicular to the electric-field gradient and further stretching.
3. When tip-to-collector distance is sufficiently great, the jet goes into the last stage, *secondary bending instability zone*, formed in the axis of the jet trajectory. In this zone, the jet suffers further stretching and thinning before it ends onto the collector surface.

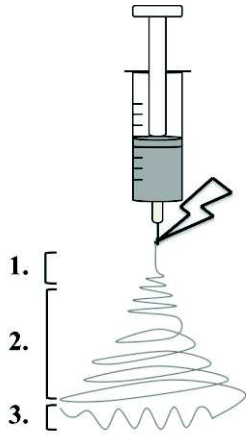

Scheme I.6. Illustration of a flying jet with divided zones of fiber formation: (1) stability zone, (2) first bending instability and (3) second bending instability zone

During the jet flight, solvent evaporates forming a thin film at the surface of the jet. This thin film will further control the evaporation kinetics being a barrier for the solvent, and leaving it entrapped inside the fibers. The presence of the solvent residue might lead to the formation of pores and voids inside and at the surface of the fibers. It is also considered responsible for various shapes of final electrospun fibers – ribbons, tubes, cylinders, etc.[33]

In fact, there are many parameters influencing the electrospinning process and consequently fiber morphology. Next section gives a detailed description of the processing and solution parameters for electrospinning as well as progressive setup development seeking for an increase of the production rate, fiber's morphology upgrade, and promotion of mechanical and physicochemical properties.

2.5.1 Electrospinning Parameters

Electrospinning process has become popular because of its simple setup. However, fiber formation during the electrospinning process is accompanied with complex physicochemical behavior influenced by both processing and solution parameters.

1.5.1.1 Solution Properties

Properties of the electrospinning solution have the most significant influence on the process itself and on the final fiber morphology. Solution parameters are:

a) Polymer molecular weight and solution viscosity

Molecular weight of the polymer is one of the main factors affecting the solution viscosity. According to Mark-Houwink-Sakurada equation, $[\eta] = KM^a$, where K and a are constants for a polymer in a given solution, an increase of molecular weight M causes the viscosity $[\eta]$ of the solution to increase.[34] Electrospinning process of continuous fiber formation entails viscous polymeric solutions for which polymer chains overlap and entangle, requiring well defined polymer chain length and concentration in a given solvent.

Scheme I.7 illustrates three concentration regimes for flexible polymeric chains and electrospun fibers obtained therefrom. In the dilute regime ($c < c^*$) (Scheme I.7A), single polymer chains are isolated. Critical concentration (c^*), marking the boundary between the dilute and semi-dilute regime, has been described by de Gennes[35,36] as the overlap concentration for which steric interactions between polymer coils start to arise in the solution. A semi-dilute polymer solution placed under high electric field, due to absence of cohesion between polymer chains, will produce a discontinuous jet of droplets, called electrospray. By increasing the concentration, polymer chains will start approaching each other, slightly merging but not enough to entangle (semi-dilute, unentangled, $c^* < c < c_e$). Critical entanglement

concentration (c_e) is the cross-over concentration from the semi-dilute unentangled and semi-dilute entangled regime. Electrospinning in the semi-dilute, unentangled regime results in bead-on-a-string formation – very fine nano fibers with micron-sized beads. Further increase in the polymer concentration (semi-dilute, entangled, $c < c_e$), leads to chain entanglement and a single continuous fiber could be formed.[37] It is determined that the concentration of 1-2 times c_e ($\geq$ 2.5 entanglements per chain) is needed to maintain the continuity of the jet during electrospinning.[38–40] However, too high polymer concentration in the solution results in a very viscous fluid, too difficult to be pumped through the needle. These highly viscous solutions may result in fast solvent evaporation and polymer drying at the needle tip. Consequently, a needle clogging will occur, hindering the electrospinning process.

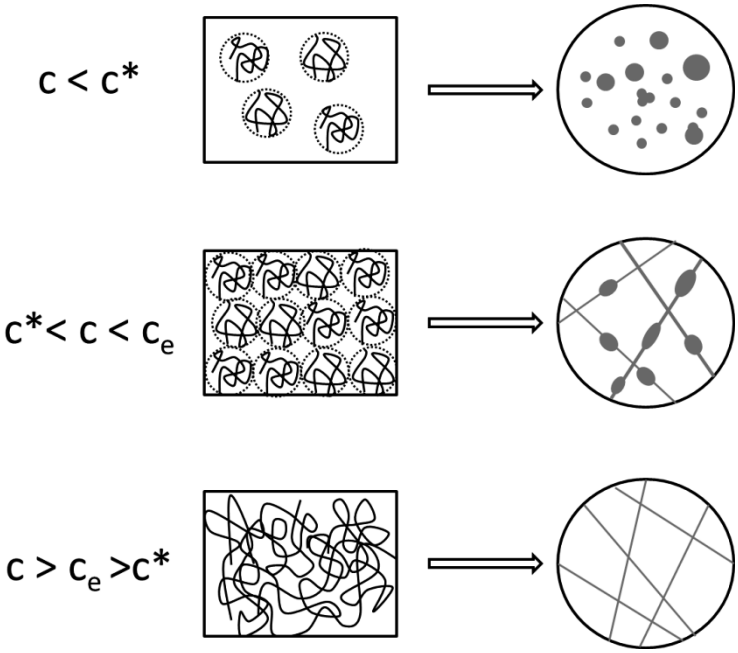

Scheme I.7. Illustration of polymer chains inside the solution from dilute ($c < c^*$) over semi-dilute unentangled ($c^* < c < c_e$) to semi-dilute entangled ($c > c_e$) regime and corresponding collected structures after electrospinning

The macromolecular chain length will directly influence the concentration where chain entanglements occur, and consequently, fiber formation and its diameter. High concentration

of the polymer solution could also discourage the bending instability. As a result, the jet path is reduced and the bending instability spreads over smaller area; polymer stretching is less pronounced and the collected fibers have large final diameters.

b) Surface tension

During the electrospinning process, under the influence of high voltage, a droplet of polymer solution at the needle tip will take a conical form, known as a Taylor cone. Surface tension of the solution will tend to decrease the surface area per unit mass of a fluid and make a spherical droplet, while high voltage will try to elongate the droplet in the direction of the electric field. When the high voltage surpasses the threshold value, and electrical forces overcome the surface tension, a liquid jet will be formed. Scheme I.8 illustrates the influence of high voltage increase on droplet morphology and solution's surface tension.

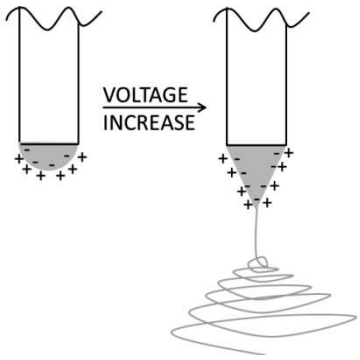

Scheme I.8. Illustration of liquid jet formation under sufficiently high voltage – when high voltage force overcomes the surface tension – from drop deformation to Taylor-cone formation

Surface tension is believed to be one of factors causing the formation of beads on the electrospun fibers due to Rayleigh-Taylor instability.[41] This phenomenon is observed in the case when adequate solution viscosity is used for electrospinning uniform fibers, but insufficient electric field is exerted onto the solution to overcome the surface tension leading to bead-on-string fiber formation.

In order to decrease the surface tension, low surface-tension solvents can be used, such as ethanol, or a surfactant may be added to the electrospinning solution.[42] Jia and Qin investigated several surfactants on poly(vinyl alcohol) (PVA)/water electrospinning solution and observed significant decrease of surface tension even with surfactant contents as small as 1%.[43] The presence of surfactant increased the solution conductivity as well as polymer crystallinity inside the electrospun fibers, while remarkably decreasing fiber diameter from 400 to 100 nm.

c) Dielectric constant of the solvent

Dielectric constant of the solvent has an important influence on electrospinning and fiber morphology. High dielectric constant of a solvent (such as DMF, acetic acid, etc.), used in electrospinning, may reduce the bead formation. Small amounts of the solvent with a high dielectric constant, could improve the electrospinnability of the solution and result in uniform fibers without beads.[44]

Guarino *et al.*[45] intensively studied the influence of solvent permittivity and dielectric constant on fiber formation (beaded or uniform fibers) in the case of poly(*ε*-caprolactone) (PCL) (Scheme I.9).

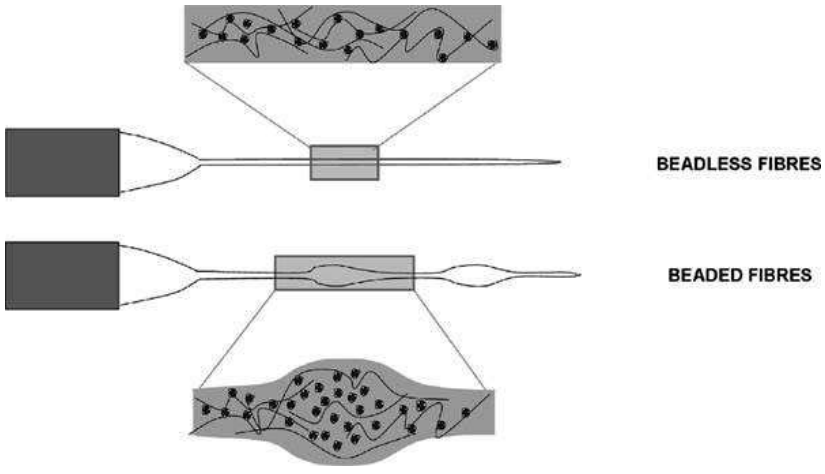

Scheme I.9. Schematic representation of bead-free and beaded fibers, alluding to the importance of the solution properties in electrospinning PCL[45]

The objective of their study was to identify the solvent properties affecting the most: fiber morphology, physical properties and biological response. Different polymer/solvent systems tested indicate the importance of solvent permittivity in the polymer chain folding during the fiber formation, thus affecting the fiber crystallinity, and consequently the bead formation.[45] They observed that polar solvents with high permittivity (highly fluorinated alcohols: TFE, HFP) were promoting the formation of sub-micron sized fibers while non-polar solvents yielded micron-sized fibers. PCL nano-fibers had higher degree of crystallinity and were more readily available for cell adhesion and viability then micron-sized PCL fibers.

d) Conductivity of a polymer/solvent system

Solution conductivity is ability of a fluid to pass the electric current, and as such, it is an important parameter in the electrospinning process.

Pattamaprom *et al.*[46,47] tested several solvents (DMF. 1,4-dioxane and chloroform) for electrospinning of polystyrene in order to determine the fiber production rate in the terms of electrospinnability of the system. They observed that the conductivity of a chosen solvent strongly influences the final fiber production. Highly electrospinnable solvents were those with reasonably high values of conductivity and dipole moment. In the case of polystyrene, DMF was found to be promoting high dipole moment and spinnability of the solution.[46]

Higher solution conductivity could be accomplished by small addition of a salt (or polyelectrolyte) to the electrospinning solution. Increased charges in the solution would increase the bending instability, favoring the thinner fiber formation.[48] Zong *et al.*[49] showed that the solution conductivity is inversely related to the fiber diameter – higher solution

conductivity results in a smaller fiber diameter. By adding a small amount of ionic salt to polylactide solutions they observed significant decrease of fiber diameter while drastically changing their structure – from bead-on-string to fine and uniform bead-free fibers.

However, the difficulty in using salts is that their crystals could be found entrapped inside or at the surface of the fibers.[50]

e) Solvent volatility

Solvent volatility depends mainly on its vapor pressure and boiling point, and thus directly influencing electrospinning process and morphology of electrospun fibers. During the electrospinning, the solvent will evaporate as the flying jet accelerates toward the collector. If the most of the solvent evaporates before the jet reaches the surface of the collector, well defined fibers will be formed. However, if the solvent used has a high boiling temperature, its evaporation process might not be complete when the flying jet arrives to the collector, and instead of fibers, a thin polymer film would be collected.

At the beginning of the fiber formation, a thin skin of polymer will be formed on the surface of the jet that will thereafter influence the solvent evaporation kinetics. Lower the vapor pressure of a solution is (and therefore lower the boiling temperature of the solvent is), faster the evaporation process would be, rapidly creating a film at the jet surface. In the case of low volatile solvents, once the skin is formed, the residual solvent will continue to slowly evaporate even after the fiber formation, leaving the cavities and voids.[51] However, the porosity is also observed when the solvent is very volatile – the premature skin formation will cause the porous structure inside the fibers while the surface might be smooth.

Koombhongse *et al.*[33] reported various cross-section shapes of electrospun fibers. They demonstrated that different polymer/solvent systems (poly(2-hydroxyethyl metacrylate)

(HEMA) and ethanol/formic acid; polystyrene and DMF; poly(vinylidene fluoride) (PVDF) and DMF/dimethylacetamide; poly(ether imide) (PEI) and hexafluoro-2-propanol) could be electrospun into distinctively different fibrous morphologies and illustrated in Scheme I.10.

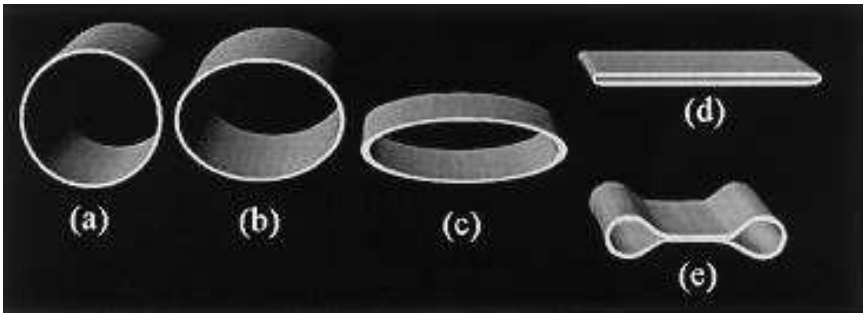

Scheme I.10. Various shapes of electrospun fibers due to a collapse of the skin on a jet: from cylinder (a) over cylinder-like shapes (b and c) to flat ribbon (d) and ribbon with two tubes (e)[33]

Depending of the kinetics of the solvent evaporation, various shapes of electrospun fibers could be observed: cylinder (Scheme I.10a), oval (Scheme I.10b, and I.10c), and, due to a collapse of the skin on a jet, ribbon like (Scheme I.10d) and ribbon with two tubes (Scheme I.10e).

1.5.1.2 Processing Parameters

Once the solution properties are defined and optimized, processing parameters should be adjusted for optimal electrospinning and uniform fiber formation. Hereafter, several important processing parameters are introduced, and their influence on the electrospinning process.

a. Voltage

Voltage is a key point of the electrospinning process. It provides the charges needed to overcome the surface tension and Taylor-cone formation, as mentioned previously. It is also responsible for the stretching of a liquid jet during the fiber in formation. At low voltages, a

still droplet is suspended at the needle tip and only small beads reach the collector (Scheme I.11B).

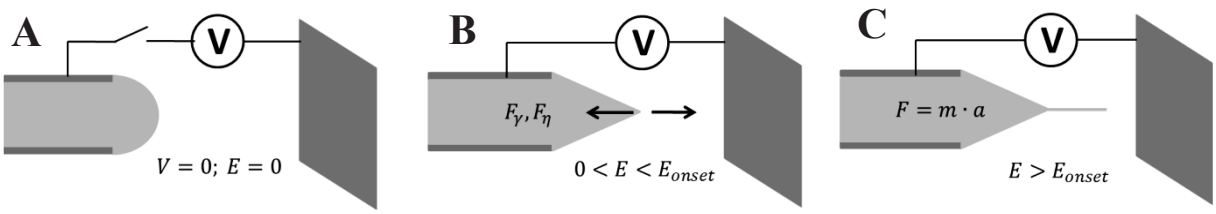

Scheme I.11. Schematic diagram showing balance of forward and backward driving forces at the needle tip when increasing high voltage

By increasing the high voltage, Taylor cone is formed, ejecting a liquid jet and uniform fibers are formed on the collector (Scheme I.11C). Further increase of high voltage might lead to Taylor cone receding inside the needle. When the voltage is too high, it causes the Taylor cone instability and jet break-up. Consequently, resulting fiber's morphology might be irregular with broad fiber diameters or even beads.[49]

b. Tip-to-collector distance

The distance between the needle tip and the collector influence the force of the electric field that will be applied to the electrospinning jet in formation. Generally, the Coulomb force F applied on a charge q, depends on the electric field E, itself dependent on the potential difference $\Delta\phi$ and the distance d as follows:

$$F = q \cdot E = q \cdot \frac{\Delta\phi}{d} \quad \text{(I.1)}$$

In the case of electrospinning process, when increasing the tip-to-collector distance (d), the electric field strength (F) will decrease.

c. Solution feed rate

Flow rate imposed to a solution determines its amount available for electrospinning (also called a feed-rate). Unlike extrusion, feed rate in electrospinning process is not a driving force for fiber formation. In order to obtain a stable Taylor cone and a continuous jet, for a given high voltage a defined feed rate should be applied. In the case of polymer solution in non-entangled regime, by increasing the feed rate of the solution, beads size will increase, and no fibers will be formed. In the entangled regime, by increasing the feed rate, the fiber diameter will increase as well, all due to the increased solution volume drawn from the spinneret. However, there is a limit of the feed-rate increase. The excess of feed rate (mainly over 0.5 mL/min) will result in nozzle overflowing by polymer solution, and consequently solution dropping onto the collector under gravity.

d. Humidity and temperature

Humidity and temperature are often neglected, but important parameters influencing morphology and surface texture of the final electrospun fibers. It has been already mentioned that solvent nature and its evaporation kinetics directly influence the fiber morphology and possible void/pore formation. In addition, air humidity in the electrospinning box affects the fiber formation in a certain extent, all depending on the type of both polymer and solvent used for electrospinning.

It has been often reported that relative humidity of the electrospinning box should be kept at minimum in order to avoid the formation of pores inside the fibers. However, for the poly(ethylene oxide) (PEO) and PVA polymer, electrospun fibers had no pores at all values of humidity tested. Contrarily, poly(L-lactic acid) (PLLA) and PS needed low humidity for smooth fibers without pores.[52] It could be therefore concluded that humidity does not have influence on pore formation for the hydrophilic polymers, while it strongly affects the pore formation during electrospinning of hydrophobic polymers. Indeed, in the course of fiber formation, when

polymer comes in contact with water from the humid air, the process of phase separation and finally polymer precipitation occurs.

While solvent evaporates, the temperature of the surface decreases, allowing water from the surrounding humid air to condensate at the surface of the fibers in formation. For a hydrophobic polymer, this may result in a sudden phase separation and polymer precipitation. Thus, for those polymers, it is important to keep the air humidity low. For hydrophilic polymers, this phenomenon does not occur and even at high humidity smooth fibers are obtained.[53] However, if the polymer is hydrophobic, pores will not necessarily form.[52] Actually, there is a competition between two phenomena: phase separation and solvent-evaporation rate as in casting porous membranes. Also, the diameter of the fibers will influence the pore formation, where micron fibers are more susceptible in forming pores while for nano-fibers the dynamics of solvent evaporation, phase separation and skin formation are too fast to allow pores to be formed.

e. Collector type – static or dynamic

Electrospun fibers may be collected in random or organized (aligned) fashion, depending of the collector type used.[54] One of many examples, showing the importance of fiber aligning, is in tissue engineering applications for nerve regeneration and growth where aligned fibers provide topographic guidance to the cells. Cooper *et al.*[55] reported that aligned chitosan-PCL fibers provide a preferable surface for nerve cell attachment, proliferation and cell growth conducting when compared to the randomly collected ones.

If the fibers are collected onto aluminum or any static conductive surface, a random network will be formed with the fibers deposited in all directions uniformly (Scheme I.12-1). However, both static and dynamic collectors could produce aligned fibers, namely, static

parallel wires or plates (Scheme I.12-2a and 2b), rotating cylinders (Scheme I.12-3), drums (Scheme I.12-3a) or discs (Scheme I.12-3b).

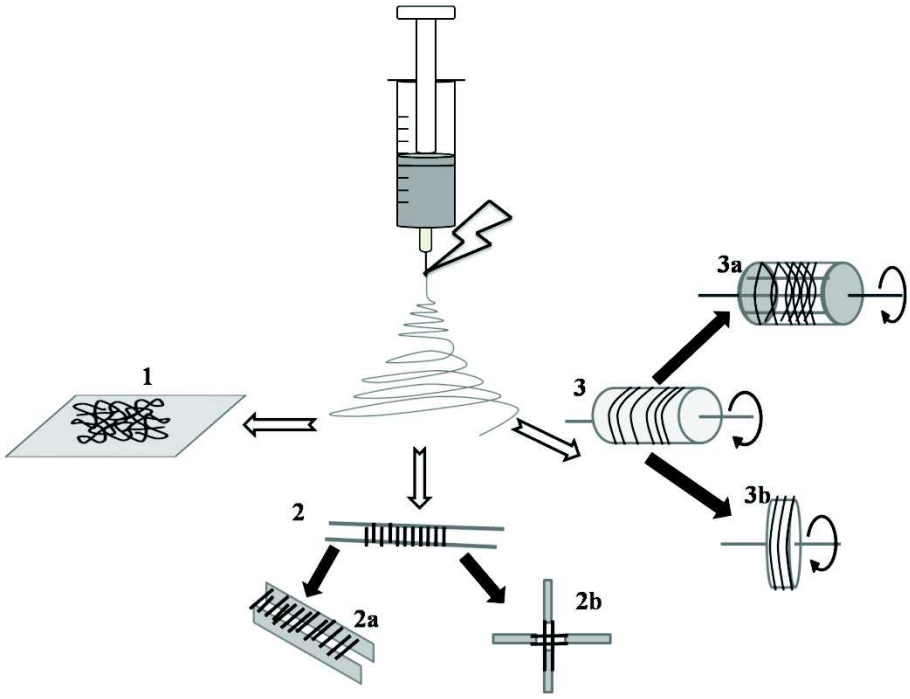

Scheme I.12. Illustration of electrospinning setup with different types of static and dynamic collectors with collected electrospun fibers: (1) classical static collector, usually an aluminum foil for obtaining randomly deposited fibers; (2) parallel wires/plates for aligning fibers (2a) uniaxially – between two parallel plates and (2b) biaxially – when 4 cross-forming plates are used; (3) rotating cylinders in the form of (3a) a drum or (3b) a disc where mechanical force is aligning fibers

In the case of *static parallel electrodes*, aligned fibers are drawn along with the electric field lines towards the edge of the parallel electrodes and are collected in aligned fashion in between.[56] When parallel electrodes, plates and wires, are used, the setup is simple and cost-effective, and fibers could be easily detached.[56–58] However, the fiber length is limited to the distance of the electrodes and thicker fibrous mats cannot be formed because of the residual charges in the fibers.

In the case of *rotating collectors*, whether discs or cylinders, the alignment process is governed by high rotation speed of the collector. When the tangential speed of the collector

reaches the whipping speed of the jet, the fibers collected onto the cylinder will start to align. Increasing the velocity of the rotating collector, the tangential force during the fiber collection will not only align but further elongate the fibers along the axial direction, leading to their significant decrease in diameter.[59,60]

Rotating cylinder uses its entire surface for collecting electrospun fibers. Consequently, a significant amount of fibers could be collected. However, as the collecting surface is large, the alignment will be only partial with the fibers only orientated in the direction of the rotation of the cylinder.

Rotating drum is a simple solution of rotating cylinder where fibers could be collected in an aligned manner with a large collecting area.[61] When compared with the rotating cylinder, the rotating drum is shown to be more effective in the fiber uniaxial orientation as well as in the amount of fibers that can be collected without disturbing the alignment.

Disc collector has as an advantage a small collecting area, guiding the fibers into high alignment.[59,62] However, when the thickness of the scaffold starts to be important, fiber alignment is less pronounced.

There are other ways of collecting electrospun fibers in an organized fashion. Lavielle *et al.*[63] used a combination of micro-patterning and electrospinning to obtain micro-structured fibrous scaffolds (Figure I.3).

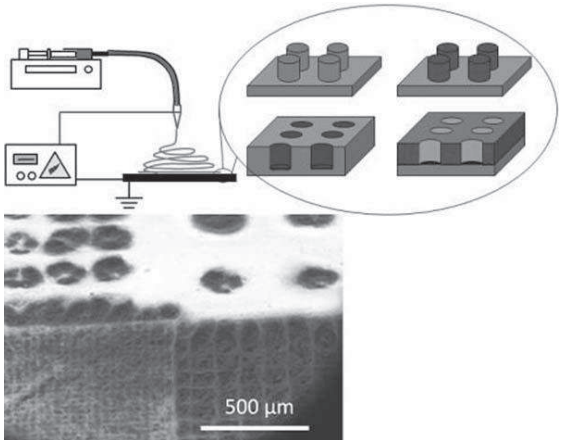

Figure I.3. Micro-patterning of electrospun fibers by using 4 different collector geometries

The above-mentioned examples go in behalf of electrospinning versatility, opening new ways for processing advanced fibrous scaffolds. Next section will be particularly dealing with the improvements of electrospinning setup and different types of electrospinning technique will be exposed.

2.5.2 Different Types of Electrospinning Technique

Electrospinning technique has rapidly developed, and to date, one could find various types of this technique, named as:

1. Melt electrospinning
2. Emulsion electrospinning
3. Co-axial electrospinning
4. Magnetic electrospinning
5. Needleless electrospinning

The first two terms refer to the properties of the electrospinning solution – polymer melt[64] or polymer emulsion[65] will be electrospun. The last three terms refer to the electrospinning setup.

Melt electrospinning is process of fiber drawing from a polymer melt, above the melting temperature. Herein, the process of fiber-formation is governed by the temperature gradient between nozzle and collector. For better temperature control, the distance between the nozzle and the collector is of few centimeters.

Melt electrospinning has an advantage of using a polymer melt and avoiding often toxic solvents for nano-fiber production. It is therefore convenient in tissue engineering purposes where solvent toxicity should be kept on minimum. Dalton *et al.*[64] applied this method for production of electrospun fibers from a PEO-*b*-PCL copolymer directly onto the fibroblast cells (Scheme I.13). They determined the order of magnitude lower feed rates and the magnitude higher viscosities needed for melt electrospinning when compared with the electrospinning from a solution. However, electrospinning onto insulating polystyrene Petri-dish plates is not a convenient solution for continuity of electric field, and it requires further research of better grounding system.

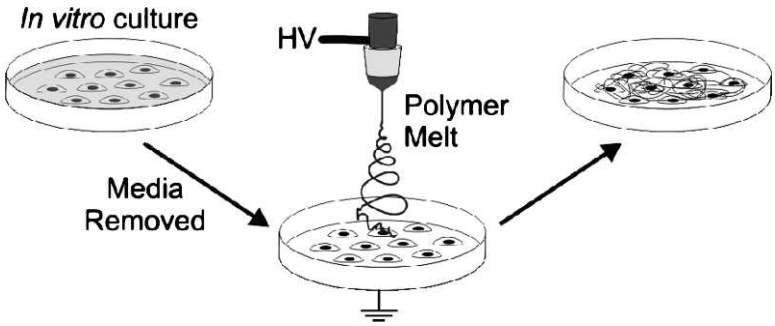

Scheme I.13. In vitro electrospinning of PEO-b-PCL copolymer melt[64]

Co-electrospinning, later called *coaxial electrospinning*, uses a special feeding system that will supply the nozzle with two different solutions in order to obtain core/shell morphology of the fibers. Sun *et al.*[66] obtained polysulfone (PSU)/PEO core/shell fibers from the coaxial electrospinning setup shown in Figure I.4. Apart from the specific morphology this method produces, it is equally attractive because it can electrospin the molecules that are otherwise not

able to form fibers by standard electrospinning technique. Usually, the electrospinnable solution is forming a shell, while core material is made of a solution not able to be electrospun.[67]

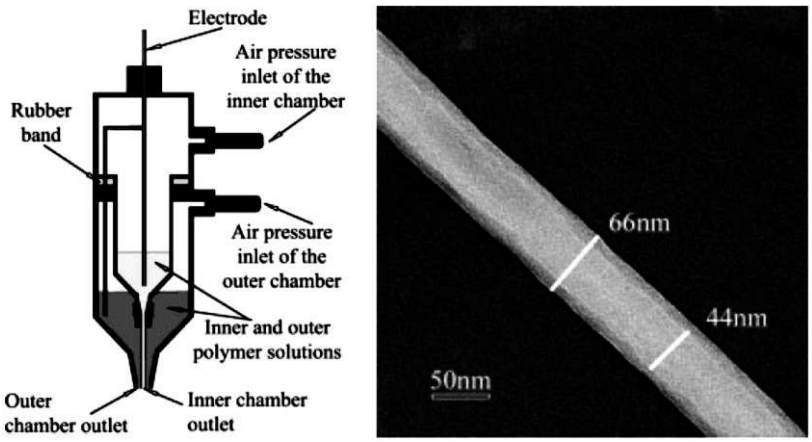

Figure I.4. Experimental setup for co-electrospinning (left) and TEM image of PSU/PEO core/shell fibers (right).[66]

Emulsion electrospinning is another way to load useful molecules inside the electrospun fibers and obtain core/shell like structures. The emulsions used in electrospinning are usually of water/oil type. They consist of an aqueous phase containing micron and submicron hydrophilic molecules, and an oil phase consisting of organic solvent in which a polymer and a hydrophobic reagent are dissolved. During the electrospinning process, two phases will form distinct core/shell structure of the fibers with, for example, hydrophilic molecules in the core and hydrophobic polymer as a shell. Xu *et al.*[68,69] were among the first to report the emulsion electrospinning, highlighting the importance of using amphiphilic block copolymer for obtaining the core/shell structure of electrospun fibers.

Li *et al.*[65] used emulsion electrospinning as a tool for protein encapsulation into biodegradable nano-fibers. Electrospun core/shell fibers were made of human-nerve growth factor (NGF) wrapped around with a poly(L-lactide-*co*-caprolactone) copolymer and able to release proteins in a sustained manner. Schematic representation of the core/shell formation is

shown in Scheme I.14. The formation process of core/shell structure is divided on micelle elongation under electric field (Scheme I.14a), partial surfactant migration to the surface of the fiber in formation (Scheme I.14b) and final formation of the core/shell structure (Scheme I.14c) with a cross-section (Scheme I.14d).

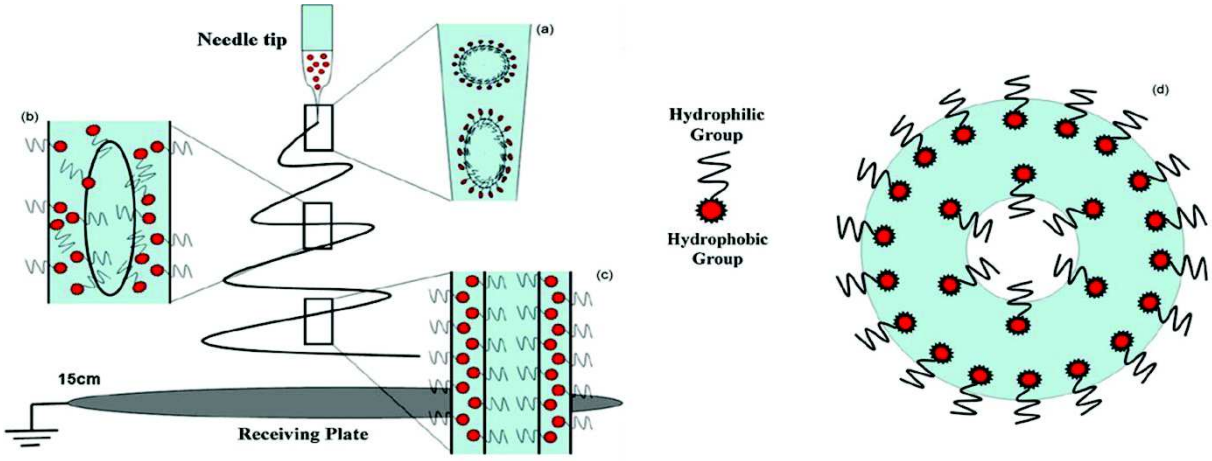

Scheme I.14.Schematic representation of a core/shell structure forming process: (a) water spheres, stabilized by surfactant, under electric force (b) some of the surfactant molecules migrate from the interface of oil (polymer) and water solution to the nano-fibers' surface (c) surfactant distribution on the longitudinal section of nano-fiber and formation of the core/shell structure; (d) surfactant illustration and its distribution on the cross-section of the nanofiber.[65]

Magnetic electrospinning is a method that generates aligned (parallel) fibers via electrospinning of magnetic-particle-doped polymers in a magnetic field.[70] This method involves only a polymer solution containing small amount of magnetic nano-particles and a magnetic field obtained between two magnets (Scheme I.15). When appropriate magnetic field is applied, polymer solution, containing magnetic nano-particles, will tend to form lines between the two magnets. Resulting electrospun fibers are aligned in parallel fashion along the magnetic field lines.

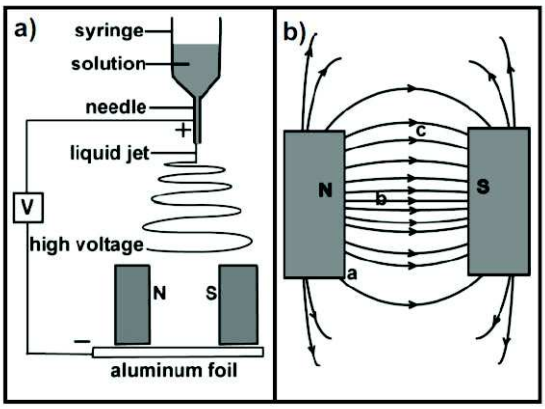

Scheme I.15. Illustration of (a) the apparatus for magnetic electrospinning and (b) calculated magnetic field strength vectors between two magnets (top view)[70]

Needleless electrospinning emerged from the need of high productivity rate and industrialization of the electrospinning process. In order to increase the productivity of the process, the main idea was to create several jets at the same time from one solution. One approach is to use multiple capillaries where each of them produces a jet. Another approach consists of producing many jets under high electric field from nearly flat liquid surface, commercialized as Nanospider™.[71]

Yarin and Zussman[72] reported needless electrospinning using a combination of normal magnetic and electric field, applied on a two-layer system: a ferromagnetic suspension as a lower layer, and a polymer solution as an upper layer. The setup for this system is presented in the Scheme I.16.

It consists of a recipient containing magnetic liquid and polymer solution separated in two phases. The counter electrode (Scheme I.16c) is placed at distance H from the liquid surface and it is connected by electrode to the liquid (Scheme I.16d) and high voltage source (Scheme I.16e). Magnetic field from the permanent magnet (Scheme I.16f) will cause the formation of small steady spikes at the free surface of the magnetic liquid. Once sufficient normal electric

field is attained, due to instabilities of magnetic fluid, a multiple jetting is observed at the free surface of polymer solution. Fibers are formed and collected at the counter electrode.

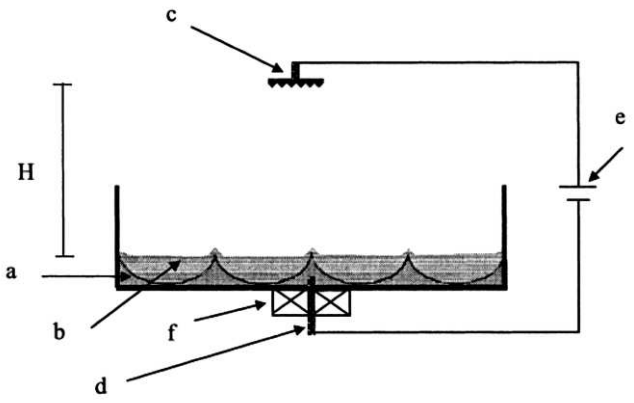

Scheme I.16. Schematic drawing of the upward needleless electrospinning setup: (a) layer of magnetic liquid, (b) layer of polymer solution, (c) counter-electrode located at a distance H from the free surface of the polymer, (d) electrode submerged into magnetic fluid, (e) high voltage source and (f) strong permanent magnet or electromagnet[72]

2 Structural Studies of Electrospun Fibers

Once drawn into solid fibers, physicochemical and structural properties of electrospun fibers are further investigated. A wealth of characterization techniques is available nowadays for characterization of the nano-structured materials at the molecular and/or supramolecular levels:

- Microscopy (optical, scanning and transmission electron microscopy, atomic force microscope, etc.),
- Spectroscopic methods (UV-vis, Raman, infrared, etc.),
- Calorimetry (differential scanning calorimetry, etc.)
- Scattering methods (small angle neutron and X-ray scattering, dynamic light scattering, etc.) and many others.

The methods for morphological evaluation of electrospun fibers employ microscopy, while scattering methods give information about the polymer's size, molecular organization and system dynamics. Owing to the micron and submicron size of electrospun fibers, surface morphology of electrospun scaffolds could be visualized using electronic microscopy techniques. Fibrous surface architecture and relief can be investigated using scanning electron microscope (SEM) and atomic force microscope (AFM), respectively, while SEM provides precise information on fiber's shape and diameter. A typical core/shell structure of coaxially electrospun fibers could be visualized by transmission electron microscope (TEM). Further insight into the fibrous structure and polymer crystallinity can be studied by X-ray diffraction (XRD). Macromolecular organization, inter- and intra-chain interactions and their dynamics in polymer solutions and solid materials are available by using: dynamic light scattering (DLS), small angle X-ray scattering (SAXS) and small angle neutron scattering (SANS) techniques.

Herein, the focus of structural studies will be put on the small angle neutron scattering technique. SANS takes an important place in polymer science investigating the structure and dynamics of polymer chains in a system of interest (solid, liquid, gel, etc.). Next section will give a brief introduction of this technique, its possibilities and applications in soft matter physics with an insight into SANS practice on electrospun fibers.

2.1. Small Angle Neutron Scattering (SANS)

Neutrons are sub-atomic particles with no net electric charge, discovered 1932 by James Chadwick. Other than particle, neutrons have wave characteristics including reflection, refraction and diffraction (scattering). When in contact with a material and its atoms, neutrons will scatter following Bragg's law:

$$\lambda = 2D\sin(\theta) \tag{I.2}$$

where D is the distance between crystallographic planes, λ is the wavelength and 2θ is the scattering angle. Scheme I.17 represents neutron elastic scattering from a sphere.

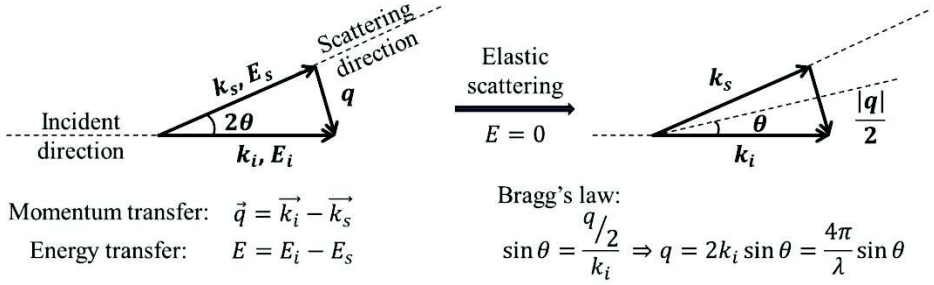

Scheme I.17. Neutron elastic scattering from a sphere

Scattering vector $\vec{q}$ is actually a subtraction of incident $\overrightarrow{k_i}$ and scattered vector $\overrightarrow{k_s}$ and therefrom could be deduced:

$$q = 2k_i\sin(\theta) = \frac{4\pi}{\lambda}\sin(\theta) \tag{I.3}$$

Combining the equations (I.2) and (I.3) gives $D = \frac{2\pi}{q}$ indicating that, for studying the small objects of 10-1000 Å, one should work at low q values: ~$10^{-3} < q < 10^{-1}$Å, at small angles ($\theta < 10°$), and using long wavelengths ($5 < \lambda < 20$ Å).

SANS measuring experiment is represented below in Scheme I.18.

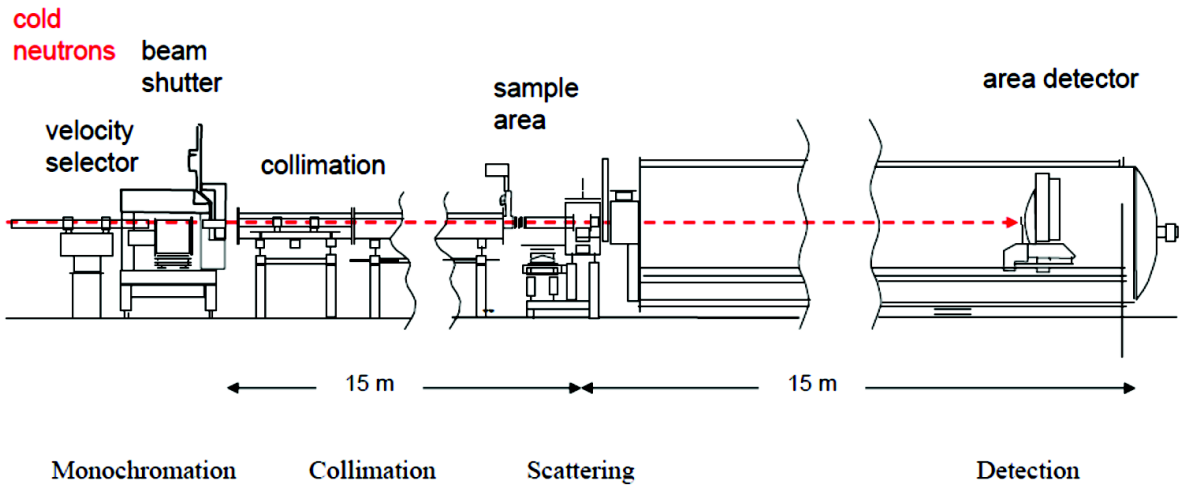

Scheme I.18. Schematic representation of SANS experiment from neutron source to detector[73]

SANS instrument uses:

1. *Monochromation* – for defining the wavelength λ and producing a monochromatic neutron beam using a velocity selector (chopper),
2. *Collimation* – for defining the size and the scattering angle θ of incident neutron beam,
3. *Scattering* from samples in various forms (solids, liquids, gels, etc.) and in various environments (heating, pressure, shear, etc.) and
4. *Detection* of scattered neutrons with an area detector forming a 2D grid.

A neutron incident beam, which goes through the sample, will scatter as a vector q having an angle theta θ, or in space coordinates $d\Omega$. If a neutron detector (neutron

diffractometer) is set to count the number of neutrons scattered into the solid angle $d\Omega$, the differential cross-section $d\sigma/d\Omega$ could be defined as:

$$\frac{d\sigma}{d\Omega} = \frac{number\ of\ neutrons\ scattered\ per\ second\ into\ a\ solid\ angle\ d\Omega}{I_0 d\Omega} \tag{I.4}$$

where I_0 stands for incident flux. Neutron diffractometer is an instrument for recording the scattered intensity as a function of the scattering wave-vector $I(q) = f(q)$. What one measures using SANS technique is a double differential cross-section: intensity of neutrons scattered by a matter as a function of q and E (energy transfer: $\hbar\omega = E_i - E_s$):

$$I(q, E) = \frac{d^2\sigma}{d\Omega dE'} \tag{I.5}$$

called *neutron scattering law*. Scattering law is proportional to the space and time Fourier Transform of the time dependent correlation function. Thus, the information about analyzed material will be obtained from a Fourier transformation and represented in reciprocal space as intensity versus scattered vector (I *vs.* q) plot.

This $I(q) = f(q)$ correlation gives us different information of the material – its structure and dynamics for different q values observed. Moving across the q values, we actually magnify the sample observed, from its morphology until its molecular structure. In order to get this information, SANS technique relies on modeling and data analysis and some of them will be introduced in the next subtitle.

2.2. Deuterium labeling in SANS

Deuterium labeling or contrast matching technique is at the center of neutron scattering. Contrast matching reduces the number of visible phases of a system, while relying on the fact that neutron scattering lengths b (interaction strength of a neutron wave with a given nucleus) for hydrogen and deuterium are very different ($b_H = -3.739 \cdot 10^{-13}\ cm^{-1}$ and $b_D = 6.671 \cdot$

$10^{-13}cm^{-1}$). Since the overall scatter of a molecule depends on the scatter of all its components, this will depend on the ratio of hydrogen to deuterium in the molecule.

To use contrast matching technique, different components of a system must scatter differently. By replacing the hydrogen with deuterium in one of the components of the system (a molecule or a solvent), the information of each part of the system can be obtained at a time. Deuterium labeling will be illustrated through the example of core/shell particle in a solvent, represented in Scheme I.19, all having different neutron scattering lengths (natural contrast). If hydrogen atoms of the solvent are replaced by deuterium ones in such a way that the new overall scattering length of the solvent matches the one of particles' core ($b_{solvent} = b_{core}$), a shell structure of the particles can be observed. If now the ratio of hydrogen atoms, replaced by deuterium atoms in solvent, gives the scattering length that matches the one of the shell ($b_{solvent} = b_{shell}$), the core structure can be observed.

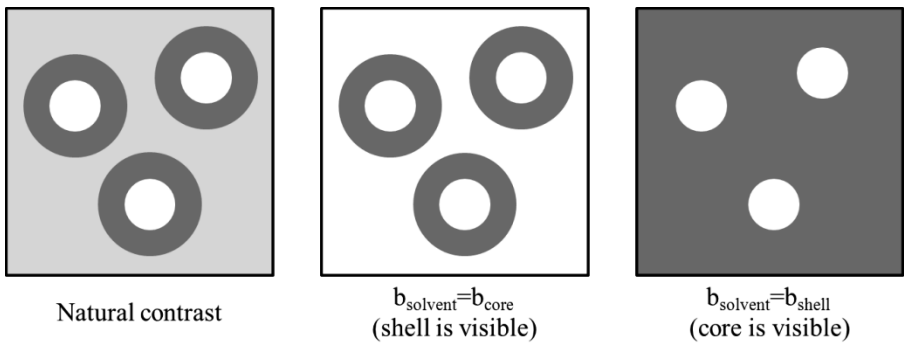

Scheme I.19. Contrast matching method for the core/shell particles in a solution

In a similar way, different systems of polymer blends and supramolecular structures (proteins, DNA, etc.) may be revealed by contrast matching technique.

Deuterium labeling relies on hypothesis that normal and deuterated molecules are identical. However, deuterium labeling and blending of hydrogenated and deuterated polymers of the same kind is not a thermodynamically inert process. Actually, notable shifts of miscibility

of hydrogenated and deuterated polymers forming a blend are observed. Bates *et al.*[74] alluded to the fact that in extreme conditions D/H pairs of polystyrene and polybutadiene may become immiscible. Specific attention to the phase separation phenomena when using deuterium labeling is therefore warmly advised.

2.3. SANS Data Analysis and Modeling

As mentioned previously, the information of the material observed with neutron scattering could be reached in reciprocal space and SANS strongly depends on models used for data analysis.

Various molecular and supramolecular structures could be visualized through the scattering intensity curves. By looking at the q value of interest, one could have indications on a particle volume, over single chain size to chain segments, as represented in Scheme I.20. Low q values ($q = 0$) correspond to low magnifying glass and only thermodynamic aspects of the system can be obtained. By increasing the q values, in the area where $I(q) = const$ and $q^{-1} \approx$ chain dimensions, one could measure size of the objects observed. In this domain, called Guinier domain, a radius of gyration (R_g) could be measured. Further increase of q gives information about statistics and persistence length (l_p) of polymer chain. It corresponds to medium magnifying glass, and the intermediate part of the curve presented in Scheme I.20. If one continues increasing q values, in the domain of high q, where q^{-1} corresponds to the length of chemical bonds, local structure of the chain can be investigated.

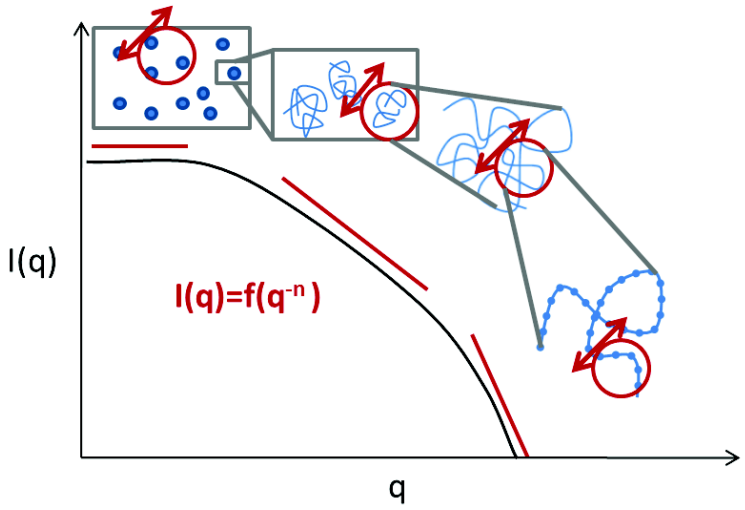

Scheme I.20. Graphical illustration of $I(q) = f(q)$ curve and its physical interpretation for polymeric systems

In order to extract the information of the material in question, for a given sector of q values, corresponding law should be applied for data analysis and fitting.

Guinier law, as mentioned previously, is applicable in the area of low q values ($q \approx 0$) and it gives information of radius of gyration (R_g). It is limited to the sector where $qR_g \ll 1$ and is defined as:

$$\ln(I(q)) = \ln(I_0) - \frac{R_g^2}{3} q^2 \tag{I.6}$$

It involves plotting $ln(I(q))$ vs q^2 in order to obtain the slope of $R_g^2/3$ wherefrom R_g could be extracted.

Porod law is defined for high values of q ($q \gg 1/D$ where D is the size of the scattering object) and it is stated as:

$$I(q) \propto q^{-4} \tag{I.7}$$

or more exactly:

$$I(q) = 2\pi\Delta\rho^2\phi(1-\phi)\frac{S}{V}q^{-4} \quad \text{(I.8)}$$

where $\Delta\rho^2$ is the scattering length density equals to $(\rho_{air}^2 - \rho_{dPS}^2)$, and ϕ is deuterated polymer ratio. Therefrom it could be extracted:

$$\frac{\pi}{q}\lim_{q\to\infty}(I(q)\cdot q^4) = \frac{S}{V} \quad \text{(I.9)}$$

suggesting that one can obtain the information about the specific surface of a material observed. Beside the surface morphology, in the area of high q values, the interface of the objects with their surrounding fluid can be analyzed as well.

Porod plot of $\log(I(q))$ vs. $\log(q)$ yields information about the so-called "fractal dimension" of the scattering objects:

$$I(q) \propto q^{-n} \quad \text{(I.10)}$$

where n varies between 1 and 4:

- 1 is for rigid rods (objects 1D)
- 2 is representing a polymer's Gaussian chain, discs and cylinders (2D objects)
- 4 is for 3D objects such as spheres and it also suggests the smooth surface of the objects
- A slope of $n = 5/3$ is for fully swollen coils while a slope of $n = 3$ is for collapsed polymer coils
- A slope between 2 and 3 is for "mass fractals" such as branched systems and gels or networks.

Zimm plot ($I(q)$ vs. q^{-2}) is used for polymer blends and its slope is proportional to the correlation length (ζ):

$$I(q) = \frac{I_0}{1+\zeta^2 q^2} \quad \text{(I.11)}$$

Kratky plot for the polymer chains emphasizes the Gaussian nature or departure from it. As Gaussian chain is defined in $I(q) \sim q^{-2}$ range, for high q values, this plot tends to a horizontal asymptote. For the low q values, the scattered intensity correlates as $I(q) \sim q^{-1}$. At the crossover point when $q^2 I(q)$ starts being independent of the thermodynamics of the system (plateau in the Kratky plot) one could obtain the information of the persistence length (l_p) of a polymer. Deviation from the horizontal asymptotic behavior indicates to the non-Gaussian character of the scattered chains.

It is possible to describe the distribution of a material in terms of a form factor $P(q)$ and a structure factor $S(q)$. $S(q)$ represents the interference of neutrons scattered from different objects. Thus, for the dilute solutions, where correlation between particles does not exist, $S(q) = 1$. $P(q)$ represents the interference of the scattered neutrons from different parts of the same object. It can be used to determine the overall size (R_g) and shape (spheres, cylinders, etc.) of the scattering objects. For Gaussian chains, one could obtain R_g from the Debye equation of form factor $P(q)$:

$$P(q) = \left(\frac{2}{q^4 R_g^4}\right)\left[exp\left(-q^2 R_g^2\right) - 1 + q^2 R_g^2\right] \quad \text{(I.12)}$$

2.4. SANS from Polymers

Small angle neutron scattering (SANS) resolves structures on 1-1000 nm length scales, and it is sensitive to light elements such as H, C or N, but also to isotopes (H and D). Because of their electrical neutrality, neutrons have a high penetration depth, making SANS a convenient technique for bulk probes (1-2 mm of sample thickness). SANS is therefore attractive for observing polymers, proteins, micelles, porous media or precipitates. As a

result, many research studies have been published around the polymers – solutions,[75,76] co-polymers,[77] blends,[78] thin films,[79] gels,[80] networks,[81] micelles,[82] liquid crystals,[83] etc.

SANS studies of *polymer solutions* are mainly based on chain conformation in various polymers (stiff, flexible, amorphous, and crystalline, etc.) and in solvent mixtures, polymer-solvent interactions, and phase transitions at ambient or high temperatures. B. Hammouda investigated poly(ethylene oxide) (PEO) chain conformation in water and other solvents as well as in solvent mixtures and determined that PEO shows better solvation in solvent mixtures rather than in the individual solvents.[84] Also, he determined that PEO coil size and correlation length decrease in the diluted regime while they both increase in the semi-diluted regime.[75] These results are indicating that one could accurately determine the overlap concentration that delimits dilute from semi-dilute solutions. Additionally, when PEO is used in a mixture of water and isobutyric acid, it shows the transformation from rod-like (helical) (Porod exponent $n = 1$) to swollen coil structure (Porod exponent $n = \frac{5}{3}$).[76]

Supramolecular structures of micelles, consisting of amphiphilic copolymers having di-, tri- or multi-block units, can be readily identified by SANS. Hadjiantoniou *et al.*[85] synthesized different multi-block amphiphilic copolymers and analyzed their structure by SANS technique. By using SANS technique, they were able to identify the copolymer arrangement inside the micelle – one type of folded chain conformations for tetra- and penta-block copolymers, and three different micellar structures for hexa-block copolymer (Scheme I.21).

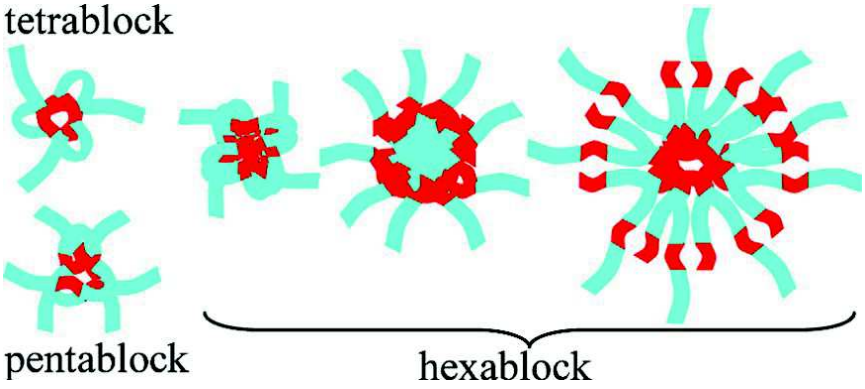

Scheme I.21. Proposed structures of the micelles formed by the multi-block copolymers in aqueous solution[85]

SANS could be used alone, as an analyzing tool, or simultaneously with other analyzing techniques for *in situ* physicochemical studies. Wu *et al.*[77] investigated chain conformation of perpendicularly-aligned multi-block *copolymer* lamellae under shear flow. They observed micro-domain alignment under shear flow and its relaxation upon cessation of shear as represented in Scheme I.22.

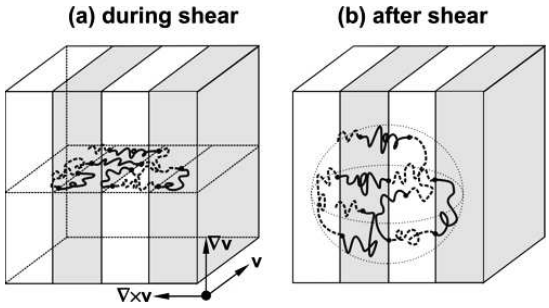

Scheme I.22. Chain conformation of perpendicularly-aligned undecablock copolymer lamellae (a) during and (b) after shear[77]

SANS technique is able to detect *structural anisotropy* in a tested sample (liquid, gel or solid material) and signal organization of polymeric chains inside that sample. Scattered iso-intensities of anisotropic materials are typically taking the form of ellipses, lozenges or butterflies.[86]

Millon *et al.*[80] studied the anisotropy inside the poly(vinyl alcohol) (PVA) *hydrogels*. These anisotropic hydrogels are produced from a physical crosslinking of PVA and repeated freeze/thaw and controlled stretching cycles. Such stained PVA hydrogels, as biomedical devices, mimic the anisotropic and nonlinear mechanical properties of porcine aorta. Small angle- and ultra-small angle neutron scattering (SANS and USANS respectively) accompanied by atomic force microscope (AFM) enabled further investigation of the source of bulk anisotropy inside these hydrogels.[87] It was determined that crosslinked PVA is formed inside the densely packed and assembled micron-sized blobs, which are under strain further arranged in an anisotropic fashion.

Further advances in SANS analysis have enabled investigation of chain conformation within confined polymeric structures. In the case of ultrathin polymer films, sample volume represents a significant problem in SANS measurements. R. L. Jones *et al.*[79] reported a successful SANS analysis of chain conformation in ultrathin polymer films from a sample stack containing many thin films obtained under identical conditions.

Development of electrospinning process and increased complexity of electrospun fibrous structures emerged the need of studying essential structure and chain dynamics of these meshes. SANS technique offers a possibility to observe these fibers and to predict their chain preferential orientation. In order to determine the level of anisotropy inside the fiber by SANS technique, it is important to form a stack of aligned fibers in order to obtain a satisfying signal-to-noise ratio. However, very few studies are reported on SANS investigations of electrospun fibers. SANS analyses on micron-sized electrospun fibers showed rather poor anisotropy even with the highest rotation speed of the collector. Additionally, voids and pores within the fiber bulk as well as ribbon-like morphology of the fibers made SANS data analysis and interpretation difficult.[88] Nevertheless, these studies raised many questions considering SANS

from electrospun fibers – is this small anisotropy due to the fiber thickness, and how the thickness problem could be overcome; what is the relaxation dynamics of polymer chains within these nonwovens, etc. These studies introduced questions about SANS technique data collecting and analysis – the sample preparation problem, guided chain relaxation and its observation considering not only the pores within the fiber bulk but the porous structure of the scaffold itself, etc. – suggesting a new chapter of SANS study on anisotropic ultra-fine structures.

3 Biomaterials Processed by Electrospinning Technique

A significant part of biomaterials, devoted to the tissue engineering applications, can be processed by electrospinning technique. The focus of this chapter will be put on biomaterials processed by electrospinning, their origin, their advantages and shortcomings, and individual characteristics that influence processing of a final product.

3.1 Definition of Biomaterial

"The single most important factor that distinguishes a biomaterial from any other material is its ability to exist in contact with tissues of the human body without causing an unacceptable degree of harm to that body", D. F. Williams.[89]

A meaning of a biomaterial is very vast, and has been causing many discussions whether one material could be declared as a biomaterial or not.[90] It should be outlined that biomaterials are usually defined by their targeting application and not by their chemical structure. However, an entity called biomaterial should be engineered in some way. Over years, the definition of the biomaterial evolved and now one finds three generations of biomaterials:

1. 1st generation biomaterial is called bio-passive ("do-no-harm") material with the minimal toxic response of the host tissue. At 1987, a biomaterial is characterized by D. F. Williams through the concept of **BIOCOMPATIBILITY**: *"biocompatibility refers to the ability of a material to perform with an appropriate host response in a specific situation"*. Later, in 2008, this definition has been extended to: *"ability of a biomaterial to perform its desired function with respect to a medical therapy, without eliciting any undesirable local or systemic effects in the recipient or beneficiary of that therapy, but generating the most appropriate beneficial cellular or tissue response to that specific situation, and optimizing the clinically relevant performance of that therapy."*[89]

2. 2nd generation biomaterials – bio-inert materials are replaced with bioactive biomaterials that could elicit a controlled action and reaction of physiological environment – **BIOACTIVITY**.[91] Another category of 2nd generation biomaterials is a resorbable (or degradable) biomaterial, summarized by L. L. Hench as: *"A second method of manipulating the biomaterials-tissue interface is controlled chemical breakdown, that is, resorption of the material. Resorption of biomaterials appears a perfect solution to the interfacial problem because the foreign material is ultimately replaced by regenerating tissues. Ideally, there is eventually no discernible difference between the implant site and the host tissue."*[92]
3. 3rd generation biomaterials emerged the concept of **BIOMIMICRY**: not only that material is doing no harm to the host tissue but it is also able to obtain a beneficial response – so-called smart or biomimetic material. Materials are interacting with the tissue and stimulating a specific cellular response on molecular level (proliferation, regeneration, etc.)[93]

The complexity of tissue architecture demands equally complex structure of a guest material. Many attempts have been put into finding an optimal solution between feasibility, availability, and physicochemical properties of the final material. However, each biomaterial represents a specific case, and physicochemical properties and structure of that material should be adjusted to the targeting purpose. The latest opinion on this matter was given by D. F. Williams, where biomaterial is defined:

"A biomaterial is a substance that has been engineered to take a form which, alone or as part of a complex system, is used to direct, by control of interactions with components of

living systems, the course of any therapeutic or diagnostic procedure, in human or veterinary medicine."[94]

3.2 Structure of Biomaterials

Biological systems consist of nanometer-length proteins and other biological macromolecules, exposing their activity within the cell or at the interface cell-wall/environment. The fibers of extracellular matrix (ECM), their interconnecting pores, or hydroxyapatite crystals present in bone tissue, have typically sub-micron dimensions. It is therefore found logical that man-made biomaterials should have a nanometer scale for mimicking the structure of a host tissue.

Stevens and George[95] indicated to the importance of material's nano-scale engineering for optimal cell adhesion, proliferation and growth as represented in the Scheme I.23. It was observed that different topography of the same material elicits different responses from the same cell.

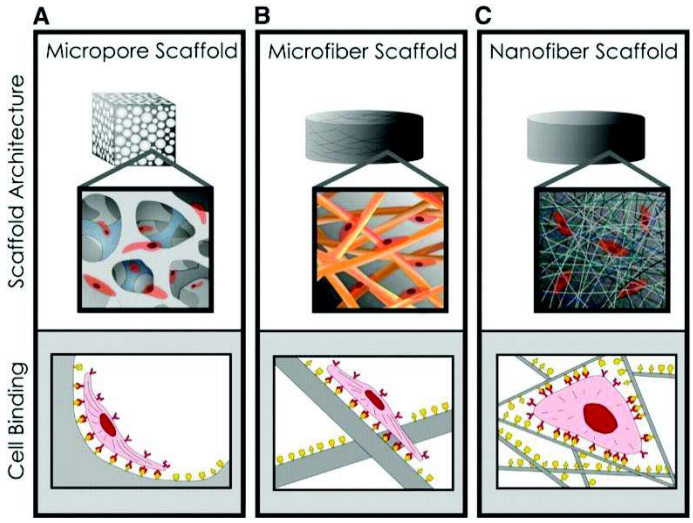

Scheme I.23. Scaffold architecture affects cell binding and spreading: (A and B) cells binding to scaffolds with micro-scale architectures flatten and spread as if cultured on flat surfaces (C) scaffolds with nano-scale architectures have larger surface areas to adsorb proteins, presenting many more binding sites to cell membrane receptors. The adsorbed proteins may also change conformation, exposing additional cryptic binding sites.[95]

However, not all nano-sized objects are biocompatible and elicit positive cell-tissue response. It is more likely that a positive response from tissue cells could be elicited from physicochemical, mechanical and structural properties of a material acting together on the cells in question. For a given purpose, biomaterials should balance between cell-response, material's chemical structure and material's architecture. Chemical structure of a material is very important because, once implemented in the living tissue, material is in direct contact with the surrounding tissue. However, the cell response will not only depend on the material's structure but its architecture as well. Biomaterials will therefore simultaneously depend on material's chemical structure and architecture in order to elicit a positive cell response.

It could be therefore concluded that man-made biomaterials represent always a compromise, and it is the final application that decides optimal physicochemical properties of a material in question. Next sections will put the accent on the role of nanotechnology and electrospinning technique in biomaterials' engineering practice, their medical applications,

available biomaterial's sources as well as physicochemical modifications desired for creating new-generation advanced biomaterials.

3.3 Applications of Biomaterials

Generally speaking, biomaterials' applications target living tissue and should therefore closely mimic its physicochemical properties and architecture. Electrospinning technique allows the production of nano-fibrous scaffolds that mimic certain aspects of ECM structure. Nano-fibers electrospun from biocompatible polymeric structures might be comfortably used for various applications in tissue engineering, drug delivery, as bandages and sutures and many other biological and medical purposes.

3.3.1 Drug Delivery

Drug delivery method and, generally, pharmaceutical applications make use of drug-containing electrospun fibers. A drug is introduced into the polymer solution for electrospinning and transformed into fibers that transport and simultaneously release active substances. Fabrication of core/shell fibrous structures has added to the versatility of these nonwovens affording a wider range of molecules to be released in a controlled manner.[96]

Hu *et al.*[97] made use of emulsion electrospinning to successfully electrospin both hydrophilic and hydrophobic drugs into the poly(L-lactic-*co*-glycolic acid) (PLGA)/gelatin fibrous mats. The core/shell fiber's structure where core carries a drug and shell, consisting of PLGA/gelatin polymer blend, enabled constant and sustainable release of Cefradine® drug.

Mickova *et al.*[98] used coaxial electrospinning setup to obtain liposome loaded PVA/PCL core/shell fibers (Figure I.5). Coaxial electrospinning was reported to preserve enzymatic activity of horseradish peroxidase encapsulated in the liposome, while monoaxial electrospinning setup caused the liposomes to break and release their encapsulated material.

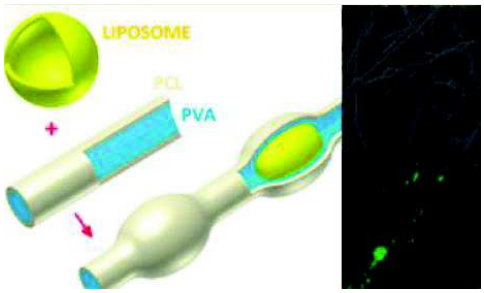

Figure I.5. Schematic representation of the PVA/PCL core/shell fibers loaded with liposome and their SEM and confocal microscopy images[98]

The efficacy of the core/shell fibers containing protein-loaded liposomes was tested in a cell culture study of mesenchymal stem cells and showed to stimulate the cells' proliferation.

Polyesters, having a slow degradation rate have been used as contraceptive devices. Dasaratha Dhanaraju *et al.*[99] incorporated contraceptive steroids into PCL microspheres. Two water-insoluble steroids were encapsulated into PCL microspheres by double emulsion-solvent evaporation process. *In vitro* drug-release tests showed prolonged diffusion of these molecules, promoting PCL microspheres as promising devices for controlled delivery of contraceptive steroids.[100]

3.3.2 Wound Dressings

Electrospun biopolymers have been employed for wound dressing applications as well, due to their high porosity and high surface-to-volume ratio enabling high absorption and gas permeation while being enough flexible to efficiently cover the wound.

Lalani and Liu[101] used a three-step process consisting of polymerization, electrospinning and crosslinking for obtaining zwitterionic poly(sulfobetaine methacrylate) (PSBMA) superabsorbent and protein-resistant scaffolds. Electrospun mats were super-hydrophilic, yet water-stable, enabling up to 350% of water uptake, while keeping gas exchange due to the high porosity of the scaffold. Additionally, these mats were tested to proteins (human plasma

fibrinogen, bovine serum albumin, and horseradish peroxidase-conjugated polyclonal goat antihuman fibrinogen), bacteria (*Pseudomonas aeruginosa* and *Staphylococcus epidermidis*) and cells (bovine aortic endothelial cells) and showed good resistance on both, making electrospun PSBMA scaffolds good candidates for wound dressing applications.

Merrell *et al.*[102] reported a curcumin loaded poly(ε-caprolactone) fibers able to sustainably release the drug while remaining bioactive. Curcumin is naturally-occurring molecule with anti-cancer, anti-inflammatory and anti-oxidant characteristics and its activity was tested once incorporated in electrospun PCL fibers. Curcumin-loaded electrospun fibers were shown to be bioactive with a potential to enhance the wound closure *in vivo* in a diabetic mouse model.

3.3.3 Tissue Engineering

Tissue engineering is one of the biomedical engineering areas where electrospun fibers have been mostly used. Electrospun scaffolds in tissue engineering could mimic the extracellular matrix fibrous structure and serve as a temporary support for cells during the tissue regeneration process. In literature, both natural and synthetic polymers and their combinations are employed for tissue engineering in the form of electrospun fibrous mats where muscle, neuronal, skin, bone and other tissue cell cultures were investigated.

Francis *et al.*[103] fabricated electrospun scaffold from a blend of adipose and poly(dyoxanone) (PDO) serving as a template for adipose stem cell culture. Adipose is a natural protein mixture consisting of collagen, laminin, and fibronectin, having herein human adipose (connecting) tissue origin. Adipose/PDO fibrous scaffolds, with 10/90 ratio, were sufficient to provoke the cell growth and survival but significantly lower number of cells was attached when compared to the adipose alone.

Ghasemi-Mobarakeh *et al.*[104] studied proliferation of nerve growth precursor (NGP) cells seeded onto electrospun poly(ε-caprolactone) (PCL) fibers. PCL electrospun scaffolds, having covalently attached Matrigel™ (a soluble sterile extract rich in laminin, collagen IV, fibronectin and heparin sulphate proteoglycans), showed higher cell proliferation when compared to native PCL fibers. These results highlight the influence of matrigel and improved hydrophilicity of the scaffolds to the NGP cell proliferation and morphology. Their studies encouraged further investigations in chemical modifications of synthetic biomaterial scaffold for tissue engineering applications.

3.4 Sources of Biomaterials

Biomaterials have as a goal to closely mimic a targeting tissue. That is why the structure of a biomaterial, expressed through physicochemical and mechanical properties, should be closely related to those found in the living tissues. Accordingly, several most important macromolecular structures, cell-friendly and often used in electrospinning technique, will be briefly introduced in the next section.

3.4.1 Natural Carbohydrate- and Protein-Based Biomaterials

In order to promote the cell adhesion and viability, electrospun scaffolds should be made out of materials that are recognized and accepted by the cell. These molecules are typically carbohydrates (oligo- and polysaccharides), and proteins (or peptides) and the same have been intensively processed into fibers for biomedical applications.[105]

Carbohydrates are an integral part of any living organism where they perform numerous roles and functions. They serve for storage of energy, as structural components, but they are also involved in diverse cellular processes, enabling communication, proliferation, and differentiation. The strategic placement of carbohydrates at the surface of the cell makes these molecules a key element in communication process (Scheme I.24). Structural diversity of

carbohydrates enables cells to communicate with different molecular structures and living organisms: proteins, antibodies, viruses, bacteria, and other cells, as illustrated in Scheme I.24. Today, both natural and synthetic carbohydrates could be considered as third-generation tissue-engineering biomaterials: they are recognized as ligands for cell-receptors; they can modulate the cell behavior or tune the cell surface recognition.[106]

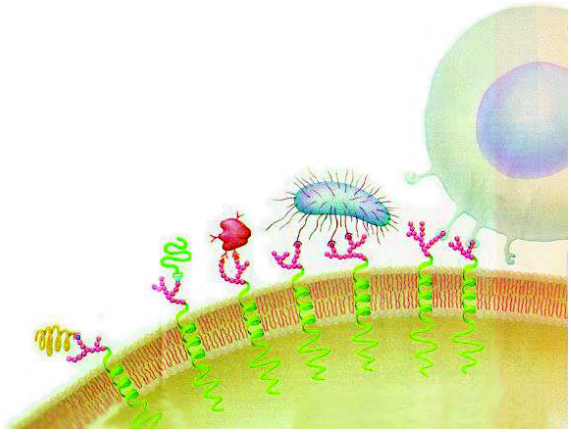

Scheme I.24. Interaction of the carbohydrates at cell wall with various molecules and living organisms surrounding the cell[107]

HNK-1 is a human natural killer carbohydrate-based epitope, involved in cell-cell and cell-substrate interactions, nerve outgrowth and is present in the kidney cancer and melanoma. Bastide *et al.*[108] synthesized a trisaccharide HNK-1 analogue and demonstrated that it cross-reacts with anti-NHK-1 antibodies, suggesting applications in nerve regeneration and cancer diagnosis.

Gentsch *et al.*[109] investigated the surface functionalization of the PCL/poly(pentafluorophenyl methacrylate) (PPpfMA) fibers with monosaccharides and showed that these functionalized fibers triggered specific interactions with antigen-presenting cells, e.g. macrophages.

Chitosan, a cationic polysaccharide issued from crustacean or fungi, is a very popular polymer for biomedical applications.[110–112] Chitosan is known for its anti-microbial activity, and chitosan-based electrospun scaffolds could find their applications in filtration and tissue engineering. Initial studies on chitosan-based fibers report the use of wet-spinning method on chitosan blend with a thermoplastic polymer for better processing feasibility.[113] Ohkawa *et al.*[114,115] observed that highly polar trifluoroacetic acid (TFA) solvent facilitates electrospinning of chitosan by destroying its crystalline structure, while neutralizing the charges on chitosan in the solution, which was found crucial for uniform fiber formation. Addition of another synthetic polymer has proved to facilitate the electrospinning of chitosan while improving the mechanical properties of the final scaffold. In order to facilitate the fabrication of chitosan into fibers, Nguyen *et al.*[116] proposed a coaxial electrospinning of chitosan with poly(lactic acid) (PLA) making shell and core of the final fiber, respectively. That way, the functionality of the chitosan is performed at the surface of the fibers while PLA in a core contributes to the mechanical properties of the final scaffold.

Extracellular matrix typically consists of natural *protein-based polymers*, such as collagen, fibrinogen and gelatin. These polymers are biocompatible and biodegradable, and as such, they have been often studied as biomaterials for tissue engineering purposes. However, electrospinning from pure proteins often results in poor mechanical properties of the fibrous scaffolds.

Collagen, *gelatin* and *elastin* represent important natural macromolecules constituting the majority of human's structural extracellular matrix (ECM). However, due to their weak mechanical properties and/or structural stability upon hydration, these proteins are often crosslinked with glutaraldehyde and/or blended with mechanically superior synthetic polymers. In such a way, McClure *et al.*[117] proposed a crosslinking of electrospun scaffolds obtained from

a blend of elastin and poly(dioxanone) (PDO). Mechanical properties of crosslinked PDO/elastin electrospun scaffolds can match those of pig and native human artery.[118] Similarly, to prevent fast degradation, gelatin is often electrospun in combination with compatible synthetic polymers such as poly(glycolic acid), poly(ε-caprolacone), poly(lactic acid) and polyurethane.[97,119–121]

Synthetic polypeptides with a well-defined amino-acid sequence could be synthesized by already established chemical methods and procedures involving microorganisms. The advantage of synthetic peptides over natural proteins is the possibility to tune the amino-acid sequences for a desired purpose, in order to avoid the organic solvents or simply to produce polymers without animals or plants.[122] Khadka and Haynie[123] electrospun synthetic polypeptide, poly(L-ornithine) (PLO), from an aqueous solution in the concentration range of 35-40 w/v %. The solubility of these nonwovens was controlled by simple crosslinking method. L-orhithine is a physiological amino acid and is a key component in urea cycle for biosynthesis of arginine, another amino acid. Soon, they efficiently electrospun another co-polypeptide made of L-glutamic acid and L-tyrosine (PLEY) from aqueous solution.[124] Similarly as PLO, PLEY fibers became insoluble after crosslinking, and additionally, compatible with fibroblast cell attachment. By using aqueous solutions to produce and electrospin PLO and PLEY polypeptides, Khadka with coworkers demonstrated a new method for obtaining biomaterials from aqueous solutions – attractive supports for tissue engineering purposes.

Naturally occurring polymers, consisting either of carbohydrates or proteins, offer good biocompatibility and biodegradability with instructive cues for cell binding and proliferation. However, some natural polymers, such as collagen and gelatin, are extracted from animal resources, and therefore considered as inconvenient for medical applications. Additionally, natural polymers showed important processing difficulties. Once electrospun into fibers, natural

polymers display poor mechanical properties. As a consequence, research studies highlight the importance of their modification, either by crosslinking for keeping the fibrous structure, or by blending with some synthetic biopolymer when superior mechanical properties are requested.

The necessity of synthetic polymers for improvement of naturally occurring macromolecules has led to a profound investigation of synthetic polymers and their possibilities as biopolymers. As a consequence, literature offers many reports on use of synthetic polymers as biomaterials covering the areas of tissue engineering, drug delivery, and wound dressing, in scientific research as well as in medical practice.

3.4.2 Synthetic Biomaterials

There are different classes of synthetic materials employed as biomaterials in the human body: *metals* and their alloys, as first dental and bone implants, were soon replaced or upgraded by *ceramics* – hard, brittle and non-adherent – used in orthopedics and in dentistry,[125] and *synthetic polymers*, covering the area of both hard and soft tissue engineering applications. Next paragraphs will give an insight into synthetic polymers and their possibilities to form biocompatible and bioactive materials and electrospun scaffolds for tissue engineering applications.

Poly(ethylene oxide) (PEO) has been quite often used for facilitating electrospinning of some biopolymer solutions that are otherwise not able to be electrospun into fibers. It is water-soluble which makes it environmentally friendly and convenient for biomedical applications and it is easily processed into fibers by electrospinning. Vega-Lugo and Lim[126] reported such use of PEO for electrospinning of whey protein isolate. Adjusting the pH of the solution to highly acidic (pH=1) enabled strong interaction between two polymers, their entanglements and jet stabilization which resulted in uniform fiber formation. Pakravan *et al.*[127] reported coaxial electrospinning of PEO and chitosan in aqueous phase. PEO as a shell solution permitted

electrospinning of chitosan inside the fiber's core while avoiding toxic organic solvents. Branched PEO has proved to have protein repellent characteristics because of the higher packing density of the PEO chains at the surface. Rieger *et al.*[128] synthesized PEO-*graft*-PCL branched polymer, confirming the amphiphilic nature of the copolymer and suggesting its use as a biomaterial where specific protein repellence is requested.

Similarly as PEO, its low-molecular-weight derivative, *poly(ethylene glycol)* (PEG), is also an important hydrophilic polymer for making biomaterials because its protein-repellent properties.[129] Sharma *et al.*[130] coated the surface of silicon-based micro-devices with PEG ultra-thin film in order to reduce the non-specific protein adhesion and improve the biocompatibility of the material. Covalently attached PEG maintained the protein-repellence characteristics even after 28 days of incubation. However, long exposure of hydrophilic PEG surface to the aqueous environment caused significant decrease of film thickness. Grafahrend *et al.*[131] synthesized poly(ethylene glycol)-*b*-poly(ε-caprolactone) (PEG-*b*-PCL) copolymer. A cell-adhesive peptide sequence, GRGDS, was further covalently attached to the polymer chains prior electrospinning. Electrospun PEG-*b*-PCL peptide-functionalized hydrophilic fibers were able to immobilize human-derived fibroblasts, their adhesion, spreading and high viability. Also, Grafahrend and coworkers indicated to the importance of selective protein adhesion on electrospun fibers for better cell adhesion and proliferation. [132]

Polyurethanes are widely used as biomaterials because of their high hydrolytic stability and biocompatibility. Wang *et al.*[133] made use of Selectophore™ polyurethanes to create electrospun nano-fibers with controlled porosity, thickness, glucose permeability and hydrophilicity. They further tested these nonwovens for coating a glucose-biosensor surface and created small implantable biosensors as novel biocompatible nano-devices.[134]

Poly(lactic acid) (PLA) is an aliphatic polyester and, processed into fibrous scaffold, it is often used as biopolymer in tissue engineering and other biomedical applications. Several reports mentioned the use of electrospun aligned poly(L-lactic acid) PLLA fibers for nerve regeneration applications.[135–137] Yang *et al.*[137] electrospun aligned PLLA scaffolds having micro- and nano-sized diameters and tested their potential for cell growth of nerve stem cells (NSC). They observed that fiber alignment improved neurite outgrowth, while the cells showed preferential differentiation on nano- than micro-fibers. However, the use of this polymer may be limited by the strong water-repellent behavior (hydrophobicity) of the polymer. As a consequence, research studies pursued a suitable method improving the hydrophilicity and cell viability of the scaffold. Cui *et al.*[138] proposed a surface hydrolysis and chitosan coating of PLLA fibers with a goal to improve their hydrophilicity and cell attachment and growth conditions onto the scaffold. A remarkable influence of the blending molecule on the physicochemical properties of the final fibers is presented by Yang *et al.*[121] The addition of gelatin into the PLLA bulk led to phase separation and surface migration of polar side groups of protein, resulting in complete wettability of the PLA/gelatin fibrous mats.

Polyesters have attracted wide attention as biomaterials for tissue engineering purposes.[139] Compared to other aliphatic polyesters, poly(ε-caprolactone) (PCL) is a most commonly used source for biomaterials – it is semi-crystalline, biocompatible and bioresorbable polymer with a very slow degradation rate.[140] The importance of this polymer is highlighted by increasing number of studies published in last ten years (Figure I.6). PCL is also approved by U.S. Food and Drug Administration (FDA).

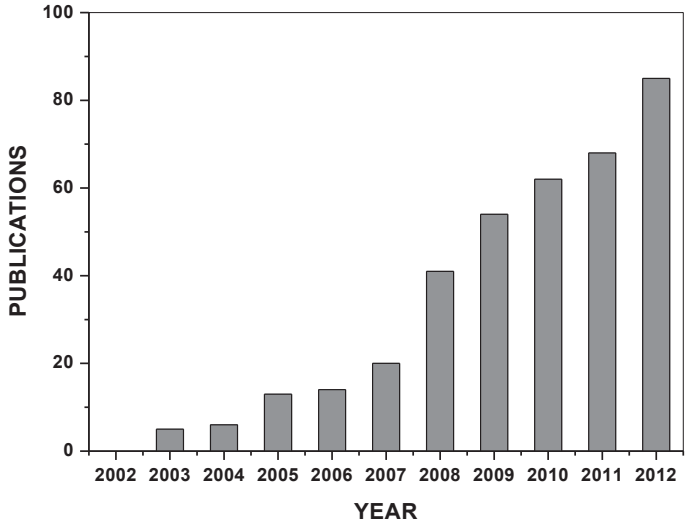

Figure I.6. Publications of electrospun PCL fibers during the period of ten years, from 2002 to 2012, sourced from ISI Web of Knowledge

An extensive literature study of Labet and Thielemans on poly(ε-caprolactone) synthesis, contributes to the general significance of PCL polymer.[141] Compared to other aliphatic polyesters, PCL does not produce copolymers during its synthesis. Almost all the elements of periodic system have been tested for synthesis of PCL. A simplified representation of the possible paths for synthesizing poly(ε-caprolactone) is shown in Scheme I.25. The catalysts for PCL were classified in three sections: metal-based (alkali, alkaline earth, aluminium, tin, transition metals – Ti, Fe, Zn, and rare earth metal-based catalysts), enzymes (lipase-based catalysts), organic compounds and inorganic acids.

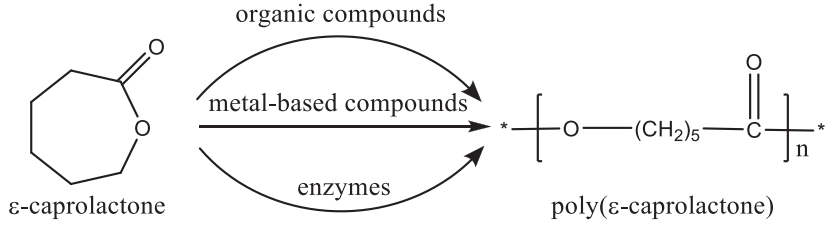

Scheme I.25. Ring-opening polymerization of ε-caprolactone and possible catalysts for obtaining poly(ε-caprolactone)

To be used as a biomaterial, polymer has to be biodegradable – to decompose its structure into smaller non-toxic units, and bioresorbable – degradation products are completely removed from the body *in vivo* with no residual side effects[142] PCL could be biodegraded by bacteria or fungi and their enzymes, or chemically by hydrolysis. PCL homopolymer will completely degrade in a period of 2 to 4 years depending of the polymer molecular weight. Several mechanisms are proposed for its degradation, generally divided into two stages:

- Firstly – a non-enzymatic hydrolytic cleavage of ester groups and
- Secondly – when the polymer is more crystalline and with lower molecular weight (3000 g mol^{-1}) – polymer undergoes intracellular degradation mechanism.[143]

In the end, PCL-degradation products are completely eliminated from the body in the citric acid cycle.[144] Accordingly, PCL can be applied in controlled drug delivery where slow degradation kinetics is required.[99] On the other hand, it can be easily copolymerized or functionalized in other way in order to adjust its degradation rate and be employed either as a short-term or a long-term degradable device for tissue engineering purposes.

However, hydrophobic nature of PCL polymer causes poor surface-wetting properties of PCL biomaterials and consequently low cell adhesion and uncontrolled biological interactions with a material. As a result, different molecular and macromolecular structures have been combined with PCL in order to enhance the hydrophilicity and cell response.

Owing to a wide concentration range and different solvents available for electrospinning PCL, a large variety of molecules could be incorporated inside the fibers' bulk. PCL-based electrospun fibers could be loaded with a crude extract of *Biophytum sensitivum* (a potential antibacterial herbal drug) targeting wound dressing applications;[145] with heparin for drug

delivery;[146] PCL could be blended with collagen for stimulating the axonal growth,[147] or with chitosan for tissue engineering purposes.[148] It is indeed the generous ability of PCL to blend easily or bond covalently with other polymers that caused the constant increase of PCL use as a biomaterial. The always-increasing interest for PCL also induced the growth of functionalization techniques having an aim to design advanced biomaterials with always expanding medical applications. In the next section, discussion will be oriented to physicochemical modifications combined with the electrospinning technique to create materials targeting tissue engineering applications.

3.5 Physicochemical Modifications of Material for Tissue Engineering Applications

From the previous section, it could be deduced that one material, whether natural or synthetically produced, cannot meet all the high standards required for biomaterials' applications at present. That is why one finds many research studies dealing with the mixtures of substances, simply blended or covalently bonded into complex structures (at all molecular levels) in order to form hybrid structures that mimic the bio-environment they will be used in.

In order to prepare biomaterials with enhanced properties, their practice has been frequently followed by additional functionalization and/or surface modifications.[149,150] Functionalization techniques applied on electrospun fibers could be sorted in several groups:

1. Blending of bioactive substances and polymers – molecules are homogeneously dispersed or oriented at the surface of the electrospun fibers (Scheme I.26A)
2. Coaxial electrospinning – localizes the molecules in the center or at the surface of the fibers (Scheme I.26B) (for more details see Chapter 1.3)
3. Physicochemical treatment: plasma and hydrolysis (Scheme I.26C)

4. Surface immobilization – covalent attachment of active molecules at the surface of the fibers (Scheme I.26D)

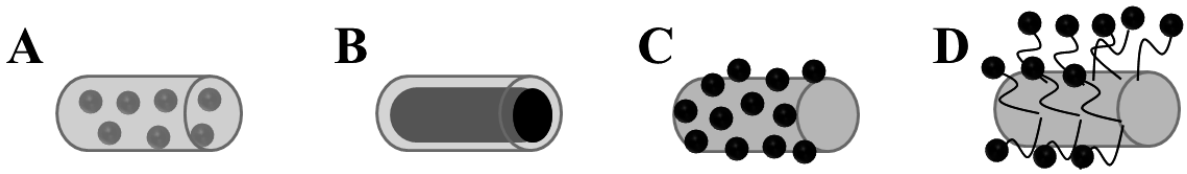

Scheme I.26. Several mechanisms of fiber functionalization: (A) blending of polymers prior electrospinning, (B) coaxial electrospinning, (C) physicochemical treatment and (D) surface immobilization

First method induces functional groups in the polymer solution for electrospinning; the second one obtains a core/shell structure where active molecules are either at the surface or inside the fiber's core. The third and the fourth method introduce functional moieties at the surface of the fibers, *after* the electrospinning process. Each of those methods will be introduced in the next section.

3.5.1 Substance Blending Prior Electrospinning Process

Simple *blending* of various forms of bioactive materials or polymers before the electrospinning process could improve physicochemical properties of the fibrous scaffolds without their deterioration. In a blend, active substances are homogeneously dispersed in the bulk and could be only partially found at the surface of the fiber. Blending method of uniformly dispersing active substances in the fiber's bulk is very convenient for a continuous and uniform degradation of the fibrous network.

Chitosan, as typically difficult to electrospun, has been often blended with various biocompatible synthetic polymers where combined properties of bioactivity from chitosan and strength from a synthetic polymer resulted in advanced biomaterials for many biomedical applications. Van der Schueren and coworkers[151–153] propose using a PCL/chitosan blend in

acetic/formic acid solvent mixture for obtaining uniform nano-fibers without beads. They improved these nonwovens by addition of Nitrazine Yellow which resulted in bioactive and stimuli-responsive fibers with an increased hydrophilic nature.[154]

3.5.2 Physicochemical Post-Electrospinning Treatment

Plasma treatment is a "dry" functionalization method, where different gases (O_2, NH_3, SO_2, CO_2, etc.), in contact with the fibrous scaffold, are changing its surface-morphology and surface-chemistry by creating different polarized groups (hydroxyl, carboxyl, amino or sulfate groups). In the case of polyesters, it serves for improving the hydrophilicity and cell-material interactions. Wulf *et al.*[155] treated the surface of PCL scaffolds with ammonia (NH_3) and oxygen (O_2) plasma in order to immobilize anti-inflammatory and anti-thrombogenic model drugs for vessel prostheses. Ammonia and oxygen plasma radiation formed amino and hydroxyl groups, respectively, at the surface of the PCL fibers that served as active places for further drug immobilization.

Hydrolysis, also called *wet-chemical method*, consists of immersing a solid material (a scaffold or a film) in an aqueous solution of sodium- or ammonium- hydroxide. After a certain period of time, hydroxyl and/or carboxyl groups are formed at the surface of a material. This method might serve to improve hydrophilicity or simply as an intermediate step for further functionalization. Croll *et al.*[156] introduced carboxyl- and amine- groups at the surface of PLGA thin films through hydrolysis method. Surface-functional groups of the PLGA film enabled covalent attachment of chitosan at the surface, while promoting the protein binding and consequently cell attachment and growth.

Plasma radiation and chemical hydrolysis methods are rather simple and available in chemistry laboratory. These methods make hydroxyl, amino or other groups easily available at the surface of the fibers. The fact that these modifications might damage fine fibrous structure

and further weaken mechanical properties of the nonwovens could also be advantageous, in the case of polyesters for example, when accelerated degradation kinetics is required.

3.5.3 Surface Functionalization

Surface functionalization can be performed by taking advantage of the polymer groups at the surface of the fibers for chemical bonding with desired molecules. It is used to improve the biocompatibility of the polymer while preserving the bulk properties of the material. Depending of chemical group available at the surface, various coupling methods could be performed.

Click chemistry, as one of such methods, is a versatile and high yielding approach for covalently coupling different molecules in homogeneous as well as heterogeneous phase, typically at the surface of a material. There are several types of reactions lying under the concept of click chemistry, with azide-alkyne cycloaddition as the most used one. The reaction between two molecules having end-available azide and alkyne groups is called azide-alkyne cycloaddition (Scheme I.27), popularly known as *click chemistry*.

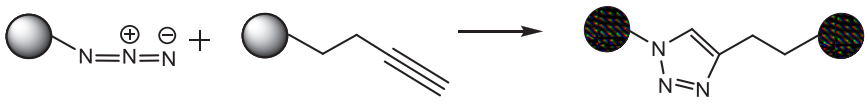

Scheme I.27. Schematic representation of click chemistry reaction between azide and alkyne ending molecules and a typical triazole ring formation

This technique is a valuable method for introducing broad functional moieties owing to its versatility and high yields. It was for the first time reported by Huisgen[157,158] under high temperatures and in organic solvents. Independently, Sharpless *et al.*[159] and Meldal with coworkers[160] discovered that copper(I)-catalyzed azide-alkyne cycloadditions (CuAAc), popularized as click chemistry, can be performed at ambient temperature and in aqueous phase. Soon, click chemistry concept becomes a simple solution for long known challenges – synthesis

of complex polymeric structures as co-polymers and dendrimers,[161] bioconjugation[162] and surface functionalization.[163] The combination of electrospinning and click chemistry resulted in several interesting studies.[164–166]

Fu *et al.*[164] reported a three-step process for obtaining solvent-resistant and thermo-sensitive crosslinked nano-fibers (Figure I.7). Firstly, they obtained poly(4-vinyl-benzyl chloride)-*b*-poly(glycidyl methacrylate) (PVBC-*b*-PGMA) copolymer by reversible addition-fragmentation chain-transfer (RAFT) polymerization which was then electrospun. Fibers collected were exposed to a sodium azide solution to obtain azide groups at the surface.

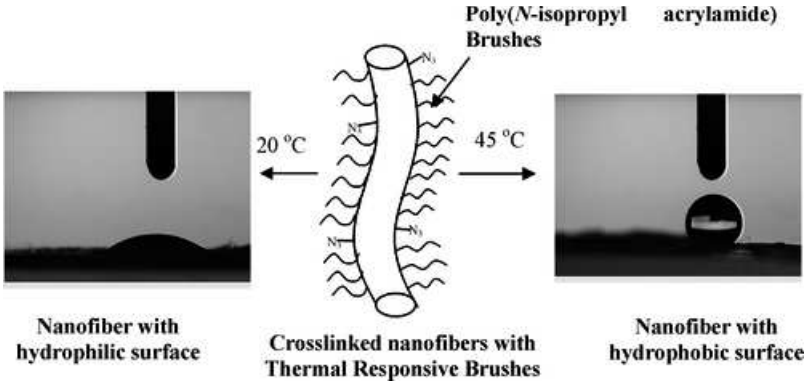

Figure I.7. Thermo-sensitive nanofibers obtained from combined RAFT polymerization, electrospinning and click chemistry[164]

Some of surface azides partially crosslinked with epoxy groups of PVBC, while the rest of the azides were covalently bonded using click chemistry to N-isopropylacrylamide (NIPAM). NIPAM was further polymerized into thermo-sensitive PNIPAM brushes at the surface of crosslinked nanofibers. Final fibrous structure showed good resistance to solvents and was able to respond on temperature stimuli by changing their hydrophilicity. However, the multi-step process before obtaining desired structure makes this approach quite complex and time consuming.

Xu *et al.*[167] investigated a convenient synthesis-approach for obtaining saccharide end-functionalized polyesters. Synthesis of saccharide end-capped polyesters could be achieved by ring-opening polymerization (ROP) of lactones or lactides initiated by saccharides, which requires many protection-deprotection steps. That is why Xu *et al.* chose a post-polymerization modification of polyesters with saccharides. They compared synthesis protocols for obtaining saccharide terminated PCL via Michael addition and click chemistry. Xu *et al.* observed that both Michael addition and click chemistry were successful in PCL end-functionalization with saccharides without degradation and side products.

As noted from previous examples of surface functionalization – click chemistry is a convenient method for making a material surface active with various physicochemical properties accessible for action and interaction with other substances.

4 Conclusions

Nano-fibrous materials with a high specific surface area and porosity are of the outmost value in the field of biomaterials science and tissue engineering. Electrospinning offers a possibility to process a wealth of biopolymers, their blends, composites and even monomers in a rather simple and a cost-effective way into ultra-fine fibrous scaffolds. The interest in this technique is reflected through many studies dealing with the improvements of processing and solution parameters and setup evolution.

From a fundamental point of view, it is important to investigate the physicochemical phenomena of both polymer solution for electrospinning and fibers obtained therefrom. There are many techniques available for studying the morphology (SEM, TEM, AFM) and polymer structure of a material, such as crystallinity (XRD, SANS). Small angle neutron scattering stands out as a powerful technique for characterization of polymeric structures on both molecular and supra-molecular level, in both amorphous and crystalline state. It has been confirmed as a sensitive tool for anisotropy evaluation in confined structures. To date, very few publications discuss SANS on electrospun fibers and more is to be revealed about polymeric structure within these nonwovens.

Biomedical research and tissue engineering in particular have shown a notable interest in electrospun fibers. With the fibrous structures and a porous architecture very similar to those of extracellular matrix, electrospun nano-fibrous mats represent an ideal candidate for cell culture and outgrowth. However, materials' structure is not enough for stimulating a positive response of targeting cells. Physicochemical properties at the surface of material are essential for cell recognition, adhesion and proliferation. Placed at the surface of the cells, carbohydrates enable communication and interaction of the cell with various molecules and other living organisms due to their structural versatility. However, their weak mechanical properties and

instability, once formed into fibers, caused the simultaneous use of carbohydrates with synthetic polymer structures. Physicochemical functionalization methods have shown helpful in bridging the gap between the structure and optimal chemical property of a biomaterial for a desired application. Click chemistry has been evidenced as appropriate technique for enriching the surface of a material in both aqueous and organic environments. The employment of click chemistry on electrospun fibers has demonstrated its great potential in drastically changing the surface properties of the fibers. Yet, complicated multi-step procedures might be an issue, and novel paths should be investigated for a simpler and versatile approach in click coupling practice.

Chain Conformation and Thermal Annealing within Electrospun Polystyrene Fibers – a Small Angle Neutron Scattering Study

Chapter II – Chain Conformation and Thermal Annealing within Electrospun Polystyrene Fibers – a Small Angle Neutron Scattering Study

Small angle neutron scattering (SANS) is ideal for probing various macromolecular and micro structures: polymers, colloids and surfactants, voids and precipitates, porous media, biological structures (proteins, membranes, vesicles in solution), nanoparticles.[168] Samples for SANS analysis could be in various forms (solid, liquid, gels, etc.) and in various environments (heating/cooling, shear, pressure, magnetic field, etc.). Diversity of polymeric materials and valuable physicochemical characteristics on both molecular and macromolecular level that can be studied have allowed a constant progress of SANS technique and made it a precious tool in structure and dynamics analysis.

Popularity of electrospinning process caused a simultaneous development and adjustment of characterization techniques for better qualitative and quantitative analysis of both process and structure of electrospun fibers. However, fast whipping-like motions of the jet prevent investigation of the fiber formation process in situ and consequently, quantification of the strain exerted on polymer chains within the fibers under high electric field. Thus, one cannot say with certainty what happens to the polymer chain inside the fiber in formation, just before it reaches the grounded collector, as the jet cannot be recorded and visualized due to the process stability. On the other hand, polymer chain conformation and relaxation dynamics, affecting

the stability within the electrospun fibers, will also have a determining role in tissue engineering as one of possible application domains. As a consequence, many researcher papers have investigated jet elongation rate and chain conformation through mechanical and spectroscopic studies. As illustrated in Scheme II.1, two distinctive points of view are noticed in the literature. Some studies highlight chain elongation that remains once the fibers are electrospun.[169,170] Others are suggesting polymer chain relaxation inside the fiber bulk until complete solvent evaporation.[88,171–173] By means of mechanical and thermodynamic properties of electrospun fibers, Arinstein and Zussman[169] determined the nonequilibrium state of the polymer matrix within the fibers and its only partial relaxation before the total solvent evaporation. On the other hand, small-angle-neutron-scattering (SANS) studies on polystyrene fibers of Mohan *et al*.[172] observed only 5% greater value of radius of gyration in electrospun fibers than in the bulk state, claiming almost complete polymer chain relaxation.

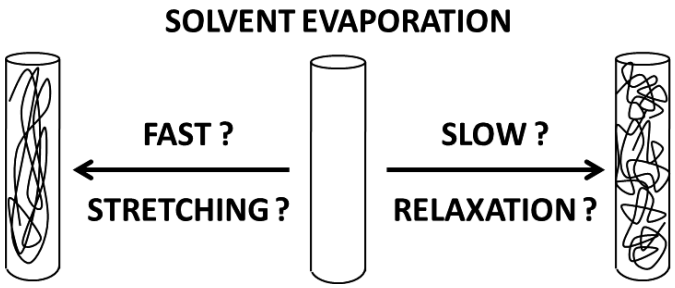

Scheme II.1. Illustration: An open question – what is the final state of polymer chains inside the electrospun fibers?

To address the problem of existing discrepancy in the literature, the anisotropy of fibers electrospun from highly monodisperse polystyrene was investigated employing SANS technique. Polystyrene was chosen as a typically amorphous polymer and there is no partial crystallization to eventually perturb the analysis of molecular organization of the polymer chains. Additionally, chain conformation in as-spun state and its evolution after thermal annealing were analyzed. Electrospun fibers made of polystyrene, having narrow molecular-

weight-distribution (MWD), were used as a model for these studies. Following chapters will be dealing with the process of preparation and electrospinning of polystyrene solutions, and finally, SANS analysis of electrospun fibers in as-spun and annealed state. Electrospinning technique will be briefly demonstrated on the polystyrene solutions, describing the fiber's structure and morphology. Next, by analyzing the electrospun fibers with SANS, the practical aspect of this technique will be introduced through the data analysis and interpretation. Both conformation and relaxation dynamics of macromolecular chains will be analyzed by SANS technique.

1. Electrospun Polystyrene Fibers – Processing and Characterization

Polystyrene was employed as a model-polymer for studying the chain conformation in electrospun fibers. Polystyrene is amorphous polymer and thus convenient to investigate the chain orientation and alignment in electrospun fibers without possible confusion of crystalline zones with the chain alignment as in the case of semi-crystalline polymer.

Two types of polystyrenes were electrospun for SANS measurements: one from Sigma Aldrich, Belgium, with large molecular weight distribution (MWD), and the other one from PolymerSource, USA, atactic, with narrow MWD. Both polymers used had close values of weight-average molecular weight, as presented in Table II.1. For all the polymers tested, MWD was determined using gel-permeation chromatography (GPC) with THF as a solvent and the results are presented together with the supplier's information of the polymer in Table II.1.

From the comparison of GPC results of both producers, one could notice that PolymerSource gives similar information on polymer number- (M_n) and weight-average (M_w)

molecular weights, while the information from Sigma is deviated from the one obtained by GPC measurements.

Polymer	M_n (supplier), g mol^{-1}	M_n (GPC), g mol^{-1}	M_w (supplier), g mol^{-1}	M_w (GPC), g mol^{-1}	MWD (supplier), (M_w/M_n)	MWD (GPC), (M_w/M_n)
PS (Sigma)	170000	98000	350000	351000	2.06	3.57
hPS (PolymerSource)	360000	367000	392000	429000	1.09	1.17
dPS (PolymerSource)	350000	322000	385000	375000	1.10	1.17
dPS (PolymerSource)$_{normalized}$	325000	299000	358000	349000	1.10	1.17

Table II.1. Number (M_n) and weight average (M_w) molecular weights and molecular-weight distributions (MWD) of the polystyrenes used, given by the supplier and measured by GPC technique

Consequently, the GPC values of MWD of PolymerSource PS and Sigma PS differ significantly from those given by the supplier, from 1.10 to 1.17 and from 2.06 to 3.57, respectively. Thus, the values of MWD found experimentally by GPC will be used in further analysis.

1.1. Preparation and Electrospinning of Polystyrene Solutions

There are many solvents available for dissolution of polystyrene. All of them were already tested in the electrospinning process.[46,47,174] In this study, preliminary electrospinning tests were done on PS from Sigma dissolved separately in THF and DMF and influence of solvent on fiber morphology was investigated (see Figure II.1). FESEM (field-emission gun SEM) images of electrospun fibers from THF (Figure II.1A) and DMF (Figure II.1B) show two distinctive structures. Fibers obtained from PS/THF solution gave flattened, ribbon-like structures with significant number of pores at the surface. On the other hand, PS/DMF solution was electrospun into cylindrical fibers with slightly rough surface but without visible pores. Additionally, fibers electrospun from THF had notably greater fiber diameters than the fibers where DMF was used as solvent.

Indeed, previous studies on PS/THF solutions reported similar observations – ribbon-like fibers with a strong affinity to pore formation.[47] Koombhongse *et al.*[33] have observed that, after the skin formation, some trapped solvent in the fiber bulk evaporate, causing the fiber collapse to the flattened structure, which results in this kind of fiber cross-section.

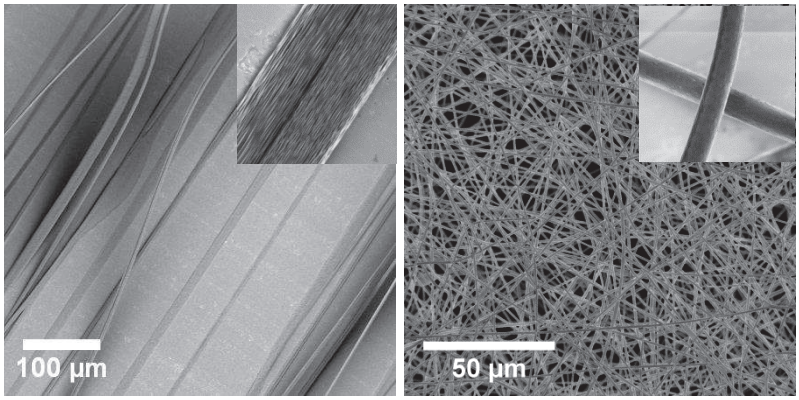

Figure II.1. FESEM images of electrospun polystyrene fibers from (A) THF and (B) DMF solvents and their magnifications as insets

Unlike THF, DMF is less effective in PS dissolution (fair solvent for PS), but it facilitates the electrospinning process and gives uniform tubular fibers.[175,176] Examples reported herein, as well as those from the literature, highlight the fact that the best solvent for dissolution is not always the optimal one for electrospinning. Therefore, it was decided that DMF will be used as a solvent for preparing PS electrospun fibers.

Electrospun PS fibers were aligned using a rotating disc. Figure II.2 represents an image capture of the electrospinning setup with the syringe containing a polymer solution, syringe pump, high voltage electrodes and the rotating disc, manufactured in our laboratory. Electrospinning setup is placed horizontally, to avoid possible solution dropping onto the collected fibrous mesh.

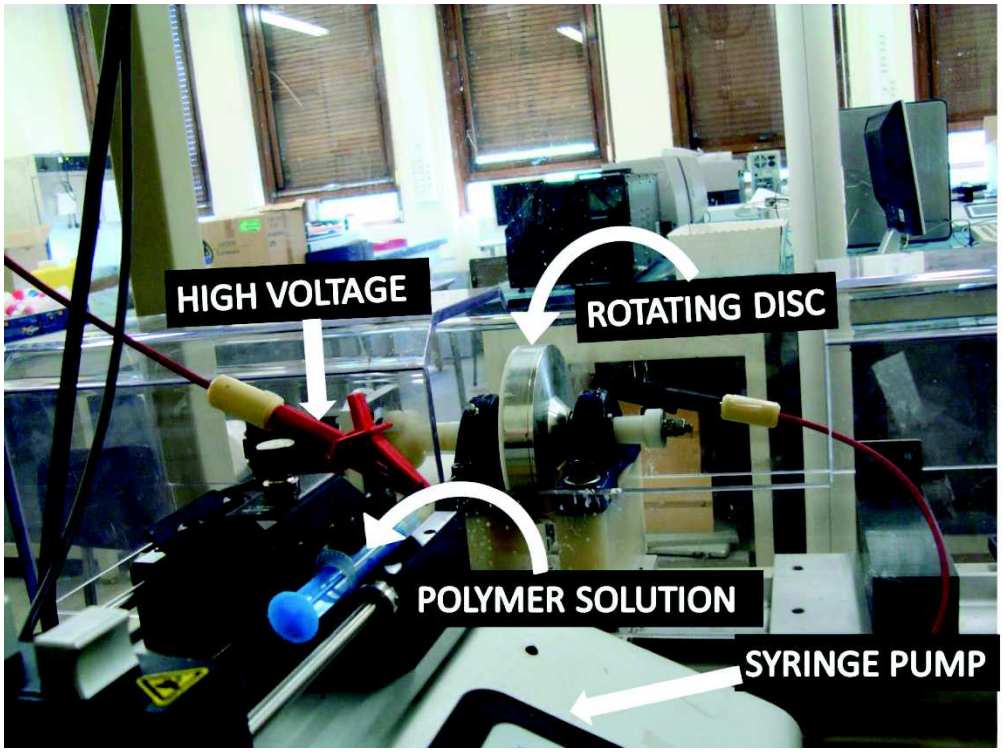

Figure II.2. Image capture of electrospinning setup with a rotating disc for collecting aligned fibers

Different types of polystyrene, dissolved previously in DMF, were drawn into fibers using electrospinning setup previously described. Solution and processing parameters were kept the same for all the polymer solutions tested and in accordance with the previous literature.[38,177–179] Fashandi *et al*.[180] implied to the pore formation at the surface of PS fibers electrospun in humid atmosphere of about 60%. On that account, in this study, humidity was kept below 20% by constant purging of dry air in the electrospinning chamber.

The concentration of 27 v/w% was determined for formation of uniform fibers without beads from the PS/DMF solution system which is in close agreement with previous reports.[177] Eda and Shivkumar studied the solvent effect on electrospinning monodisperse polystyrene and the fiber diameters obtained therefrom.[181] For a polystyrene of M_w = 393400 g mol^{-1} (MWD~1) in DMF, they reported uniform fibers without beads for a concentration of 24 w/v%, which is very close to our 27 w/v% concentration used. The fibers obtained from PS (Sigma), hPS and

blend hPS/dPS (PolymerSource), were named f-PS, f-hPS and f-hPS/dPS, respectively, and are presented in the Figure II.3. Similar morphology was observed, with a rough surface without pores and a cylindrical shape of all three types of electrospun fibers. It is important to notice that the addition of perdeuterated PS did not influence the formation or morphology of f-hPS/dPS fibers, indicating good blending of hPS and dPS and no phase separation between these two polymers.

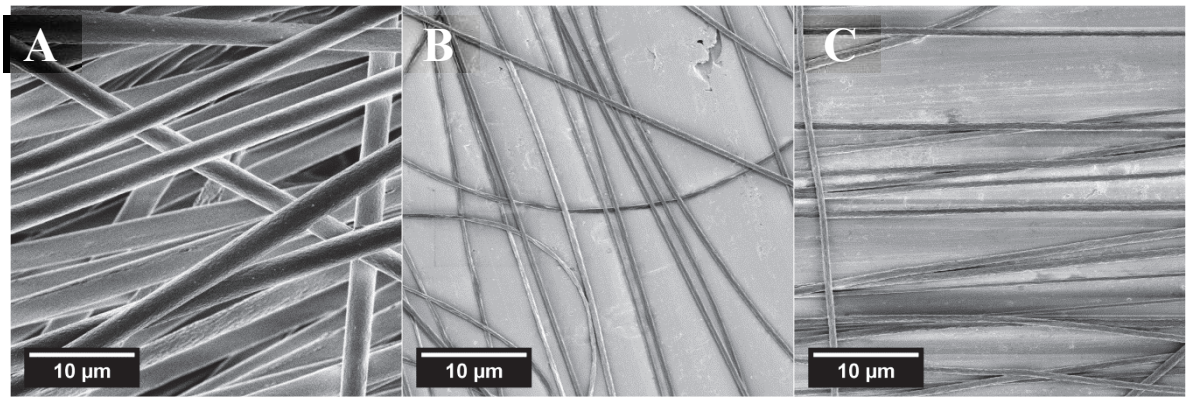

Figure II.3. FESEM images of electrospun: (A) f-PS, (B) f-hPS, and (C) f-hPS/dPS polystyrene fibers

Rough surface observed on the FESEM image (Figure II.4A) is suggesting fast skin formation at the surface of the jet and possible solvent residues, followed by formation of pores after the solvent evaporation. In the doubt of porous structure inside of f-hPS/dPS electrospun fibers, the transection of the fibers was done and their morphology was observed. Polystyrene fibers were entrapped inside the resin and a thin sample was cut using microtome instrument. Figure II.4B represents the TEM image of the f-hPS/dPS fibers' transection. Some of the fibers, colored in light gray on TEM image, form irregular ellipses, suggesting the fusion process via fiber surface contact. Considering the size of these ellipses of about 2.5 µm, it is most likely that the fibers were fused during the resin solidification process. Under low humidity conditions, there are no pores observables at the surface or inside the fiber bulk at this

magnification. Rough surface morphology observed, is therefore only a result of fast solvent evaporation during the electrospinning process.

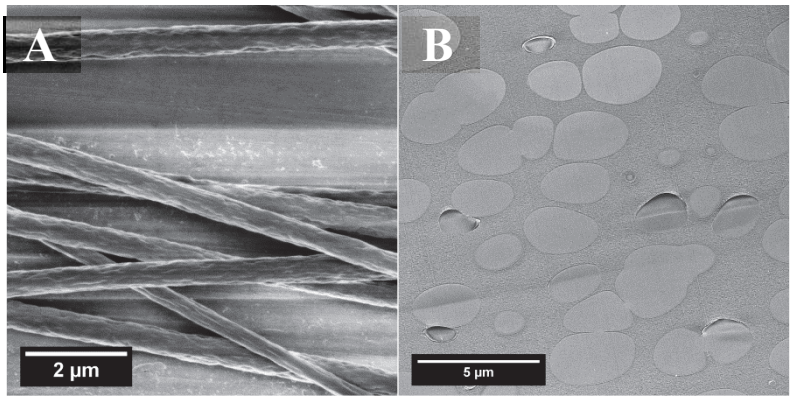

Figure II.4. f-hPS/dPS electrospun fibers observed by (A) FESEM and (B) TEM (microtome transection of resin-entrapped fibers)

Further investigations of electrospun PS fibers through FESEM technique were conducted toward analysis the fiber diameter statistics and alignment.

1.2. FESEM Imaging Analysis of Fiber Diameter of PS Nonwovens

Statistical analysis of fiber diameter distribution of electrospun f-PS, f-hPS and f-hPS/dPS fibers was studied. On Figure II.5 are shown fiber diameter distribution curves of hydrogenated PS collected in aligned (monodisperse) and randomly (mono- and polydispersed) fashion. Fibers electrospun from a polydisperse polystyrene (PS) (MWD=3.6) had average fiber diameters of 1363±267 nm, while monodisperse polystyrene (hPS) (MWD=1.2) of the same M_w was electrospun into fibers having average diameters of 360±91 nm (Figure II.5). Also, it was observed that randomly collected fibers were of diameters inferior to the ones of aligned fibers. Additionally, diameter distribution trend of polydisperse PS were significantly wider than for monodisperse PS. These results are showing that, for the same solution and processing conditions of the same polymeric structures, molecular-weight distribution of that polymer will have a significant influence on fiber diameter and diameter-distribution trend. While

monodisperse PS will be electrospun into fibers having submicron diameters and narrow diameter distribution, polydisperse PS will give micron-sized fibers with large diameter distribution trend.

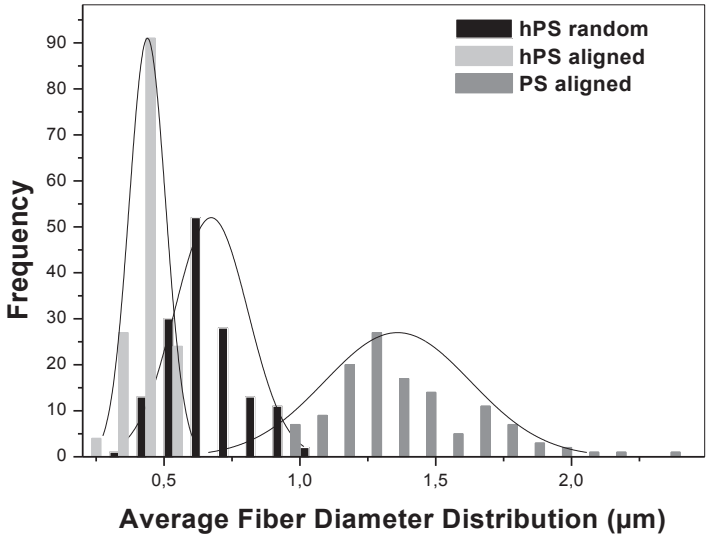

Figure II.5. Average fiber diameter distributions of aligned polydisperse PS (dark gray columns) and monodisperse PS (light gray columns) as well as randomly collected monodisperse PS (black columns)

Investigating the role of chain entanglements on fiber formation, Shenoy *et al*.[38] gave the correlation between the polymer molecular weight and the concentration for fiber formation without beads. However, they do not mention nor study the MWD within their correlation model. Our results are clearly showing that not only molecular weight and viscosity index but also the molecular-weight-distribution factor is influencing chain entanglements and fiber formation.

It was hypothesized that the polymer chains, having narrow MWD, equally participate in entanglement formation, while for polymer with broad MWD only longer chains entangle while the smaller coils are left un-entangled and isolated. As a consequence, for a given

concentration, electrospun fibers from narrow-MWD polymer will have smaller fiber diameters when compared with the fibers issued from broad-MWD polymer (Figure II.5). Gupta *et al*.[37] implied to the similar observation when studying electrospun poly(methylmethacrylate) (PMMA) fibers. In their case, the difference in MWD (from 1 to 2) influenced drastically the fiber formation at the same concentration: while uniform fibers were formed from PMMA having narrow MWD, only droplets were observed of PMMA having broader MWD. They explain that in a narrow-MWD polymer all chains have nearly the same hydrodynamic volume leading to the same relaxation dynamics. Contrarily, polymers with broad MWD have wide distribution of the hydrodynamic radii and consequently, their relaxation times. When electrospinning a polymer with broad MWD, smaller polymer chains with a smaller hydrodynamic volume and lower chain entanglement density will cause a premature jet break, resulting in a formation of polymer droplets.[37]

In the light of the previous observations, it could be concluded that the molecular weight distribution plays a key role in the fiber's formation. Therefore, the influence of MWD on fiber formation should be included in the calculations of the chain entanglement number (n_e) and concentration (c_e). Additionally, electrospinning of hPS/dPS polymer blend for SANS measurements produced fibers having average fiber diameters close to those obtained with the pure hPS polymer (360±91 nm and 442±80 nm, respectively). This result is indicating that the perdeuterated polymer had no significant influence on polymer-solvent and polymer-polymer interactions in the blend, or on the morphology of electrospun fibers.

1.3. FESEM Imaging Analysis of Polystyrene Fiber Alignment

A single fiber processed by electrospinning of nano- and micro-sized diameters is not practicable for SANS as it gives a weak signal of scattered neutrons. In order to obtain a satisfactory signal-to-noise ratio, a bundle of uniaxially aligned fibers is required.

A rotating collector was used to collect a membrane of aligned fibers. Several rotating velocities were tested on monodisperse atactic hPS, in the limit of our setup capacities. Once the fibers were electrospun, average fiber diameters were calculated as an average value of 150 measurements and the results are presented in Table II.2. By simply changing the collector conditions, fiber direction could be regulated.

By regulating the collector speed, fiber orientation and diameter size could be controlled. At the rotational speed of zero, fibers are randomly deposited onto the collector. While the speed increases, a preferential orientation of collected fibers will start to get noticed. When linear speed of rotating disc equals downward speed of flying jet, collected fibers will start to align.[60] Further speed increase will cause additional fiber extension due to mechanical drawing of the polymer chains. At that point, the speed of the collector is greater than the speed of fiber formation during electrospinning. As a result, fiber diameter will decrease. However, at certain point, the force of mechanical stretching of the jet will overcome the physicochemical bonds in the solution and its surface tension, causing the jet break-up, and consequently, fiber diameter increase.[172]

sample	velocity (m s^{-1})	AFD (nm)
hPS-0	0	0,673±0,136
hPS-1	1.33	0,520±0,124
hPS-2	2.30	0,430±0,101
hPS-3	3.25	0,396±0,086
hPS-4	4.17	0,377±0,083
hPS-5	5.26	0,390±0,083
hPS-6	6.21	0,360±0,091

Table II.2. Statistical results of average fiber diameters (AFD) at different collector velocities for f-hPS electrospun fibers

Rotational speeds employed in this study were in the range of fiber alignment and polymer stretching, before the jet break-up. This is important to know as there is no scientific interest in observing the chain elongation rate after the jet break-up point.

From the Table II.2 it could be noticed that, for the rotational speed-range investigated, the average fiber diameter decreased with increase of the rotational speed. It could be thus concluded that, in this range, mechanical stretching of the jet by the rotating disc did not cause the jet break-up. Finally, the rotational speed for aligning the PS fibers for SANS measurements was fixed at the upper speed limit of 6.21 m s^{-1}. Alignment rate was studied from FESEM images represented in the Figure II.6 and presented in a form of statistic graphic in Figure II.7.

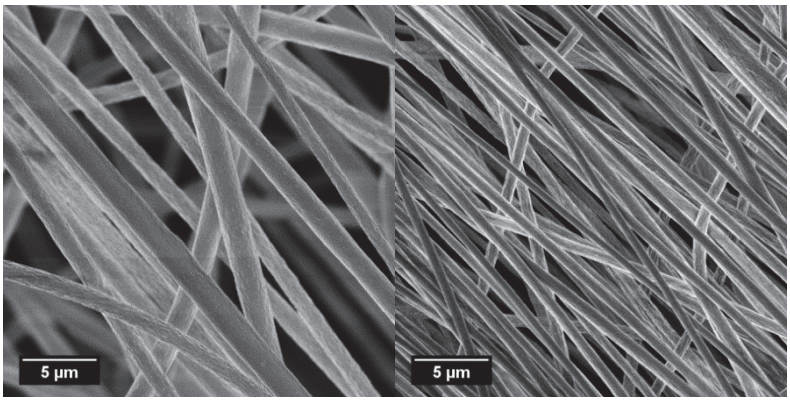

Figure II.6. FESEM images of aligned (A) PS, and (B) hPS/dPS-based fibers

Preferential direction of collected fibers is clearly evident from FESEM images (Figure II.6). However, it could be also observed that some fibers took arbitrary directions. It is hypothesized that during time, charge repulsions between isolating fibers increase by increasing the fiber's thickness, and consequently cause the fluctuation in the fiber alignment. As a consequence, fiber alignment will gradually decrease with the increase of sample thickness. In our case the aberration from imposed direction, observed at the surface of the fibrous scaffolds, does not overpass 30° (Figure II.7).

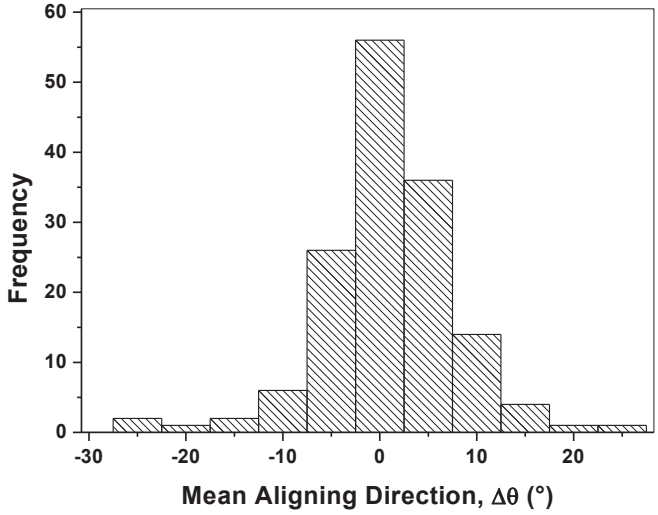

Figure II.7. Statistical graphic of the average alignment direction (°) of the f-hPS/dPS fibers

After the characterization of fiber morphology, SANS measurements were performed, and further data analysis and interpretation are the subject of the following sections.

2. SANS from Electrospun Polystyrene Nanofibers

SANS experiments on electrospun fibers were done in Laboratoire Léon Brillouin, Saclay, on PAXY spectrometer at room temperature and atmospheric pressure. Scattered neutrons, forming a 2D contour plot of iso-intensities, were further transformed by Fourier transformations into a scattered intensity I as a function of q vector (Scheme II.2A). For studying the influence of electrospinning process on polymer chain conformation and relaxation dynamics, two directions, lying in the detector plane, will be studied: parallel (//) and perpendicular (⊥) to the fiber alignment axis (Scheme II.2B). Simultaneously, a completely isotropic strain-free sample of electrospun fibers will be investigated.

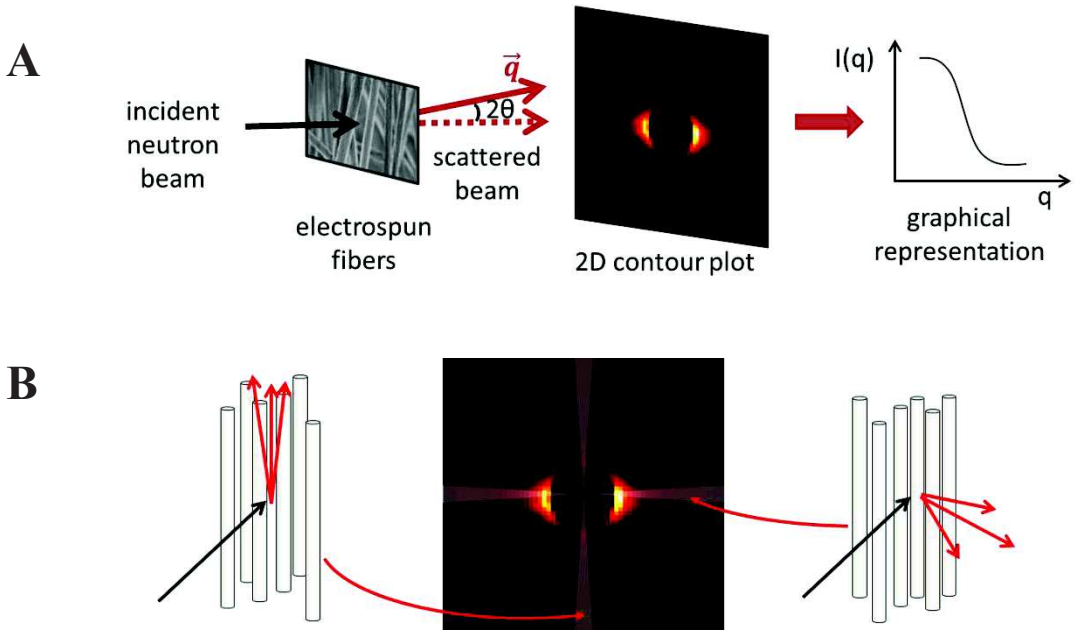

Scheme II.2. Simplified representation of SANS experiment: scattered neutrons from a fibrous sample were collected into a 2D contour plot and further transformed into a I(q) vs. q curve (A), and sectors chosen for further analysis in the direction parallel (//) and perpendicular (⊥) to the fiber alignment axis (B)

As mentioned previously, only few papers were dealing with the SANS analysis of electrospun fibers. SANS studies of Mohan *et al.*[88,172,173] on polystyrene fibers were done on micron-sized electrospun fibers (~10 µm). Their choice of producing and observing micron fibers could be justified considering the strong scattering from the interface air-fiber (strong Porod effect in the Guinier regime) of these nonwovens. So as to reduce the specific surface of the fibers and consequently the Porod effect, they fabricated fibers with larger diameters. However, it is well known that polymer chain organization and further mechanical properties are different in micron- and nano-sized objects[182–184] and this size-dependent behavior should be taken into account when studying the electrospun fibers. We therefore aimed toward submicron diameters of PS electrospun fibrous scaffolds. Deuterium labeling was achieved by blending of perdeuterated and hydrogenated PS in 50-50 % ratio and the blend was further electrospun into f-hPS/dPS fibers. Deuterium-labeled scaffolds were analyzed by SANS

technique in order to investigate the polymer chain conformation and its potential relaxation dynamics after thermal annealing.

2.1. SANS from Completely Relaxed Polymeric Chains

With the purpose of preparing an isotropic sample from f-hPS/dPS fibers having polymeric chains completely relaxed, the fibrous scaffold was annealed above its glass-transition temperature ($T_{g_{PS}}$=100 °C) for a long period of time (128 °C for 140h). The same was further analyzed with SANS technique and the curve of scattered intensity *I(q)* versus *q*, with the corresponding 2D contour plot, is presented in Figure II.8.

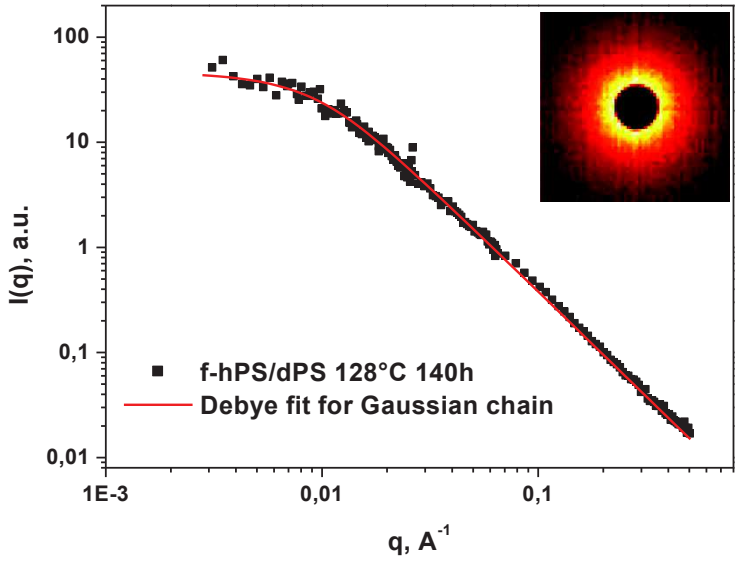

Figure II.8. Scattered intensity from completely relaxed f-hPS/dPS fibers, annealed at 128°C 140h (filled squares), and corresponding Debye fit for Gaussian chain (red line); the inset shows 2D contour plot of this sample

2D contour plot of iso-intensities shows uniform scattering pattern in all directions. It could be concluded therefrom that f-hPS/dPS scaffold, annealed at 128 °C for 140h, is

completely relaxed. However, for quantitative analysis of the chain conformation and polymer relaxation dynamics, the radius of gyration (R_g) should be determined.

For completely relaxed polymeric chains, radius of gyration can be calculated theoretically from the following equation:

$$(R_g)_{theory} = 0.275\sqrt{M_w} \tag{II.1}$$

For the polystyrene used in this study ($M_{w_N} = 0.5M_{w_{hPS}} + 0.5M_{w_{dPS_N}}$= 389 kg mol^{-1}), it is calculated to be (equation II.1):

$$(R_g)_{theory} = 171 \text{ Å}$$

A standard procedure for defining the chain dimensions and radius of gyration values of polymeric chains from SANS experimental data can be estimated from the Guinier plot in low q range ($qR_g \ll 1$):

$$I(q) \propto \exp\left(\frac{-q^2R_g^2}{3}\right) \tag{II.2}$$

From the curve $\log I(q)$ vs. q^2 in the low q range, radius of gyration can be obtained as a slope, and it was estimated to be: $R_{g_{Guinier}}$ =120±74 Å. It could be seen that this result is notably different from the theoretically predicted value, with a significant error in data fitting. It is hypothesized that the discrepancy between the theory and experiment may be due to a narrow q range data were analyzed in.

Another possibility is to make use of the intermediate part of the scattered intensity curve, and, by employing the Debye equation, deduce the value of radius of gyration,[185] while avoiding the influence of the interface scattering:

$$I(q) = I_0 \left[\frac{2}{q^4 R_g^4} \left(\exp\left(-q^2 R_g^2\right) - 1 + q^2 R_g^2 \right) \right] \quad \text{(II.3)}$$

Experimentally collected data of isotropic f-hPS/dPS sample were also analyzed by using the Debye law for Gaussian chains (equation II.3) in the larger, intermediate, q range. The data fitting gave $R_{g_{Debye}} = 156 \pm 4.3$ Å, which is close to the theoretical predictions of $R_g = 171$ Å. Former studies of thin films ($D \sim 10R_g$) observed that the chains in the thermal equilibrium take unperturbed Gaussian chain conformation and R_g values are close to those in the bulk in the direction parallel to the film surface.[79,186,187] Herein, the polymeric chains, confined within the cylindrical ultra-fine fibers ($D \sim 20R_g$), showed similar trend of R_g value in the direction of the alignment axis.

For the q range obtained from the SANS experiment, better evaluation of the radius of gyration of polymeric chains within the electrospun fibers can be obtained from the Debye than the Guinier fit. This is thought to be due to the larger data range analyzed in the intermediate domain than the domain of q below the $\frac{1}{R_g}$ value. For that reason, in this study, the experimental value of $(R_g)_{iso} = 156$ Å, obtained from the Debye fit of f-hPS/dPS scaffolds annealed at 128 °C for 140h, will be used in further analyses.

2.2. SANS Analysis of As-Spun PS Fibers

Herein, the qualitative observation of the typical SANS curves will be discussed. The subsequent comparison of the as-spun with the isotropic f-hPS/dPS electrospun fibers will follow the discussion remarks.

In Figure II.9, the scattered intensity I as a function of q for as-spun f-hPS/dPS fibers is represented, with a 2D contour plot as inset. The contour plot of iso-intensities has an elliptical

shape, suggesting an anisotropic character of electrospun fibers. Indeed, Figure II.9 shows that, at low q values, $I(q)_{\parallel}$ and $I(q)_{\perp}$ in the direction parallel and perpendicular to the alignment axis, respectively, are not superposing, and thus indicating the anisotropy of the samples.

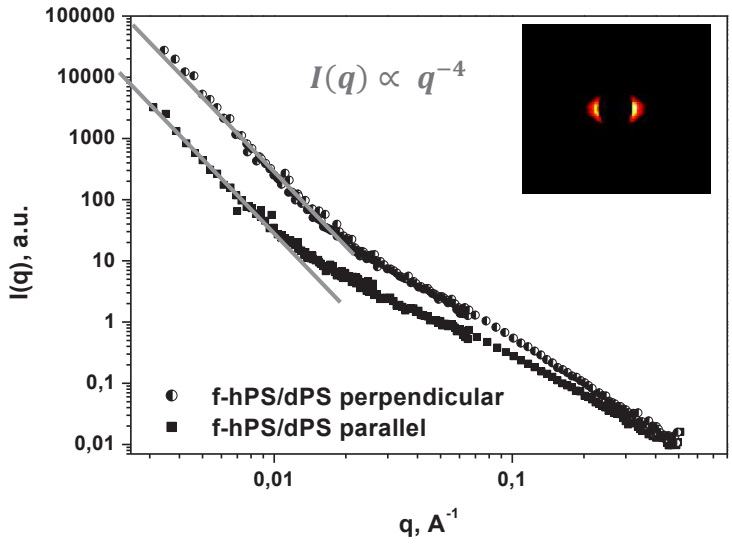

Figure II.9. Scattered intensities (I(q) vs. q) of as-spun f-hPS/dPS fibers in parallel (filled squares) and perpendicular (half-filled circles) direction; 2D contour plot as inset

The scattered intensity functions $I(q)$ in directions // and $\perp$ to the fiber's axial direction, exhibits power-law dependence at low q with an exponent of 4, characterizing strong surface scattering and Porod effect. It has been already observed that the contribution of surface roughness of thin films to the scattering data manifests itself at low q values.[79] Indeed, FESEM images showed previously (see Figure II.4A), clearly visualize rather rough surface morphology that could partially explain strong Porod effect observed on SANS curves of electrospun f-hPS/dPS fibers. Strong scattering at low q values, observed by Mohan *et al.*[172], was assigned to the scattering from the voids inside the electrospun fibers, but it is thought herein to be more likely a sum of neutron scattering from voids inside, and pores between the fibers.

In Figure II.10, $q^2I(q)$ is plotted versus q for the as-spun fibers in parallel (open circles) and perpendicular (open triangles) direction to the alignment axis. Looking at this Kratky-Porod representation, f-hPS/dPS fibers in ⊥ direction show a maximum and constant increase in // direction, while isotropic sample displays a plateau characteristic for Gaussian chains. This behavior had been thoroughly investigated and reported by F. Boué.[188] Curves $q^2I(q)_{\parallel}$ and $q^2I(q)_{\perp}$ are suggesting once again the anisotropic behavior of electrospun fibers, converging to the isotropic plateau at high values of q . At small q values, the descending trend in both // and ⊥ directions of as-spun fibers stands for the Porod effect, observed previously in Figure II.9 in the same q-range.

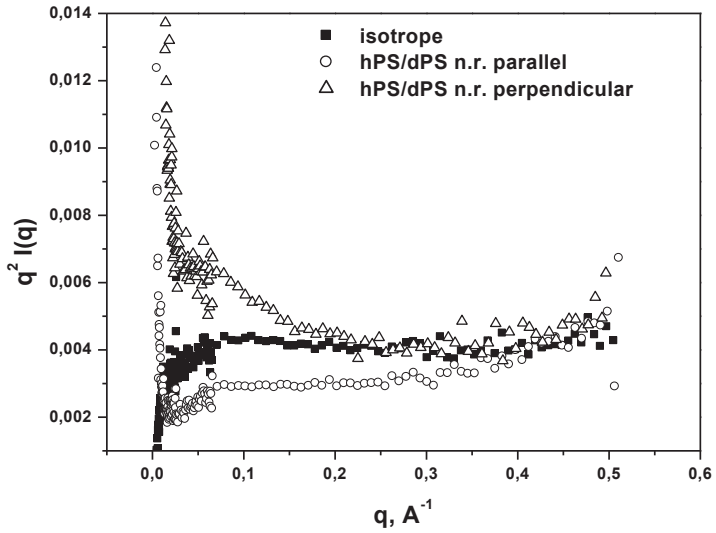

Figure II.10. Kratky-Porod representation of as-spun f-hPS/dPS fibers in direction parallel (open circles) and perpendicular (open triangles) to the alignment axis, and of completely isotropic f-hPS/dPS fibers, annealed at 128°C 140h (filled squares)

The anisotropy observed might be simply due to the fiber alignment, but could be also reflecting the anisotropic conformation of polymeric chains. In order to investigate the source

of this trend, the analysis of polymer chain dimensions and their elongation ratio were next discussed.

2.3. Chain Conformation within Electrospun Fibers

It is known that the electrospinning process induces high elongational strain of the polymer jet during the whipping motions and bending instability.[189] However, later stages of polymer jet evolution during its flight are not yet investigated, which endures the question whether polymer chains are stretched within the polymer jet, and if so, are they relaxed (partially or entirely) or not once the solid fiber is formed.

Next sections will be investigating the chain conformation within as-spun polystyrene fibers and different analyzing techniques will be employed.

2.3.1 Radius of Gyration

Radius of gyration (R_g) gives direct information about the existing anisotropy of polymeric chains. As mentioned previously, R_g of electrospun fibers can be quantified by fitting the scattered intensity $I(q)$ with either Guinier or Debye law in the corresponding q domain.

Figure II.11 shows the comparison of experimental and theoretical curves $I(q)$ vs. q in both parallel and perpendicular direction to the alignment axis of as-spun fibers and a corresponding isotropic sample, respectively. A notable difference was observed between as-spun and isotropic scaffold at the low q range, where R_g value could be commonly calculated, showing the strong scattering from the fiber's surface and Porod effect. For that reason, the chain dimensions within the electrospun fibers cannot be obtained by standard Guinier method, and a different approach should be considered.

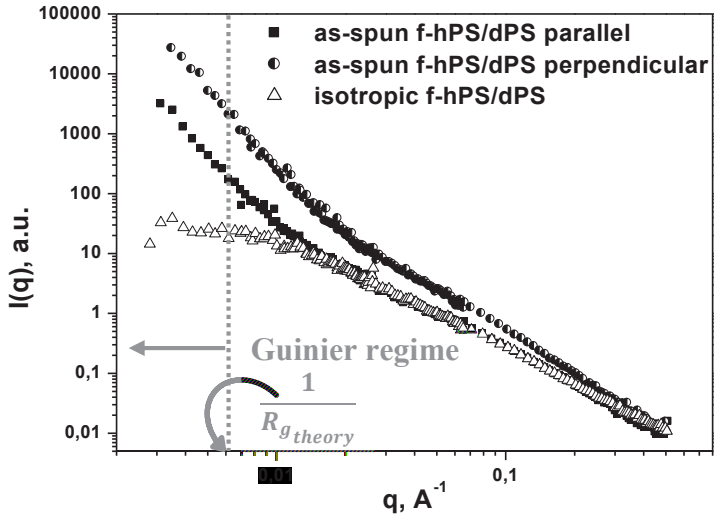

Figure II.11. I(q) vs. q plots of as-spun f-hPS/dPS fibers in perpendicular (half-filled circles) and parallel (filled squares) direction, and isotropic f-hPS/dPS fibers (open triangles); gray dotted line marks the validity limit for Guinier regime

As previously noted, a better R_g-estimation was found by using the Debye fit. Similarly, for the valorization of the R_g of as-spun f-hPS/dPS fibers, only the Debye fit will be used. Still, there are some inconveniences that should be taken into account when using this equation for fitting the scattered intensity from as-spun fibers. Debye fit is devoted to evaluate the radius of gyration of spherical objects. In order to minimize the possible errors in fitting analysis, Debye fit should be used for scattered intensity in the parallel direction where the Porod effect is less pronounced (see Figure II.11).[185] Also, in this intermediate region of q one cannot talk about the *absolute* radius of gyration because it overpasses the regime of Guinier where this value could be accurately determined. Therefore, the value of R_g calculated from the experimental data will be named hereafter as *apparent* R_g. In order to obtain this value, Debye fit was performed without taking into account the scattered intensities in the low q domain. For the as-spun f-hPS/dPS fibers, value of apparent R_g was found to be:

$$R_{g_{\parallel}} = 211 \pm 41 \text{ Å}$$

Significant error obtained from this fit is hypothesized to be a result of: *(i)* very sensitive nature of this fit due to the strong interface scattering and Porod effect, and *(ii)* as Debye fit is dedicated to typically Gaussian polymer chains (spheres) it will not completely follow and fit the tendency of elongated chains in electrospun fibers.

It could be concluded from these studies that it is possible to use Debye fit to obtain the information of the chain conformation within as-spun fibers. However, the fitting process is highly sensitive to the data range selected due to the strong Porod effect, which further contributes to the quality and accuracy of the fit.

2.3.2 Elongation Ratio

There is, however, another possibility to quantify the anisotropy inside the electrospun fibers without going into sensitive data modeling. It is known that iso-intensity curves join all the detector cells which have counted the same number of neutrons in all directions (q vector). Therefrom, for equal scattered intensity, the q values in the direction parallel and perpendicular to the fiber alignment axis could be obtained. It is known that affinely deformed samples should give ellipses with an elongation ratio:[185]

$$\lambda = \left[\left(\frac{q_{\perp}}{q_{\parallel}}\right)_{I=const.}\right]^{2/3} \tag{II.4}$$

If now the curve $\frac{q_{\perp}}{q_{\parallel}}$ vs. q is considered, both deformation ratio due to the fiber alignment and deformation ratio due to the chain elongation can be visualized (Figure II.12). From this figure, at q values higher than 0.4, corresponding to the polymer chain segments smaller than 15.7 Å, the $\frac{q_{\perp}}{q_{\parallel}}$ ratio equals 1. It could be concluded that, at this scale, the sample is completely isotropic. The anisotropic character of the system starts to be notable for $q < 0.4$ and it increases with the

decrease of q. For $q < 0.1$, experimental data exhibit a significant departure from the fit. The anisotropic signature in the low q region ($q < 0.1$) is probably due to the interface scattering, as observed previously, while the anisotropy in the intermediate q values is likely reflecting the polymer chain conformation within the fibers.

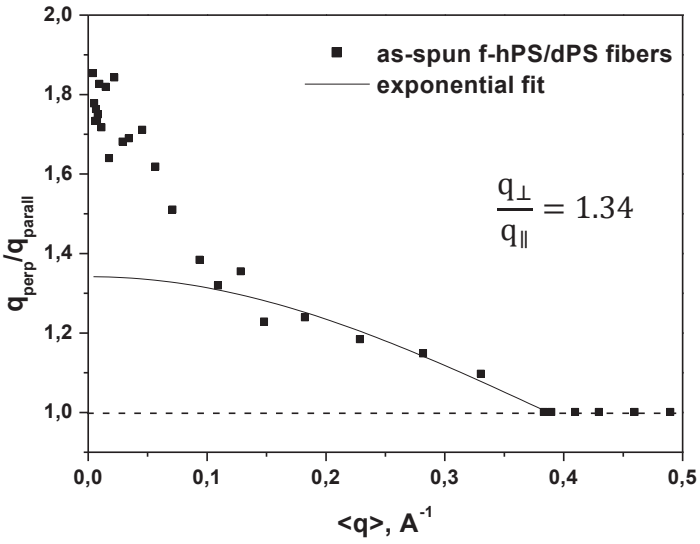

Figure II.12. The $\frac{q_\perp}{q_\parallel}$ ratio as a function of $\langle q \rangle = \frac{q_\parallel + q_\perp}{2}$; solid line corresponds to the exponential fit in the domain of chain elongation; dashed line highlights the line of isotropic sample

By using the polynomial fit for the intermediate region, where $\frac{q_\perp}{q_\parallel}$ corresponds to $\left(\frac{q_\perp}{q_\parallel}\right)_{R_g}$, and equation (II.4), the elongation ratio of the polymer chains was determined:

$$\lambda = \left[\left(\frac{q_\perp}{q_\parallel}\right)_{I=const.}\right]^{2/3} = (1.34)^{2/3} = 1.22$$

Indirectly, by using the elongation ratio, apparent radius of gyration of the f-hPS/dPS scaffold in both // and ⊥ direction to the fiber alignment axis, can be obtained from the following equations:

$$R_{g_{\parallel}} = \lambda \cdot R_{g_{iso}} \quad \text{(II.5)}$$

and

$$R_{g_{\perp}} = \frac{R_{g_{iso}}}{\sqrt{\lambda}} \quad \text{(II.6)}$$

For the as-spun fibers, the calculated values of $R_{g_{\parallel}} = 1.22 \cdot 156 = 190$ Å and $R_{g_{\perp}} = \frac{156}{\sqrt{1.22}} = 141$ Å are found. Radius of gyration obtained from the elongation-ratio analysis is similar (slightly inferior) to the value obtained experimentally from the Debye fit. Nevertheless, the results from Debye fit and elongation ratio analysis are both suggesting the anisotropic structure of polymer chains within the electrospun fibers.

2.4. Chain Relaxation Kinetics of PS Electrospun Fibers

It has been demonstrated that, indeed, strong chain elongation and stretching during the fiber formation lead to the strained polymer chains along the fiber's axis. A further analysis of polymer matrix within the electrospun fibers will include relaxation kinetics study after thermal annealing – very few-investigated domain of strain-induced electrospun fibers by SANS technique.

Herein, the chain relaxation was investigated through thermal annealing of electrospun fibers at different temperatures above the glass-transition temperature (T_g), during different periods of time. In order to wisely choose the temperature and corresponding time needed for partial or complete chain relaxation, it is important to know the terminal relaxation time (τ_{ter}) of a material at a given temperature. The terminal relaxation time for different temperatures was calculated from the following P. Cassagnau[190] relationships:

$$\tau_{ter}(T) = \frac{a_T}{a_{T_0}} \cdot \tau_{ter}(T_0) \quad \text{(II.5)}$$

and

$$\ln(a_T) = 1620 \cdot \left(\frac{1}{T-49} - \frac{1}{T_0-49}\right) \quad \text{(II.6)}$$

Where T_0=160 °C is a reference temperature and $\tau_{ter}(T_0) = 2.75 \cdot 10^{-18} \cdot M_w^{3.44}$ is the terminal time for that temperature and a_T is scaling parameter in time-temperature superposition. The calculated values of a_T and τ_{ter} for M_w = 390000 g mol^{-1} and different temperatures are given in Table II.3.

Temperature, °C	a_T	τ_{ter}, h
105	1,68 E6	21951
115	2,10 E4	274
122	1992	26
128	369	4,8

Table II.3. Calculated values of termination time τ_{ter} for different annealing temperatures

Electrospun f-hPS/dPS fibers were then annealed at different temperatures above T_g during the short time periods. As discussed earlier, strong Porod effect at low q range disables fitting of Guinier law and attaining accurate R_g. The curves of scattered intensity versus q in the fiber's axial direction were therefore fitted with Debye law, having in mind all the shortcomings of this method evoked previously. The values of radius of gyration as well as elongation ratio (λ) of annealed fibers, for different annealing temperatures and periods, are presented in Table II.4.

T, °C	t, min	$R_{g_{\parallel}}(fit)$	$R_{g_{\parallel}}/R_{g_{iso}}$
105	30	226±34	1.45
115	30	198±25	1.27
122	30	198±8	1.27
128	20	194±13	1.24

Table II.4. Chain dimensions ($R_{g_{\parallel}}$) and affine ratio ($R_{g_{\parallel}}/R_{g_{iso}}$) of electrospun f-hPS/dPS fibers annealed at different temperatures and for different time periods, in direction parallel to the alignment axis, obtained from Debye fit

As it could be observed from Table II.4, while increasing the annealing temperature, a constant decrease of R_g and consequently λ, were observed. By increasing the temperature from 105 °C to 128 °C, the elongation ratio slowly decreased from λ=1.45 to λ=1.24, respectively. Accordingly, $R_{g_{\parallel}}$ decreased from 226 Å for the fibers annealed at 105 °C for 30min, to 194 Å for those annealed at 128 °C for 20min. On the contrary, the ratio $\frac{(R_g)_{\parallel}}{(R_g)_{\perp}}$ noted by Mohan *et al*.[172] was around 1.05 (equals to λ=1.03) and did not overpass the value of 1.2 (equals to λ=1.13) at the highest collector speed. Even though they expected the elongation ratios of the same grandeur as observed macroscopically by measuring the extension ratio, $\frac{(R_g)_{\parallel}}{(R_g)_{\perp}}$ ratio and birefringence analyses were both indicating to the small level of molecular anisotropy.[172]

Indeed, there are several distinguishable differences between the study of Mohan and coworkers, and the one reported herein:

1) While they used as thick as 10 μm fibers, electrospun fibers in this study did not overpass the submicron diameters and were of the order of 360 nm.
2) Mohan *et al*. confronted the problem of skin formation during the electrospinning process that further caused the solvent entrapment inside the fiber bulk and consequently the ribbon-like fiber formation. The fast skin-

formation problem was overpassed herein by electrospinning the fibers under low humidity atmosphere (< 20%). As a result, the fibers formed were having cylindrical structures.

3) Electrospun fibers, obtained by Mohan *et al*., were containing many voids and pores within the fiber bulk, probably as a result of residual solvent which might have been causing the polymer chains to relax and therefore resulting in small anisotropy measured by SANS. Due to the low humidity atmosphere used herein, electrospun polystyrene fibers did not contain voids or pores inside the fibers.
4) In the former studies Mohan *et al*. reported wide polymer molecular weight distribution of the polystyrene used. It has been already observed that chain dynamics within the fibers made of the same polymer is not the same for large and narrow MWD.[37] For that reason, the polystyrene having narrow MWD was used in this study for more accurate and more rigorous investigation of chain dimensions in as-spun state as well as chain dynamics during thermal annealing.

The solvent evaporation kinetics, compared between nano- and micron-sized fibers, is not the same, simply because of the longer diffusion trajectory until the fiber's surface. To that matter, polymer chains inside those fibers have much more time to relax and therefore could have less stress-induced conformation what could explain their small anisotropic behavior observed. Additionally, it is known that, broader the molecular weight distribution is, higher the concentration is needed to attain chain entanglements,[191] which at the same time results in thicker fibers. The arguments described previously go in behalf of the small anisotropy ($\lambda_{max} = 1.13$) they observed as well as the R_g values similar to the bulk.[172,173] However, Mohan *et al*.[173] did observe that R_g value increased with the decrease of fiber diameter, confirming the

importance of the fiber diameter and size-dependent physicochemical characteristics of electrospun fibrous mats.

2.5. A Comparative Study of Polymer-Chain and Surface-Relaxation Kinetics of Electrospun Fibers

Beside the short annealing periods of electrospun polystyrene fibers discussed so far, longer annealing periods have been studied as well, in order to simultaneously analyze surface and chain relaxation of the fibrous scaffolds. These studies are important to further determine a characteristic relaxation time of the polymer of interest. The characteristic relaxation time could provide the information about the polymer stability inside the electrospun fibers – an important parameter for degradation processes in tissue engineering applications.

Two types of relaxation kinetics have been investigated. Polymer chain relaxation has been evaluated through the time dependency of the apparent radius of gyration within the electrospun fibers. The R_g value was obtained by fitting the Debye equation for Gaussian chains (see equation II.3) in the intermediate q range, giving the apparent radius of gyration ($R_{g_{\parallel}}$) for different annealing periods. The surface relaxation kinetics was extracted through the evolution of the Porod law ($q^4 I(q) \propto q$) at low q range, providing a surface-to-volume ratio of the fibers: $\left(\frac{S}{V}\right)_{\parallel}$ (Table II.5). Both surface and chain relaxation kinetics were investigated in the direction parallel to the alignment axis.

Surface annealing was materialized through Porod constant A in the parallel direction obtained from the following equations:

$$I(q) = A \cdot q^{-4} \tag{II.7}$$

$$A = const. = 2\pi\Delta\rho^2 \frac{S}{V}\phi(1-\phi) \tag{II.8}$$

where $\Delta\rho^2$ is a scattering length density difference between air and sample, and ϕ is perdeuterated polymer ratio in the blend ($\phi = 0.5$). Therefrom, the surface-to-volume ratio $\left(\frac{S}{V}\right)$ of electrospun scaffolds and their evolution during the thermal annealing can be evaluated from the following equation:

$$\frac{S}{V} = \frac{A}{2\pi\Delta\rho^2} \tag{II.9}$$

Annealing temperature (°C)	Annealing period (h)	$R_{g_\parallel}$, (Å)	$A_\parallel$ (for a constant Porod)	$\left(\frac{S}{V}\right)_\parallel$, (Å^{-1})
0	0	248.6±67	1.12E-6	8351
115	2	178.1±4.4	1.62E-7	1208
115	4	149.1±2.7	1.38E-7	1029
115	6	136.5±2.5	1.03E-7	768
115	11	112.2±2.1	9.13E-8	681
128	1.5	114±2	5.60E-8	418

Table II.5. Radius of gyration (R_g) and Porod constant (A) for different thermal annealing temperature and time intervals

From the Table II.5, a descending trend of the Porod's constant *A* and the corresponding surface-to-volume $\left(\frac{S}{V}\right)$ ratio of the fibrous mats was observed. About 85% of the total surface-to-volume ratio relaxed in the first two hours of thermal annealing at 115 °C to further slowly relax over 91% for the next 4h, until the relaxation of 95% of the specific surface after 1.5h at 128 °C.

As observed previously on the short-time annealing periods, by increasing the time of polymer annealing above T_g and by enabling the chain movements, radius of gyration (R_g) will decrease. R_g obtained after longer annealing periods is found to follow a similar trend (Table II.5). Significantly different values of evolution of the chain dimensions are observed and

considered as a result of both data and modeling uncertainties. Aware of this difficulty, the R_g values will be used herein only as a *guide* for predicting a *tendency* of the characteristic relaxation time.

The classical way to determine the terminal relaxation time of a material is through analysis of the deformation ratio (λ) of polymeric chains as a function of time – from strained to completely annealed polymeric materials. Due to encountered difficulties in the data processing and extracting the value of radius of gyration of the as-spun fibers, another approach was employed in this study. In the time-window of interest, polymer chain and surface kinetics of the scaffold are reported as a function of the equivalent time $t \cdot a_T$. In Figure II.13, polymer chain relaxation kinetics was displayed as R_g ratio ($R_{g_{\parallel as\ spun}} / R_{g_{\parallel annealed}}$), while the kinetics of surface relaxation was displayed as a ratio of Porod constant A ($A_{\parallel as\ spun} / A_{\parallel annealed}$), of as-spun and annealed fibers in the direction parallel to the fiber alignment axis. Solid line in Figure II.13 is an exponential fit following the annealing trend of polymeric chains. Dashed line in the same figure serves only as an eye guide for the surface relaxation tendency.

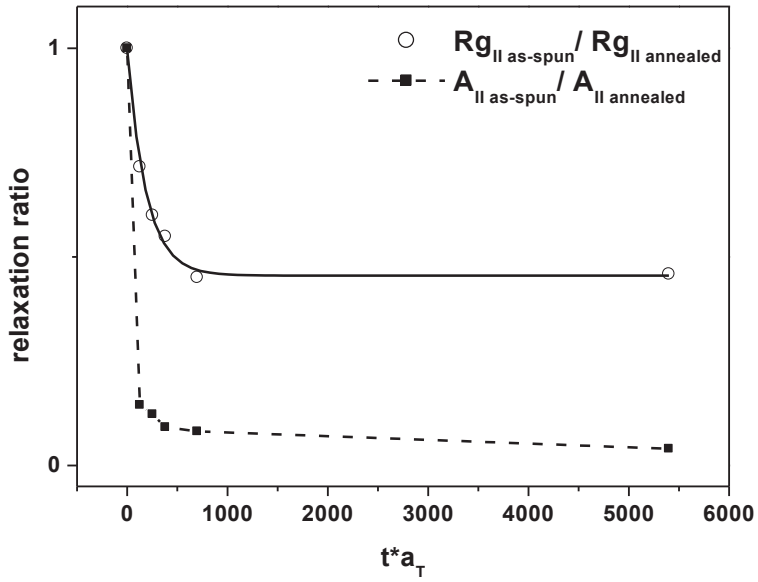

Figure II.13. A plot of relaxation ratio vs. time of radius of gyration $R_{g_\parallel}/R_{g_{\parallel iso}}$ and Porod's constant $A_\parallel/A_{\parallel iso}$ in the direction parallel to the fiber's alignment axis; reference temperature for time-temperature superposition parameter a_T is 128 °C

It could be seen from the Figure II.13 that majority of the surface relaxed in the short time periods, while the relaxation of polymer chains took significantly more time. By using the exponential fit for the chain relaxation curve, we tried to extract the information about the characteristic relaxation time of those chains. Normalizing the $\frac{R_{g_{\parallel as\ spun}}}{R_{g_{\parallel annealed}}} = f(t \cdot a_T)$ curve to the temperature of 128 °C, the characteristic time of $\tau_{exp} = 2.98 \cong 3h$ was determined. This experimental relaxation time is significantly shorter than the theoretically predicted terminal relaxation time for the polymeric chains of M_w = 390000 g mol^{-1} ($\tau_{theory} = 4.8h$), but both values are of the same order of magnitude.

The surface relaxation kinetics of electrospun fibers is presented as filled squares in Figure II. 13. The $\frac{(A_\parallel)_{as-spun}}{(A_\parallel)_{annealed}}$ vs. $t \cdot a_T$ curve shows two types of time kinetics – the first one is

rather fast and after only 2h of annealing at 115 °C, the majority of the surface relaxed. The second part of the curve shows rather slow and constant surface-relaxation trend. The fast surface relaxation trend is likely to reflect the rapid relaxation of the surface tension of the material while the second part is thought to be the result of relaxation and fusion of polymer chains at the surface.

A qualitative validation of the fast relaxation kinetics of the fiber's surface was accomplished with scanning electron microscopy imaging (FESEM). The representative images of as-spun and annealed fibers and their corresponding SANS 2D contour plots are shown in Figure II.14.

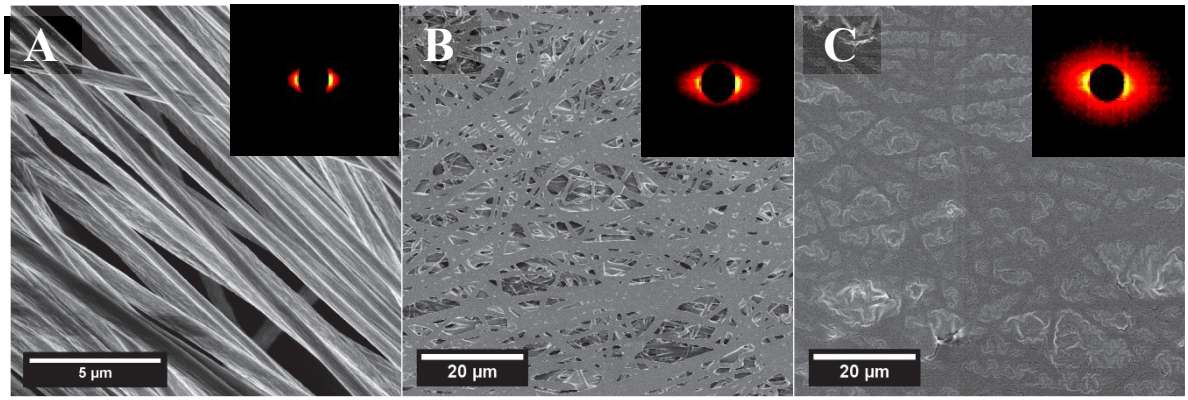

Figure II.14. SEM images of (A) as-spun and thermally annealed f-hPS/dPS fibers at (B) 115 °C for 6h and (C) 128 °C 1.5h and their corresponding SANS 2D contour plots as insets

By looking at the FESEM images of the surface of fibrous scaffolds, a drastic difference can be observed from as-spun (Figure II.14A) and annealed samples (Figure II.14B, C). It could be seen that the majority of the specific surface relaxed, and only fiber contours are visible. The temperature increase, from 115 °C (for 6h) to 128 °C (for 1.5h), caused the fibers to almost completely merge into each other, leaving the continuous surface of the sample (Figure II.14C).

3. Conclusions

The study exposed in this chapter was focused on investigation of the morphological properties of electrospun fibers, the anisotropy of polymeric chains within the fiber's bulk as well as their stability. Electrospinning process was studied through polystyrene as an amorphous polymer-model. Structural characteristics of the fibers were analyzed microscopically (SEM) while chain conformation and thermal relaxation dynamics were analyzed by SANS technique.

The first important information obtained from this study is the crucial influence of the molecular weight distribution (MWD) on fiber diameter. It was determined that, for the same polymer/solvent system and the same concentration, polydisperse polymer will produce micron-sized fibers, while monodisperse polymer will give nano-fibers under the same processing conditions.

Another important point discussed in this chapter is the thermal annealing of electrospun fibers, and furthermore, their stability over time. Small angle neutron scattering studies of monodisperse PS within the fiber bulk showed distinctive anisotropy and elongation in the direction of the alignment axis of the fibers. The short-time annealing periods showed constant and progressive decrease of anisotropy materialized through elongation ratio and radius of gyration. The long-time annealing periods enabled us to determine the characteristic relaxation time and consequently the stability of the polymeric chains in confined fibrous structures. Furthermore, while the chain relaxation was slow but continuous, the surface of the fibers relaxed almost completely in the first two hours of annealing at 115 °C.

Functionalization and Bio-Activation of PCL Nano-Fibers Using Click Chemistry

Chapter III – Functionalization and Bio-Activation of PCL Nano-Fibers Using Click Chemistry

---

Poly(ε-caprolactone)-based nonwovens have been confirmed as a promising material for biomedical applications because of their biodegradability and biocompatibility.[143,192] However, their hydrophobicity and absence of functional groups have triggered many studies dealing with PCL modifications.[104,193,194] These modifications were mainly focusing on improvements of hydrophilic properties for establishing a friendly interface for living cells. Recently, the attention has been paid to overcome the problem of non-specific protein adsorption on the electrospun fibers. A significant step toward specific protein adsorption using bio-functionalized polymeric fibers was made by D. Grafahrend and coworkers.[195–199] They highlighted the importance of the polymer choice for electrospinning as well as the choice of active species at the fibrous surface. Therefore, for producing bioactive PCL-based materials, not only hydrophilic but also protein- and cell-recognized molecules should be used. Typical examples of such structures are carbohydrates.

Carbohydrates perform numerous roles in living organisms. They serve as energy storage, or as structural components, but they are also involved in diverse cellular processes, enabling communication, proliferation, differentiation. Functionalization of polymers, such as polyolefins, with sugars has been explored periodically as a possible way to improve their biodegradability.[200] Over time, carbohydrate-conjugated polymers have attracted attention for

their biomedical applications. Chua *et al.*[201] demonstrated that galactose-conjugated nanofiber meshes promote cell-substrate interaction, suggesting potential scaffold application in the liver tissue engineering. Equally, sugar-conjugated polymers were employed for immobilization of proteins,[202] as cell's surface mimics,[203] cell adhesion as well as for many other pharmacological and biomedical applications.[204]

There are various methods of chemical functionalization, notably wet chemical methods[156] and plasma treatment[155] as mainly studied. Although these methods are simple and easy to use, they induce changes in surface morphology and a partial degradation of a material. Azide-alkyne cycloaddition, popularly called click chemistry; is a valuable technique for introducing broad functional moieties owing to its versatility and high yields.[157,159] The reaction of cycloaddition is produced from any two end-functionalized azide and alkyne molecules into a triazole ring leaving no side products. It is high yielding in both aqueous and organic solvents, as well as in homogeneous and heterogeneous phase. The combination of electrospinning and click chemistry resulted in a number of interesting studies.[164,165,205] However, these reports reveal complex preparation of a desired polymer from a previously modified monomer. Thus, it is of significant importance to investigate a simple yet non-aggressive path for obtaining highly decorated surface of biocompatible nanofibers, able to immobilize various bioactive molecules by means of click chemistry.

Searching for linear PCL from commercial sources (herein we referred to Sigma Aldrich source), typically two types of PCL could be found (Scheme III.1):

1. PCL diol having hydroxyl groups at both ends of the chain, available with several lower molecular weights: M_n = 530, 1250, 2000 and 10000 g mol^{-1}, and
2. PCL, synthesized typically from a monohydric alcohols, available in high molecular weights: M_n = 45000 and 70000 – 90000 g mol^{-1}

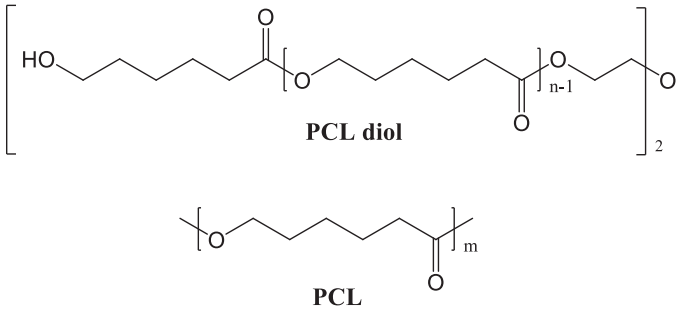

Scheme III.1. Chemical structures of commercial poly(ε-caprolactone)s: low molecular weight α,ω-poly(ε-caprolactone)-diol (PCL diol) and high molecular weight PCL

For electrospinning purposes, polymer molecular weight is a critical parameter for uniform fiber formation without beads. In the case of PCL, mainly used molecular weight is of 80000 g mol^{-1} (henceforth named as PCL_{80}) giving smooth bead-free fibers from the solutions having as low as 7.5 w/v% of polymer.[192] However, PCL_{80} has only one hydroxyl end group that could be converted into azide/alkyl group for click coupling. Additionally, slow segmental motions, considering high molecular weight, might directly influence the yield of the final product. Nevertheless, once functionalized, high molecular weight allows direct electrospinning. On the other hand, low-molecular weight PCL could be easily put into solution and submitted to chemical modifications. Yet, it cannot be directly electrospun and it needs to be blended with some other polymer having longer macromolecular chains.

Thus, in this study, we chose to chemically modify low-molecular-weight PCL, having M_n of 2000 g mol^{-1} (henceforth named as PCL_2), and to further implement it in the electrospun fibers made of high-molecular-weight PCL_{80}. This choice has several advantages:

- low viscosities of reaction mixture, better Brownian chain motions leading to higher yields,

- final product, introduced in the fiber, could offer various physicochemical properties depending of the functional group it contains (henceforth referred to as a bulk functionalization),
- if a functional group introduced is available to react by click coupling (alkyl or azide), fibers could be subsequently surface-decorated (henceforth referred to as a surface functionalization),
- and finally, the quantity of functional polymer in the fiber could be adjusted by changing its ratio in the blend with PCL_{80} polymer.

This chapter will be therefore dealing with the chemical transformations of PCL_2 polymer, processing of PCL-based fibers, their surface- and bulk- functionalization, and finally, characterization of the nonwovens obtained. The functionalization of the fibrous surface using click chemistry coupling will be performed in both homogeneous (in the polymer solution) and heterogeneous phase (at the surface of the fibers). The availability of the surface azides and their activity was visualized by fluorescence from a fluorescent dye introduced onto the fibers by surface click coupling. Most importantly, model bioactive molecules: mannose and galactose were surface-coupled using click chemistry approach and their specific recognition by proteins was analyzed. Carbohydrate coupling with PCL, in solution or at the fibrous surface, has as an objective to make of PCL fibrous scaffolds not only biodegradable but bioactive and biomimetic structures for tissue engineering purposes.

1. Electrospinning of High-Molecular-Weight PCL into Nanofibers

Two commercially available PCLs of high molecular weight (M_n = 45000 and 70000 – 90000 g mol^{-1}) were tested in the electrospinning process and fiber morphology was observed

through optical microscopy, FESEM electronic microscopy, and X-ray tomography. The choice of a convenient solvent for electrospinning PCL into fibers was discussed. Once the optimal polymer/solvent system was identified, their physicochemical and rheological properties were examined.

1.1. The Choice of Solvent for PCL

Solvent choice is an important parameter for optimal electrospinning as it influences both electrospinning process and quality of resulting fibers. For the Taylor cone to be formed and therefrom a liquid jet, high voltage has to overcome the surface tension of the solution used. By choosing a solvent with the low surface tension, Taylor cone formation could be facilitated. Concerning the quality of the fibers, for a given polymer, one could obtain porous, smooth, or ribbon-like fibrous structures where the solvent used for electrospinning plays an important role.[33,47] Additionally, humidity should be carefully controlled as it has a strong influence on solvent evaporation kinetics and consequently, the morphology of resulting fibers.[52] Thus, all these factors should be taken into consideration when choosing a solvent for electrospinning. Moreover, if the final purpose of the fibrous scaffolds is for tissue engineering, toxicity of the solvent and possible residues should be kept to a minimum.

There are many solvents suitable to dissolve PCL: chloroform, dichloromethane (DCM), dichloroethane (DCE), toluene, acetic and formic acid, tetrahydrofuran (THF), trifluoroethanol (TFE), etc. Table III.1 displays the solubility of PCL in each solvent and the morphology of electrospun fibers obtained. For a given solvent, dielectric constant (ε) and boiling temperature (T_b) reflect conductivity and volatility of that solvent. Mainly used solvents for electrospinning of PCL are chloroform, DCM and THF.[192] It is interesting to mention the successful use of acetone for electrospinning of PCL. Using acetone, which is a non-solvent for

PCL, Reneker *et al.*[206] electrospun uniform fibers without beads. However, the electrospun fibers obtained had micron diameters and large fiber diameter distributions.

solvent	solubility	ε*	T_b** (°C)	Fiber morphology
chloroform	high	4.81	61	smooth[44]
dichloromethane	high	8.93	40	smooth[44]
dichloroethane	high	10.45	84	smooth[207]
acetic acid	good	6.2	118	droplets[152]
formic acid	good	58	101	smooth[44]
tetrahydrofuran	good	7.58	66	smooth[44]
toluene	good	2.38	111	droplets[44]
trifluoroethanol	good	26.14	74	smooth[119]
acetone	poor	21.4	56	smooth[206,208]
methanol	poor	33	65	beads
N,N-dimethylformamide	poor	36.71	153	beads

*ε – dielectric constant at 20 °C; **T_b – boiling temperature

Table III.1. Physicochemical properties of solvents used for electrospinning of PCL; PCL solubility and fiber morphology

A frequent use of a solvent mixture in electrospinning of a polymer could be noticed in the literature.[192,209] Usually, that mixture consists of both solvent and non-solvent for polymer. This practice is introduced when fiber's morphology and/or processing conditions are not satisfactory when using only one solvent. Typically, small values of dielectric constant, low volatility, or a high surface tension of the polymer's solvent are adjusted with addition of a polymer's non-solvent. Ameliorated solution properties could then lead to increased efficiency of electrospinning process, influencing the fiber diameter and morphology.

Acetic acid alone does not allow electrospinning of PCL, and it is therefore used in combination with formic acid.[44,153] However, it is known that these acids trigger polymer

degradation over time.[210] When the solvent residue is present in the electrospun fibers, even after drying under vacuum, these acids might progressively deteriorate the mechanical properties of the electrospun scaffolds.[44]

Lee *et al.*[211] showed that between DCM alone and mixtures DCM/toluene and DCM/DMF, the latter one facilitates the electrospinning process while decreasing the fiber diameter drastically. DMF is also combined with the chloroform or THF[212–215] and successfully electrospun into fibers.

Another non-solvent often used for amelioration of solution conductivity is methanol. Pham *et al.*[216] used chloroform/methanol for electrospinning of PCL into multilayer nanofiber/microfiber scaffolds. Using dichloromethane/methanol solvent mixture, Luong-Van *et al.*[217] prepared uniform submicron PCL fibers with narrow fiber diameter distribution for controlled heparin release.

The choice of the solvent to be used in electrospinning of PCL in this study was established on the criteria of volatility, conductivity and targeting applications. In this study, it was aimed for less toxic, more volatile and conductive solvents to be used. Between the organic solvents at disposal for PCL, we chose the one that is volatile (chlorinated solvents over THF and organic acids), and less toxic (DCM over chloroform). DCM is a good solvent for PCL, volatile, thus easy to remove from the electrospun fibers. However, this solvent has rather low conductivity (dielectric constant ε_{DCM}=8.93 at 20 °C; see Table III.1) and additional solvent with higher conductivity should be introduced. Most commonly used conductive solvent is N,N-dimethylformamide (DMF), with its remarkable conductivity, but very low volatility (Table III.1). On the other hand, methanol (MeOH) has acceptable both conductivity and volatility (Table III.1). Thus, we chose DCM (solvent) and MeOH (non-solvent) to be used as electrospinning solvent mixture for PCL.

1.2. Morphology of Electrospun PCL Scaffolds

As mentioned previously, there are two options of commercially available PCL having high molecular weight: M_n = 45000 (PCL_{45}) and 70000 – 90000 g mol^{-1} (PCL_{80}). Before making a final choice of PCL to be adopted in future experiments, both PCL_{45} and PCL_{80} were tested in the electrospinning process. Different concentrations of these polymers were dissolved in dichloromethane/methanol 4/1 solvent mixtures and their morphology was observed with FESEM electron microscopy. It should be noted that DCM and MeOH are not miscible, and make a "micro-emulsion". However, as major solvent in the mixture is DCM, that is, a solvent for PCL, the emulsion character should not affect the solubility of PCL_{80} polymer. Addition of methanol was used to facilitate the charge conduction through the solvent during electrospinning.

Figure III.1 represents fibers electrospun from two different concentrations of PCL_{45} in DCM/MeOH 4/1 binary solvent system. f-PCL_{45}-20 (Figure III.1A) and f-PCL_{45}-30 (Figure III.1B) fibers were electrospun from 20 and 30 wt. % solutions of PCL_{45} in DCM/MeOH 4/1 binary solvent system, respectively. As it could be noticed from Figure III.1, f-PCL_{45}-20 fibers exhibit two distinctive diameter distributions: one of few hundreds of nanometers and the other one of several micrometers. f-PCL_{45}-30 fibers, on the other hand, show uniform fiber diameter size in the area of few microns. However, both concentrations demonstrated discontinuous trend of fiber formation with clearly visible breaking points, suggesting insufficient chain entanglements in the solution. Yet, higher concentrations led to very viscous solutions and consequently needle clogging before the liquid jet could be formed.

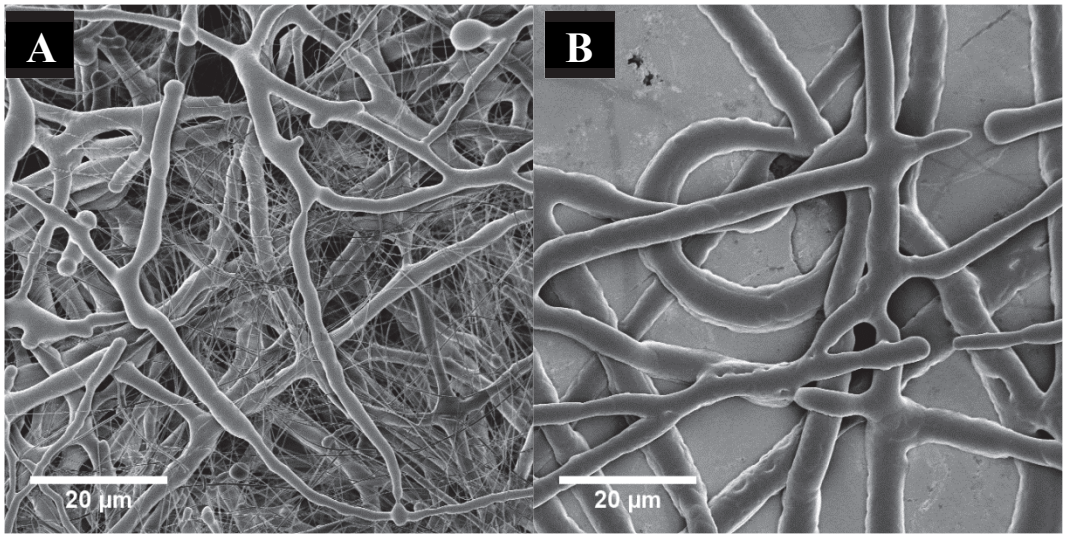

Figure III.1. FESEM images of (A) f-PCL_{45}-20 and (B) f-PCL_{45}-30 fibers electrospun from 20 and 30 wt. % of PCL_{45} in DCM/MeOH 4/1 solvent mixture

PCL_{80} was electrospun from several concentrations (5, 6, 7, and 8 wt. %) in DCM/MeOH 4/1 solvent mixture. Fibrous structures were collected onto the glass plates in the course of electrospinning and preliminary observation was done with the optical microscope in transmission mode (Figure III.2).

Figure III.2. Optical microscope images in transmittance of: (A) 5 wt. %, (B) 6 wt. %, (C) 7 wt. % and (D) 8 wt. % of PCL_{80} in DCM/MeOH 4/1 solvent mixture

In Figure III.2, the influence of polymer concentration on the fiber morphology could be observed. At low concentrations of 6 wt. % only beads were collected (Figure III.2A). By increasing the concentration to 7 wt. %, the "bead-on-string" phenomenon is observed (Figure III.2B). Further concentration increase lead over irregular (Figure III.2C) to uniform fiber

formation (Figure III.2D) without beads. It was therefore concluded that the optimal concentration of PCL_{80} in DCM/MeOH 4/1 mixture should not be lower than 8 wt. %. Indeed, the lowest PCL_{80} concentration reported so far in the literature is 7.5 wt. %.[218]

The concentration of 8 wt. % PCL_{80} was additionally tested in DCM/MeOH having two different volume ratios: 4/1 and 3/1 and electrospun fibers were observed with FESEM microscopy (Figure III.3). In similar electrospinning conditions, electrospun fibers from DCM/MeOH 4/1 (Figure III.3A) had thinner fiber diameters than those obtained from DCM/MeOH having 3/1 ratio (Figure III.3B).

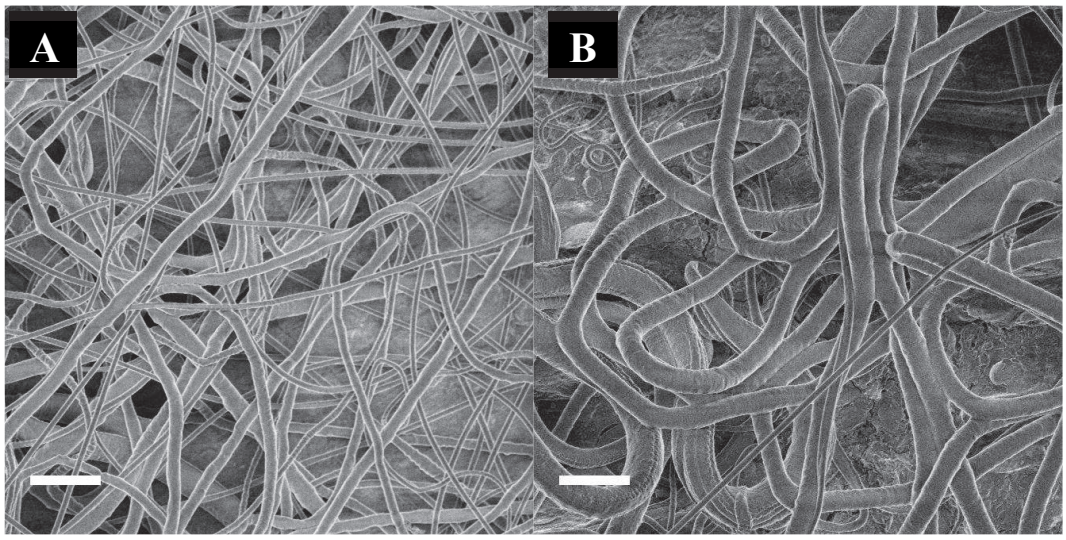

Figure III.3. Electrospun PCL fibers from 8 wt. % solutions of PCL_{80} in (A) DCM/MeOH 4/1 and (B) DCM/MeOH 3/1 solution mixtures; scale bar is 5 µm

According to previous observation, it was chosen DCM/MeOH solvent mixture with 4/1 ratio to be used for electrospinning of PCL.

1.3. Porosity of Randomly Collected PCL Fibers

An absolute method for determining the porosity of one material is by a mercury porosimeter. This method uses high pressures so the mercury could penetrate the smallest pores

of a material. In the case of electrospun fibers, porous structure is obtained by the slight merging of fibers at the juncture point. Using mercury porosity at high pressures, connection between the fibers and the inter-connected pores might be perturbed, misleading the results.[219] Nevertheless, this method could be successfully used for characterization of the pores present at the surface of electrospun fibers.[180]

Another possibility in determining the porosity of the fibrous scaffolds might be obtained from SEM images. The shortcoming of this method is that the porosity obtained is the one at the surface of the fibers.

The possibility of observing electrospun fibers using X rays from synchrotron source at ESRF facility in Grenoble was a unique opportunity for better understanding of 3D structure of these meshes. Herein, a nonwoven mesh of randomly deposited PCL fibers was observed with X-ray tomography technique (Figure III.4). A 3D cliché was reconstructed by stacking the individual image slices one on top of the other. From 3D image of PCL fibers, as high as 82% of porosity was determined, testifying the highly porous structure of electrospun nonwovens. These results should be however taken with precaution as the results strongly depend of the quality of image thresholding.

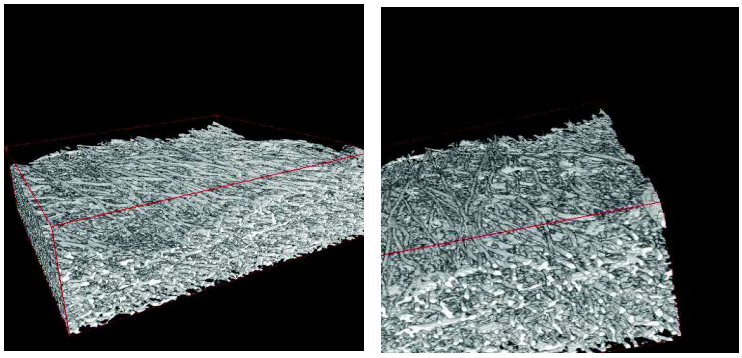

Figure III.4. Tomography-X images of randomly deposited f-PCL$_{80}$ fibers

Even though the images obtained by X-ray tomography cannot give the exact value of the porosity of PCL fibrous scaffold, they undoubtedly admit the highly porous structure that electrospinning process affords.

1.4. Viscosity Measurements of PCL_{80} in DCM/MeOH Solvent Mixture

Only when polymer chains are entangled in a solution, continuous liquid jet could be produced during electrospinning, leading to uniform and uninterrupted fiber formation.[38,177,220] It was determined that the polymer not only has to overcome the chain overlap concentration (c^*), but the entangled concentration (c_e) as well. McKee *et al.*[221] were the first to study rheological behavior of linear and branched polyesters, and later on polyelectrolytes,[222] predicting empirical correlations of solution rheology with electrospun fiber formation. Gupta *et al.*[37] studied linear PMMA-based homopolymers in a good solvent and gave a semi-empirical relationship between the fiber morphology (beads, beaded fibers, or uniform fibers) and polymer concentration and molecular weight.

Herein, using controlled-stress rheometer, the rheological study of PCL_{80} in DCM/MeOH 4/1 solvent mixture was carried out. The particularity of our case is a high volatility of the solvent mixture used. Thus, rheological measurements were performed at temperature lower than the ambient (15 °C) with anti-evaporation equipment. Figure III.5 represents the concentration dependence of zero-shear viscosity for PCL_{80} in DCM/MeOH 4/1 solvent mixture. Dashed lines are indicating the change in slope and three different concentration regimes. The first regime depicts semi-dilute concentration with unentangled polymer chains and lower viscosities; the second one is intermediate or semi-dilute entangled regime, and the last one, concentrated regime, with high viscosity. The boundary between semi-dilute unentangled and semi-dilute entangled regime represents the entangled concentration (c_e), while the second one marks the onset of the concentrated regime.

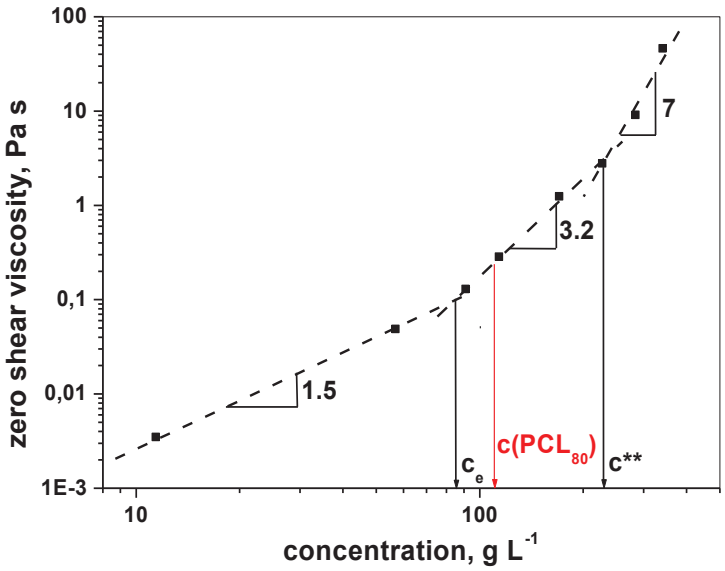

*Figure III.5. Zero-shear viscosity dependence from polymer concentration of PCL_{80} in the DCM/MeOH 4/1 solvent mixture at 15 °C with marked c_e and c** concentrations; dashed lines serve as an eye guide*

The concentration chosen in this study is 8 wt. % or about 110 g L^{-1}. Lying in the entanglement regime, this concentration ensures sufficient chain entanglements needed for continuous electrospinning process and uniform fiber formation.

Once the optimal solution and processing parameters of non-derived PCL_{80} were established, fiber bio-activation with carbohydrates using click chemistry concept followed. Hereafter, the study continues in the direction of PCL functionalization as:

- Low-molecular-weight PCL_2 end-modifications,
- Fiber's bulk-functionalization, and
- Surface-functionalization of electrospun fibers.

2. Chemical End-Modifications of PCL_2 Polymer

As mentioned previously, α,ω-poly(ε-caprolactone)-diol (PCL_2) was chosen to be chemically modified with clickable azide groups. The choice of azide over alkyl groups is particularly interesting as it offers the possibility to apply either copper-catalyzed[158] (using aliphatic alkyl moieties) or copper-free click chemistry[223] (using strained alkynes). We focused on copper-catalyzed click chemistry reactions, as a starting research point, while copper-free chemistry is envisioned for further development of the studies exposed herein.

In order to make bioactive materials out of PCL fibers, the carbohydrates were covalently coupled to the PCL chains using *bulk* and *surface* functionalization methods. The schematic representation of the strategies adopted is presented in the Scheme III.2.

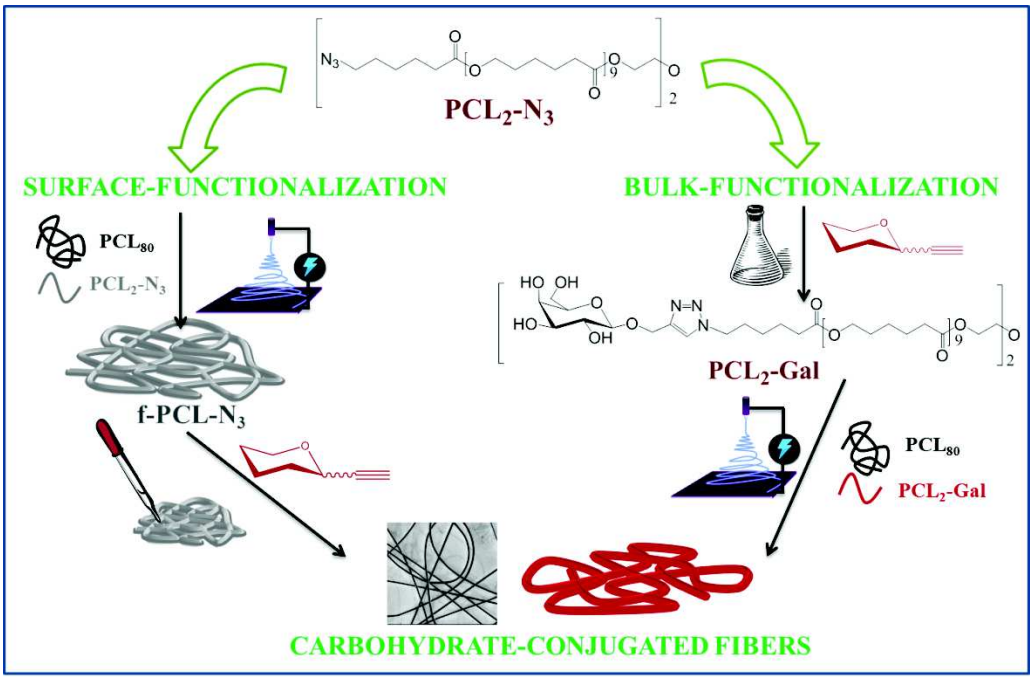

Scheme III.2. Illustrated representation of the bulk- and surface- functionalization process towards carbohydrate-decorated fibers

Bulk functionalization refers to PCL glycosylation in the fibrous bulk by simple blending of carbohydrate-modified low-molecular-weight PCL_2 with native high-molecular

weight PCL_{80}. This strategy offers the simplicity of carbohydrate coupling in the solution by using click chemistry and the variety of carbohydrate quantity to be loaded inside the fiber bulk.

Surface functionalization strategy relies on surface decoration of azide-functionalized fibers obtained from blending of azide-modified low-molecular-weight PCL_2 with native high-molecular weight PCL_{80}. Surface functionalization was obtained from click coupling of azido-fibers and alkyl-carbohydrates. This strategy has as advantage localization of bioactive carbohydrates only at the fibrous surface where they could reveal their activity.

Next chapters will be dealing with both bulk- and surface-modifications, defining their virtues and weaknesses within the qualitative and quantitative analyses.

2.1. Synthesis and Characterization of *α,ω*-Azide-poly(*ε*-caprolactone)

Modifications of the PCL_2, as depicted in Scheme III.3, took place at the chain ends, having as an objective to replace hydroxyl with azide groups. Reaction steps consisted of tosylation, giving an *α,ω-p*-toluenesulfonyl-poly(*ε*-caprolactone) (PCL-OTs) intermediate (52% yield), followed by nucleophilic substitution with sodium azide to finally afford *α,ω*-azide-poly(*ε*-caprolactone) $PCL\text{-}N_3$ (98% yield) as already described by Krouit *et al.*[224]

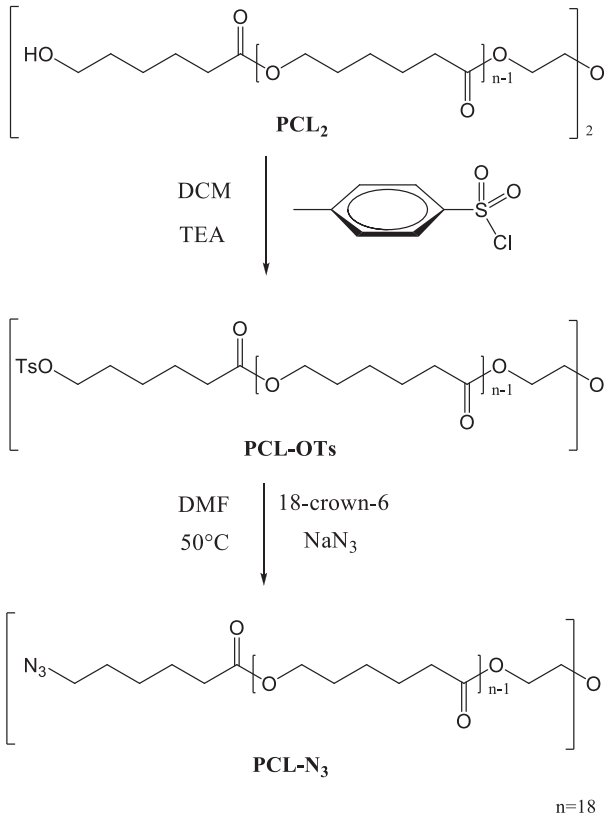

Scheme III.3. Preparation of PCL-N_3

Chemical transformations of the hydroxyl groups into tosyl and azido moieties were evidenced by ^{1}H NMR as represented in the Figure III.6A. Efficiency of the tosylation reaction was confirmed by the presence of characteristic signals of both aromatic and methyl group at 7.77-7.31 ppm and 2.42 ppm, respectively. Final substitution of the tosyl group into the azide functions was represented with the characteristic triplet at 3.26-3.23 ppm.

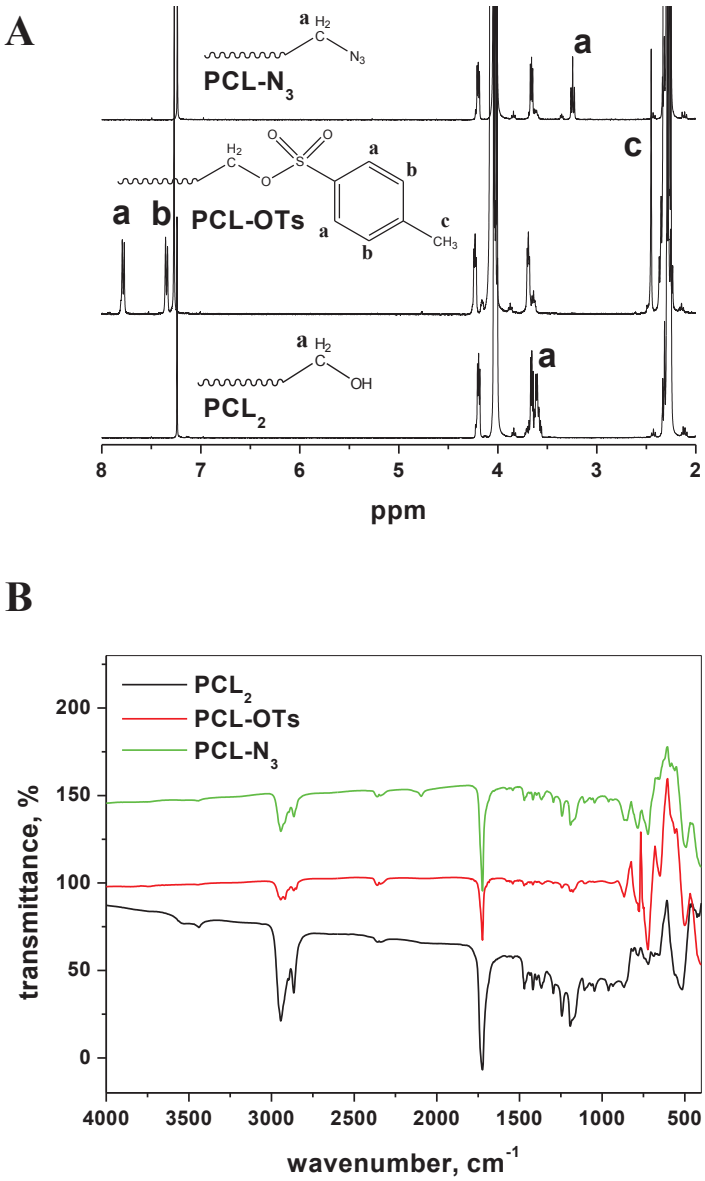

Figure III.6. (A) ^{1}H NMR (400 Hz) in $CDCl_3$ and (B) FTIR (CaF_2 optics) superposed spectra of the PCL_2, PCL-OTs and PCL-N_3 polymers

Figure III.6B represents FTIR spectra of: native PCL_2 (black line) and end modified PCL_2-OTs (red line), and PCL_2-N_3 (green line) polymers. PCL_2-OTs spectrum showed characteristic absorptions at 790 cm^{-1} attributed to aromatic ring and 720 cm^{-1} for (C-O-S) groups. PCL_2-N_3 spectrum, clearly showing absorption at 2100 cm^{-1} of (N=N) azide groups, confirms the chemical transformations of the PCL_2 polymer.

MALDI-TOF MS analyses were done as additional test for confirmation of successful PCL end-modification. PCL-OTs polymer was found to be functionalized at both ends. However, from MALDI-TOF MS spectrum of PCL-N_3 polymer, NH_2-derivatized PCL was observed. Li *et al.*[225] noticed that polymers containing azide groups are sensitive to form metastable ions in MALDI-TOF mass spectroscopy. The phenomenon of azide reduction into amines was observed by Peltier *et al.*,[226] denoting that end-functionalization of PCL_2 with azides did take place.

2.2. Synthesis and Characterization of *α,ω*-galactosyl-poly(*ε*-caprolactone)

Carbohydrate-conjugated polymers have emerged as important biomaterial systems.[227] Numerous reports testify their use for immobilization of proteins,[202] as cell's surface mimics,[203] cell adhesion as well as for many pharmacological and biomedical applications.[204]

Ring-opening polymerization has been reported by Persson *et al.*[228] and Xu *et al.*,[167] to provide access to carbohydrate-functionalized PCL. In this study, we used click chemistry approach onto previously synthesized PCL-N_3 polymer to provide covalently attached galactosyl ligands to the PCL_2 chains. The synthesis was followed by characterization with NMR, FTIR and MADLDI-TOF mass spectroscopy.

^{1}H NMR signals (Figure III.7A) of PCL_2-Gal spectrum at δ=8.03 ppm, indicate the formation of triazole ring, and those at δ=4.81 ppm of anomeric proton of *β*-D-galactoside show successful PCL end-functionalization.

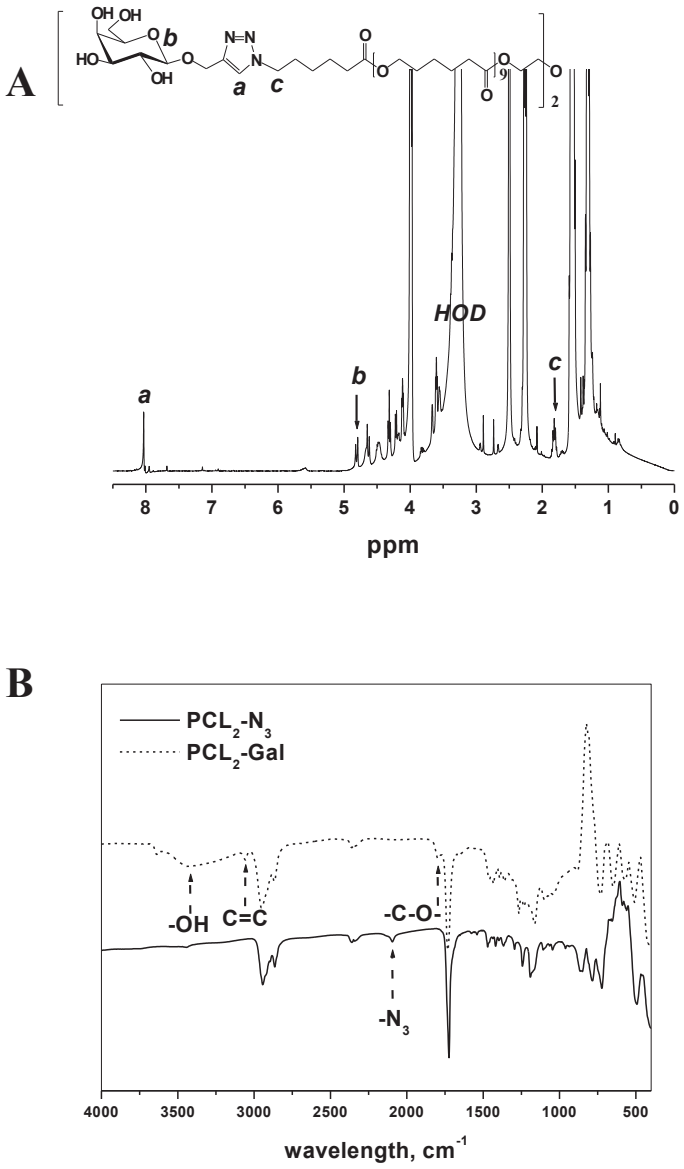

Figure III.7. (A) ^{1}H NMR spectrum of the PCL_2-Gal in DMSO-d_6 and (B) FTIR spectra attesting of chemical transformation from PCL_2-N_3 to PCL_2-Gal

FTIR spectra on Figure III.7B show the transformation of PCL_2-N_3 to PCL_2-Gal polymer. Azide groups identified by the peak at 2100 cm^{-1} were successfully transformed into triazole ring, covalently associating the galactose units with the PCL macromolecular chain. The presence of galactose and triazole ring were confirmed by stretching vibrations at 3500 cm^{-1} (O-H), 3060 cm^{-1} (C=C), 1792 cm^{-1} ($C=C_{triazole}$) and 1650 cm^{-1} (C-O).

The MALDI-TOF MS spectrum of PCL_2-Gal is given in Figure III.8. The distribution of mass population in centered around m/z = 3355.3 corresponding to the α,ω-galactoside propargyl poly(ε-caprolactone) having degree of polymerization of DP=24. The distance between other isotopic peaks is constant and corresponds to the molecular weight of ε-caprolactone monomer unit. This spectrum undoubtedly confirms the successful PCL_2 functionalization with β-D-galactoside at both chain ends.

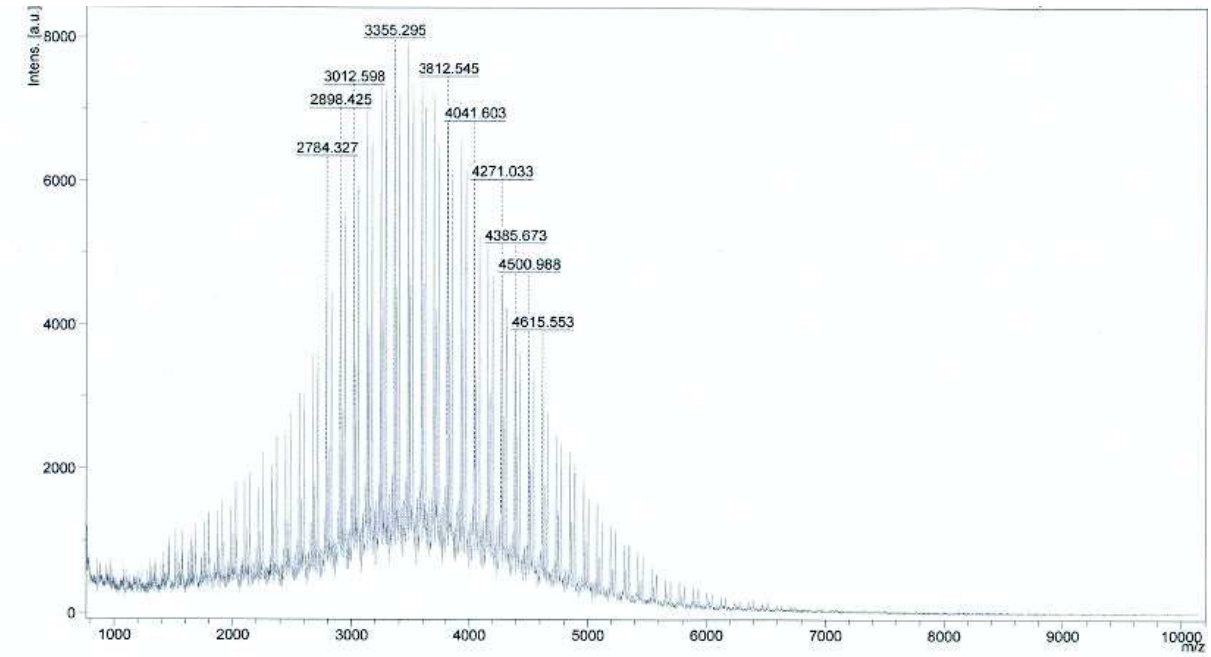

Figure III.8. MALDI-TOF MS spectrum of PCL_2-Gal polymer in linear mode

Further use of PCL_2-Gal polymer for fiber functionalization purposes was exposed in the next subtitle on the subject of fiber's bulk functionalization. The bulk functionalization consists in simply blending PCL_2-Gal and PCL_{80} in DCM/MeOH solvent mixture. Surface morphology and physicochemical properties of electrospun fibers were studied and discussed extensively.

3. Bulk-Functionalization of PCL Fibers Through Blending of End-Functionalized and Native Poly(ε-caprolactone)s

Blending of non-derived polymer with another functional molecule prior to electrospinning could significantly enrich the physicochemical properties of the final fibers.[229,230] One of such examples is the study of Yu *et al.*[231] who fabricated biodegradable PCL fibers from PCL/collagen blend and those scaffolds were successfully applied as nerve guide conduits. Yang *et al.*[121] turned hydrophobic poly(L-lactic acid) (PLLA) fibers to completely hydrophilic mats by blending and further crosslinking of gelatin with PLLA.

In this study, in order to introduce the functionalities into PCL fibrous meshes, end-modified PCL_2 polymers were blended with native PCL_{80} and electrospun in different mass ratios. Depending of the functional group introduced at the chain ends (azide of sugar), different fibrous structures were obtained. Their morphology and physicochemical characteristics will be discussed in detail in the chapters that follow.

3.1 PCL_{80}/PCL-N_3 Fibers – Their Processing and Morphology

Blends of high-molecular-weight PCL_{80} (M_n ~ 80000 g mol^{-1}) and low-molecular-weight PCL_2-N_3 (M_n ~ 2400 g mol^{-1}) were used in different ratios in the electrospinning process. PCL_{80} provides optimal electrospinning conditions and good mechanical properties[212,232] of the fibers while PCL_2-N_3 is used to functionalize the fibers. Different concentrations of PCL_{80}/PCL_2-N_3 blend were prepared prior electrospinning and their detailed solution composition and electrospinning parameters are presented in Table III.2. Polymer solutions were prepared in such a way that individual PCL_{80} concentration was always kept above its entanglement concentration (c_e) determined previously.[37,221]

Electrospun fibers	Total Polymer wt. %	PCL_{80} wt. %	PCL_2-N_3 wt. %	Flow rate mL/min	Voltage kV	RH[a] %	AFD[b] nm
PCL_{80}	8	8	0	0,01	13	5	591 ± 283
f-PCL-N_3 -20	10	8	2	0,015	14	9	567 ± 301
f-PCL-N_3-40	16	9,6	6,4	0,015	14	0	547 ± 68
f-PCL-N_3-60	23	9,2	13,8	0,02	13	6	694 ± 149

[a]Relative humidity

[b]Average fiber diameter ± standard deviation

Table III.2. Electrospinning parameters for non-derivative PCL_{80} and azide-functionalized fibers: f-PCL_2-N_3 -20, -40 and -60 and their mean diameter

PCL_2-N_3 polymer was blended with PCL_{80} at different ratios, and electrospun fibers were marked as f-PCL-N_3-20, f-PCL-N_3-40, f-PCL-N_3-60, corresponding to 20 wt. %, 40 wt. % and 60 wt. % of PCL_2-N_3 respectively. 60 wt. % of functionalized PCL_2-N_3 in the blend was the upper limit for obtaining the uniform bead-free fibers with submicron diameters.

Fibers were closely observed with FESEM microscopy. FESEM images in Figure III.9A-D show uniform and smooth fibers with comparable size diameters of both native f-PCL_{80} and azide-functionalized f-PCL_2-N_3 fibers. This trend indicates that the presence of azide-functionalized PCL_2 does not influence significantly the diameter and morphology of the fibers.

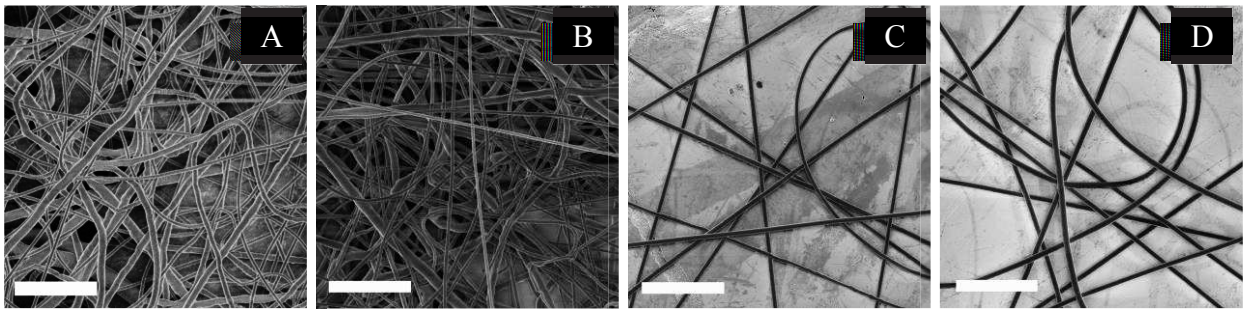

Figure III.9. FESEM images (A-D) of f-PCL_{80} fibers containing: 0 wt. % (A), 20 wt. % (B), 40 wt. % (C) and 60 wt. % (D) of PCL-N_3. Scale bar 10 µm

Using FESEM images, the average fiber diameter was obtained as a mean value of 150 diameter measurements. The statistical analysis of all fiber diameters measured show rather constant value of about 600 nm (see Table III.2) and a slender fiber-diameter distribution under dry air atmosphere. It is interesting to notice that keeping the PCL_{80} concentration nearly constant while increasing the concentration of PCL_2-N_3 did not influence the fiber diameter. This could be explained by the fact that only high-molecular-weight polymer influences the chain entanglements and therefrom the fiber formation. Thus, if the concentration of PCL_{80} is kept constant, as it is the case here, additional content of low-molecular-weight polymer, herein functionalized PCL_2, would not give contribution to chain entanglement nor fiber formation.

However, before going into any deeper consideration of fiber-diameter trend, additional analyses have to be made. Consequently, the influence of solution composition on their rheological behavior was investigated. Relationship between the solution rheological properties and final diameter of electrospun fibers is discussed in the next subtitle.

3.1.1 Rheological Analysis of PCL_2-N_3/PCL_{80} Blends

The effect of azide groups and low-molecular-weight PCL_2 chains on rheological behavior of the solution was investigated. Figure III.10 represents the zero-shear viscosity as a function of shear rate for PCL_{80} homopolymer solution and PCL_{80}/PCL_2 and PCL_{80}/PCL_2-N_3

80/20 blends in DCM/MeOH 4/1 solvent mixture. In the range of shear rate investigated, all polymeric solutions showed a Newtonian behavior.

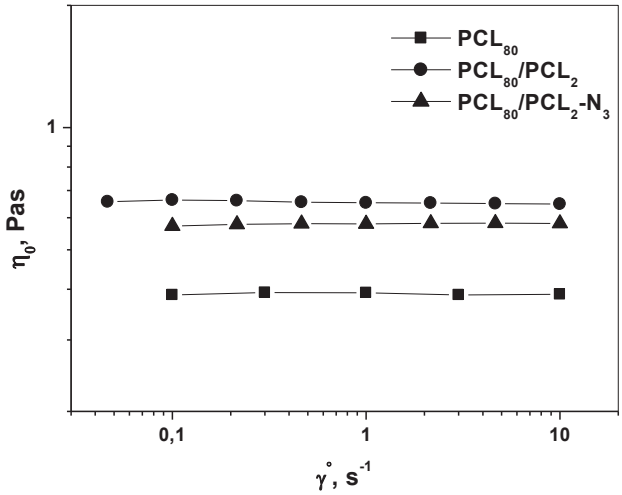

Figure III.10. Zero-shear viscosities of 8 wt. % PCL_{80} polymer solutions in DCM/MeOH 4/1 solvent mixture containing: 0 wt. % additives (■), 2 wt. % PCL_2 (●) and 2 wt. % PCL_2-N_3 (▲) measured at 10 °C

In the presence of low-molecular-weight PCL_2, the viscosity curve of blends is slightly shifted towards higher values, due to increase in concentration, but not sufficiently to increase the fiber diameter. Consequently, the fiber diameter appears to be directed by high-molecular-weight polymer chains, as previously suspected. Moreover, viscosity curves of functionalized PCL_{80}/PCL_2-N_3 and non-functionalized PCL_{80}/PCL_2 blends are nearly superimposed, showing that no significant associative interactions between the azide groups and PCL chains occur in this blend. Indeed, the density of azide groups is low and the solvent mixture is mostly nonpolar, restricting intra and intermolecular associations through hydrogen bonding. These results could explain the constant diameter of the electrospun fibers observed by FESEM.

3.1.2 Quantification of Azide Groups Present on the Surface of the Fibers

To the best of our knowledge there is no direct test for quantification of azides. In order to quantify azide groups available at the surface of electrospun f-PCL-N_3 fibrous scaffolds,

some indirect method should be employed. Punna *et al.*[233] reported a convenient colorimetric test for identification of aliphatic azides. Their method consists of azide reduction to amine by phosphine followed by standard ninhydrin (Keiser) test. Specific for amine quantification, ninhydrin method was successfully applied on solid electrospun fibers. While Mattanavee *et al.*[193] used this method for quantification of amines, Zander *et al.*[194] quantified grafted proteins at the surface of electrospun PCL fibers.

In this study, we adjusted the azide-detection method described previously for quantification of azides present only at the surface of the fibers. Surface azides of f-PCL_2-N_3 fibers were reduced with triphenylphosphine (PPh_3) in heterogeneous conditions (fibers-ethanol). Resulting amino-fibers were dissolved in 1,4-dioxane and finally quantified using ninhydrin assay.[234,235] Concentrations of the PCL_2-N_3 on the surface were calculated from the calibration curve (Figure IV.1, Materials and Methods).

The results of the ninhydrin assay are summarized in Figure III.11. Weight percentage of PCL_2-N_3 on the surface represents experimentally-found mass of PCL_2-N_3 per total mass of the sample, and it is expressed as experimental value (in grey) while initial concentration of PCL_2-N_3 in the electrospinning solution is represented in white. Total amount of azides (Figure III.11, white columns) is the amount of PCL_2-N_3 initially present in the solution (Table III.2). The difference between gray and white column stands for a non-accessible PCL_2-N_3 mass per cent inside the fibers or the film. Figure III.11 clearly points out that, for the electrospun fibers, about 80% of functionalized azide groups are located on the fiber's surface. Additionally, one could see that by increasing the PCL_2-N_3 concentration in the solution (from 20 to 60 wt. % of total polymer weight) the concentration of azides at the surface of the fibers increased accordingly. It should be noted that, without the PPh_3 reducing agent, these fibers showed no

specific coloration under ninhydrin assay, proving that the azide groups were intact during the electrospinning process.

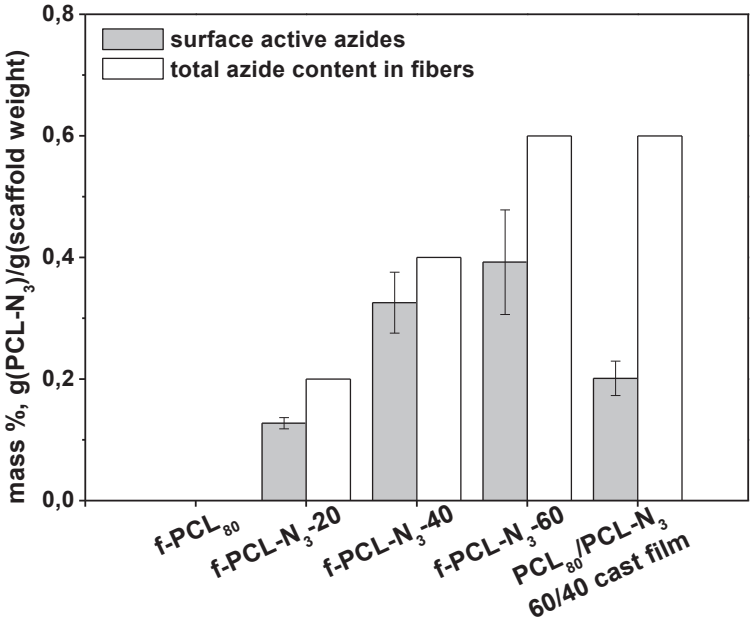

Figure III.11. Quantification of azides groups on the surface of the f-PCL_{80}, f-PCL-N_3-20, f-PCL-N_3-40, f-PCL-N_3-60 fibers that contain 0, 20, 40, 60 and 60 mass % of the functionalized PCL_2-N_3, respectively and PCL_{80}/PCL_2-N_3 40/60 cast film

Colorimetric results, done on all the f-PCL_2-N_3 fibers, suggest a surface aggregation of the azides groups. The question is if this phenomenon is caused by a spontaneous aggregation of azide groups to the solution/air interface or induced by the electric field? Hardman and coworkers[236] observed that addition of even small quantities of fluorocarbon (CF) functionalized polymer additives to polystyrene solution results in their surface segregation during electrospinning. However, they remind that the segregation of CF groups occurs even without the action of the electric field.[237] Stachewitz and Barber[238,239] indicated to the chemical group orientation at the surface of electrospun fibers due to polar contribution of polyamide 6 chains. They observed similar behavior in a cast film after mechanical drawing above the glass-

transition temperature. As clearly demonstrated by Fu *et al.*,[240] for PS bearing polar alkyl-bromide group (C-Br), such segregation can be significantly enhanced by the polarization of chemical groups induced by the electric field. Indeed, positive charges of polymer jet drive alkyl bromide groups to the surface by electrostatic interactions, while for the nanofibers electrospun with an anode positioned at spinneret, unpolarized C-Br groups remain in the bulk. Sun *et al.*[241] showed that the electric field used in electrospinning could promote surface segregation of not only small chemical groups but also large peptide segments. On the other hand, Gentsch *et al.*[242] highlight that polymer aggregation at the fibers' surface is not always due to the electric field applied. In the study of Sun *et al.*,[241] surface functionalization of peptide-polymer conjugate is field-driven. Analyzing the electrospun fibers of a synthetic peptide, Gentsch *et al.*,[242] showed that electric field played minor role, while the polarity of the solvent mixture was primarily responsible for the peptide surface aggregation. It is therefore important to reveal the real nature of azide aggregation phenomenon observed in this study.

It is known that azide groups can be polarized and bear partially negative charges (δ-).[243] In our case, PCL_{80}/PCL_2-N_3 fibers have been obtained by using a cathode on the spinneret (Scheme III.3). Consequently, it is reasonable to consider that azide group migration at fiber's surface could be induced principally by electric field even if the spontaneous migration of azide groups towards the air/liquid interface cannot be excluded.

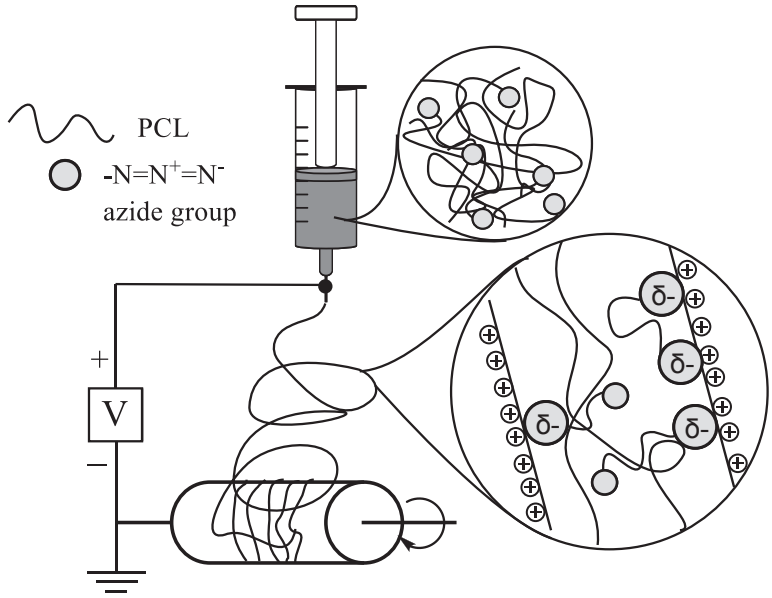

Scheme III.3. Schematic representation of the electrospinning setup with illustrated electrostatic attractions between negatively polarized azides (δ-) and positively charged surface during the electrospinning

In order to investigate possible spontaneous azide migration to the surface, a cast polymer film from the PCL_{80}/PCL_2-N_3 (40/60) blend in DCM/MeOH (volume ratio 4/1) solvent mixture was prepared. Azide groups at the surface were quantified following the same procedure as for the fibrous scaffold. The colorimetric measurements performed on the cast film showed only 20% of the azides on the surface (see Figure III.11). Considering the slow evaporation kinetics of few minutes for the cast film, polymer chains as well as chemical groups have the ability to find spontaneously preferable conformation. This result has to be compared with the extremely fast evaporation kinetics of about few milliseconds for the electrospun fibers where about 80% of azide groups were located at the fiber surface. The evaporation process of volatile solvents is extremely fast during electrospinning and this spontaneous migration, hindered by the sharp increase of the solution viscosity, is only partial. Consequently, surface segregation of azide groups is likely due to electrically induced polarization rather than spontaneous interface attraction.

3.2 Electrospinning of PCL_2-Gal/PCL_{80} Blend and Fiber Morphology Analysis

Blending of PCL_2-Gal with native PCL_{80} was employed to improve the bioactivity of electrospun nonwovens. Carbohydrate-conjugated polyesters have already shown beneficial results in cell-material interactions. Thus, they are often used as scaffolds for tissue engineering.[227,244]

Glycosylated polymer, PCL_2-Gal, was blended with a high molecular weight PCL_{80} in dichloromethane/methanol (DCM/MeOH 4/1) solvent mixture. PCL_{80}/PCL_2-Gal 80/20 and 60/40 blends were electrospun and f-PCL_{20}-Gal_B and f-PCL_{40}-Gal_B fibrous mats were obtained, respectively.

Fiber morphology was analyzed with the FESEM electronic microscope. The images obtained, show rather interesting fiber-diameter trend (Figure III.12). While the average fiber diameter of native PCL_{80} was 591 nm, it increased to 1.1 µm for f-PCL_{20}-Gal_B and reached 2.4 µm for f-PCL_{40}-Gal_B fibers. Concurrently, the increasing content of PCL_2-Gal reduced the ability to electrospin the blend and led to heterogeneous fibers in diameter (Figure III.12D). While introducing PCL-N_3 within the bulk fibers did not alter the fiber morphology (see previous subtitle 3.1. of this chapter), galactose moieties in f-PCL-Gal_B nonwovens changed dramatically both morphology and diameter of final fibers.

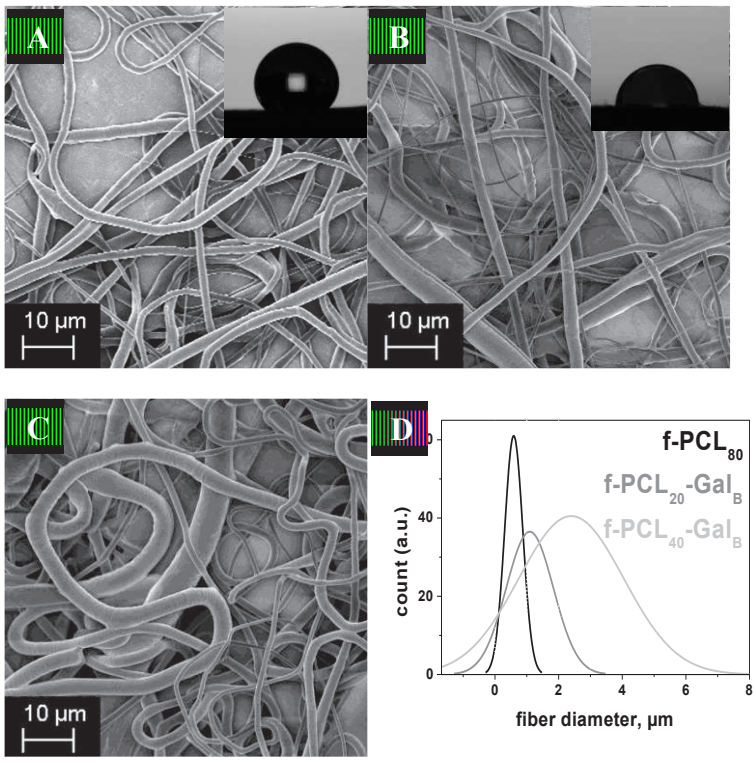

Figure III.12. (A-C) FESEM images of Pt-coated: (A) f-PCL$_{80}$ non-derived fibers, sugar-decorated: (B) f-PCL$_{20}$-Gal$_B$ and (C) f-PCL$_{40}$-Gal$_B$ fibers and (D) their graphical representations of fiber diameter distributions. The insets A and B represent the water sessile drops onto the PCL$_{80}$ and f-PCL$_{20}$-Gal$_B$ fibers, respectively

Hydrophilicity of the electrospun fibers was investigated using water-contact-angle (WCA) measurements. WCA of native f-PCL$_{80}$ and bulk-functionalized f-PCL$_{20}$-Gal$_B$ fibers are presented as inset in Figure III.12A and III.12B, respectively. In the case for f-PCL$_{40}$-Gal$_B$ fibers, the contact angle was not measured as the polymer solution showed low electrospinnability and a sufficient fibrous layer for the WCA observations could not be formed. Water contact angles (WCA) of f-PCL$_{80}$ and f-PCL$_{20}$-Gal$_B$ fibers show gentle decrease from 130° to 90°, respectively. These findings indicate to the presence of Gal units on the surface of the fibers. Yet, WCA gives only an estimation of the fiber functionalization success, and further quantification of the galactoside moieties will succeed.

3.2.1 Quantification of Galactose Present at the Fiber's Surface

Quantification analysis of the carbohydrates, present at the surface of bulk-functionalized fibers, was carried out by a combination of enzymatic hydrolysis and Dubois assay. Enzymatic hydrolysis of carbohydrates is based on their catalytic decomposition in the presence of enzymes, in aqueous media and at specific pH and temperature conditions. Phenol-sulfuric acid colorimetric method, known also as Dubois assay, is used for detection of micro-quantities of reducing sugars, oligo- and polysaccharides and their derivatives.[245] In the presence of concentrated sulfuric acid and phenol, strong orange-yellow coloration of the solution appears, indicating to the presence of carbohydrates in the solution. The intensity of the solution coloration is a linear function of the sugar concentration in that solution.

f-PCL_{20}-Gal_B and f-PCL_{40}-Gal_B fibers were exposed to enzymatic treatment with β-galactosidase (*Aspergillus oryzae*), followed with Dubois assay on the supernatant reaction to determine the concentration of the sugars released. Colorimetric results showed rather small content (2-3 wt. %) of galactose in both f-PCL_{20}-Gal_B and f-PCL_{40}-Gal_B fibers, indicating a low surface functionality of the drawn fibers. Nevertheless, phenol-sulfuric acid test, done directly on the glycosylated fibers, confirmed the initial concentration of carbohydrates present in the blend of PCL_2-Gal with PCL_{80} prior electrospinning, showing that the electrospinning process does not harm the chemical structure of carbohydrates.

Detailed study of physicochemical properties of bulk-functionalized fibers, showed the tendency of moderate improvements of both wetting and surface functionalization of f-PCL-Gal_B fibers as well as their micron diameters with the large diameter distributions. These results open several questions:

- What caused such drastic difference in fiber morphology between azide- and galactoside- bulk-functionalized fibers if only polymer chain ends were modified?
- While azide groups of PCL_2-N_3 showed high tendency of surface aggregation, why such a small surface decoration is observed when PCL_2-Gal is used?
- Might this trend be related to inter-, intra-molecular interactions or rather polymer-solvent interactions?

To answer these questions, interactions between the polymer chains as well as polymer-solvent interactions were studied through dynamic light scattering (DLS) and viscosity measurements, detailed in the next subtitles.

3.2.2 Dynamic Light Scattering Analysis of PCL_2-Gal in DCM/MeOH 4/1 Solvent Mixture

Dynamic light scattering (DLS) might offer the information of the particles' size in the solution and their possible organization (aggregates, micelles, etc.). Figure III.13 represents the DLS size distribution curves of the DCM/MeOH 4/1 solution alone and containing PCL_2-Gal polymer in small amounts.

In the case of the DCM/MeOH 4/1 solvent mixture alone the objects with a radius of few tens of micrometers are observed. It alludes to the emulsion character of the two partially miscible solvents, with MeOH droplets dispersed in the DCM medium. In the presence of polymer PCL_2-Gal, an additional peak at R_h ~ 350 nm is observed. These results are indicating the formation of aggregates of PCL_2-Gal polymer in DCM/MeOH solvent mixture (~350 nm), together with MeOH droplets (~40 µm).

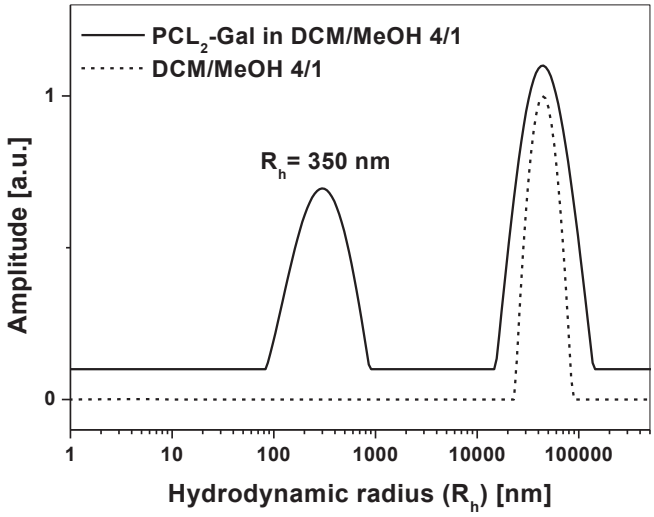

Figure III.13. Size distribution of DCM/MeOH 4/1 solvent mixture alone (dashed line) and with PCL_2-Gal dissolved in it (solid line), at 90°

At that point, it should be kept in mind that the DLS size distribution shown on the Figure III.13 is mass-weighted: larger objects contribute much stronger to the amplitude. To convert in a simple way this mass-weighted into number-weighted distribution, the equation given somewhere else is used:[246] since ~350 nm and ~50 µm objects are present, and since the percentage of the total surface area corresponding to the surface area under the peak related to the small objects is ~29%, one obtains $N_{Small} \sim 10^6 \times N_{Big}$ (N_{Small} and N_{Big} designate the number of small and big objects, respectively). Thus, small particles represent the majority in number.

3.2.3 Rheological Analysis of PCL_2-Gal/PCL_{80} Blend in Solution

Viscosity measurements were performed on polymer solutions of PCL_{80} (8 wt. %) and on blends PCL_{80}/PCL_2, PCL_{80}/PCL_2-N_3 and PCL_{80}/PCL_2-Gal at ratio of 80/20 and total polymer concentration of 10 wt. % and at 10 °C. Figure III.14 shows the viscosity of polymer solutions as a function of the shear rate of all the solutions tested. PCL_{80} and blends of PCL_{80}/PCL_2 and PCL_{80}/PCL_2-N_3 are Newtonian in the shear-rate range explored. As expected, the viscosity of blends is higher than the pure PCL_{80}. The slight decrease of PCL_{80}/PCL_2-N_3 viscosity compared

to that of PCL_{80}/PCL_2 could be assigned to a decrease of the density of intermolecular hydrogen bonding induced by the presence of N_3 groups. However, the flow behavior of the sugar-conjugated PCL_{80}/PCL_2-Gal solution is extremely different, exhibiting a significant shear-thinning behavior at low shear rates.

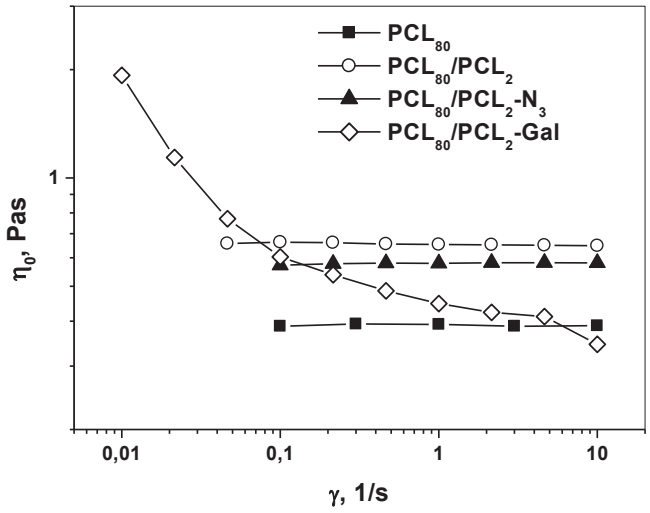

Figure III.14. Zero-shear viscosity/shear rate profiles for polymer mixtures of 8 wt. % PCL_{80} and: (■) without PCL_2, and with: (○) 2 wt. % of PCL_2, (▲) 2 wt. % PCL_2-N_3 and (◇) 2 wt. % of PCL_2-Gal

It was hypothesized that the amphiphilic structure of PCL_2-Gal might lead to the formation of a transient network of PCL chains and intermolecular interactions between the galactose groups and PCL chains. The schematic representation of this hypothesis is shown in the Scheme III.4. PCL chains are represented as irregular gray lines, and galactose units, attached to the shorter PCL chains, are represented as orange dots, all dispersed in DCM medium. It is hypothesized that the galactose units, non-soluble in DCM, will be stabilized in the methanol domains or as aggregates within hydrophobic PCL chains orientated towards DCM medium. These complex lyophobic/lyophilic polymer-solvent and polymer-polymer interactions might lead to the transient network formation in the solution.

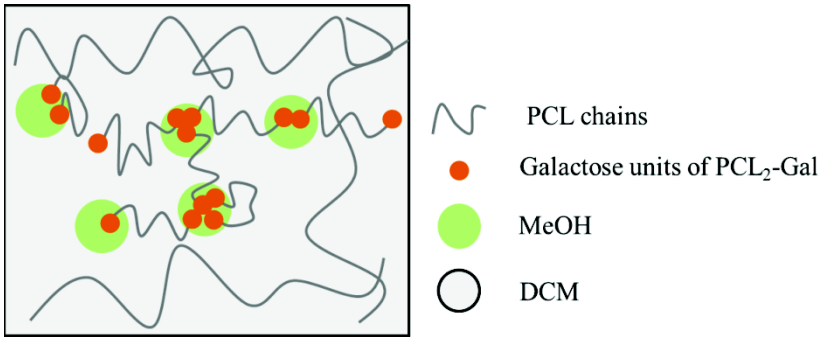

Scheme III.4. Schematic representation of the PCL_2-Gal/PCL_{80} polymer organization in the DCM/MeOH 4/1 solvent mixture

The presence of inter-chain complexes could further induce the steric interactions responsible for the significant increase in the solution viscosity and the polymer fibers' diameter. This behavior was observed by Yu *et al.*[247] in a mixture of phosphatidylcholine surfactant and polyvinylpyrrolidone (PVP) polymer in chloroform. Indeed, in the solvent mixture of DCM (polar, aprotic, good solvent for PCL) and MeOH (polar, protic, non-solvent for PCL but good solvent for galactose) (4/1), galactosyl units of PCL_2-Gal might tend to aggregate inside the methanol "microemulsions", forming aggregated galactose domains in MeOH and PCL chain domains in DCM, as illustrated in Scheme III.4. Gentsch *et al.*[242] already observed the aggregation phenomenon of the low-molecular-weight peptide-PLLA amphiphile in chlorinated solvents.

DLS and rheological results in this study suggest that, during the electrospinning process, galactose units would tend to stay enclosed in the MeOH domains, ending inside the electrospun fibers and leading to their irregular and micrometric diameters as observed by FESEM images. Enzyme hydrolysis and water-contact-angle tests go in behalf of such hypothesis, confirming that the galactose remained inside the fiber bulk and limited the surface functionality of these fibers.

4. Surface-Functionalization of f-PCL-N_3 Fibers

While previous chapter was studying the fiber functionalization from the bulk, this one will be dealing with the functionalization at the surface of the fibers. Because of the strong affinity for azide surface aggregation under high electric field, clickable f-PCL-N_3 fibers were chosen as a basis for further surface functionalization.

The aim of surface functionalization was to efficiently decorate the surface of the electrospun fibers with carbohydrates as bioactive molecules. The availability of azide groups at the fibrous surface was visualized by attaching the fluorescent dyes. The resulting fluorescent fibers were then characterized with confocal microscope. Carbohydrate-decorated fibers were characterized using colorimetric Dubois assay, enzyme-linked lectin assay, contact angle and FTIR spectroscopy measurements.

4.1 Fluorescent Labeling of f-PCL-N_3 Fibers

Fluorescent labeling of f-PCL-N_3 fibers with FITC-alkyne fluorophore using click chemistry enabled us to investigate the accessibility and reactivity of the surface azides. f-PCL_{80}, f-PCL-N_3 -20, -40 and -60 fibrous scaffolds were incubated with the FITC-alkyne fluorophore dissolved in acetonitrile/water 1/1 solvent mixture, with and without copper(I)/sodium ascorbate catalysts.

In Figure III.15, the fluorescent (E-H) and bright-field (A-D) images of f-PCL_{80} (A, E), f-PCL-N_3-20 (B, F), f-PCL-N_3-40 (C, G), and f-PCL-N_3-60 (D, H) fibers are showed after 48h incubation with FITC-propargyl fluorophore without the copper(I)/ascorbate catalysts. As it could be seen, without the catalysts, all tested samples exhibited no fiber coloration, demonstrating that non-specific adsorption of the FITC fluorophore on the PCL does not occur.

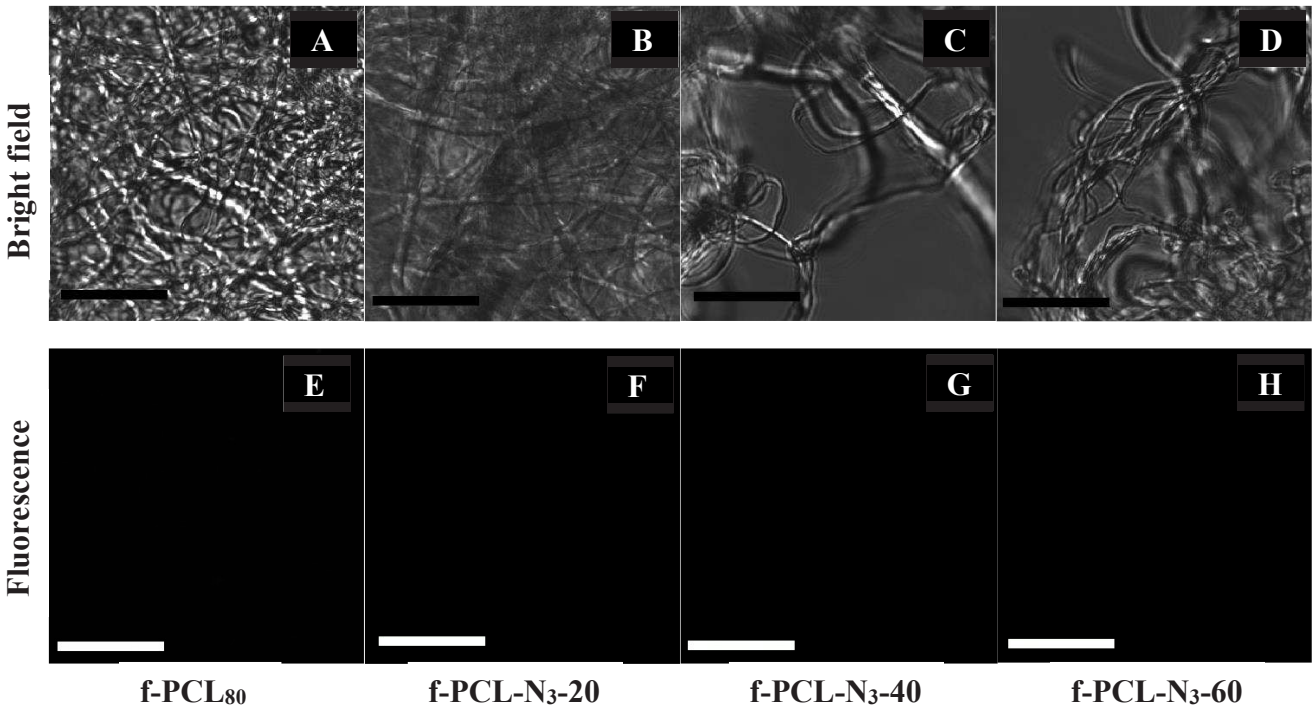

Figure III.15. Bright field images (A-D) and fluorescent images (E-H) of f-PCL$_{80}$, f-PCL-N$_3$-20, f-PCL-N$_3$-40 and f-PCL-N$_3$-60 fibers, respectively, after 48h with FITC-alkyne in acetonitrile/water solution without the catalysts; scale bar 20 µm.

Figure III.16 represents the same *f-PCL$_{80}$, f-PCL-N$_3$-20, f-PCL-N$_3$-40 and f-PCL-N$_3$-60 fibers* after 48h incubation in the acetonitrile/water solution containing both FITC-propargyl fluorophore and click catalysts. In the presence of catalysts, f-PCL$_{80}$ remained non-colored while azide-containing fibers f-PCL-N$_3$-20, -40 and -60 showed strong fluorescence at 520 nm and uniform coloration on the surface (Figure III.16E-H). These results are attesting not only the accessibility and reactivity of the surface azides but also a high selectivity of the click coupling reaction.

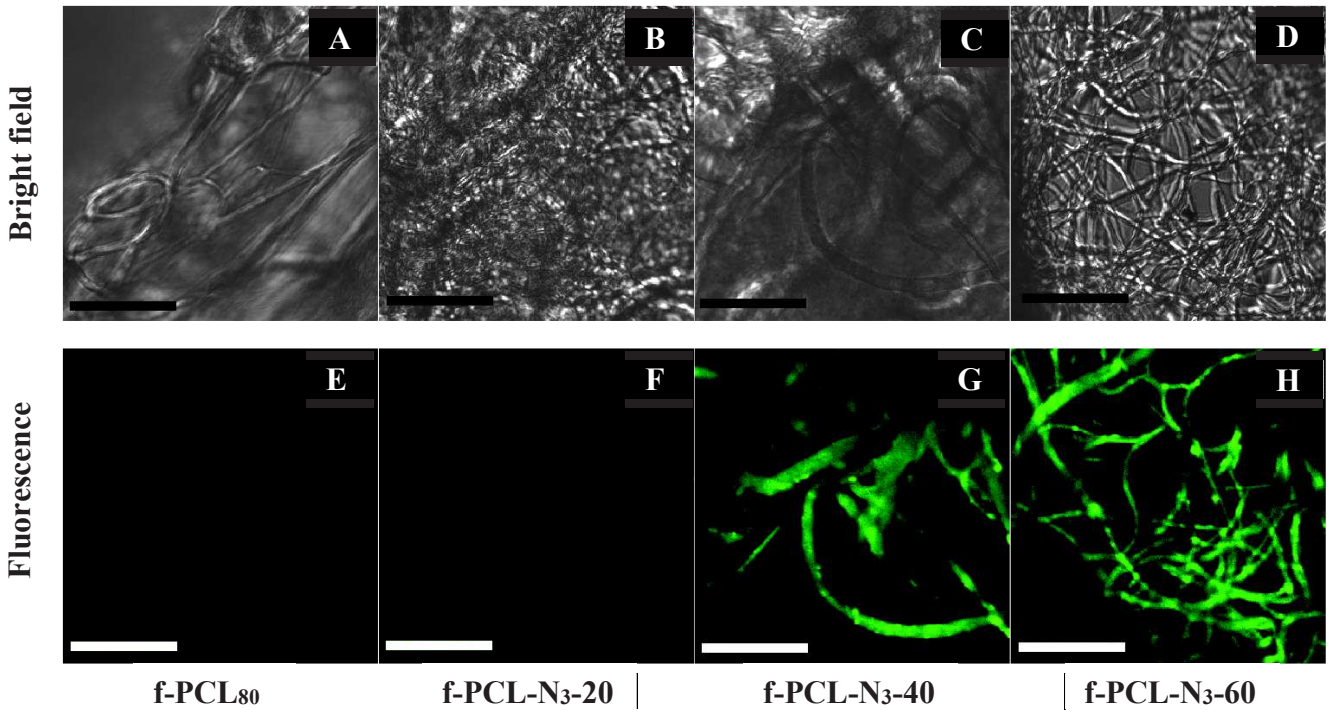

Figure III.16. Bright field images (A-D) and fluorescent images (E-H) of f-PCL$_{80}$, f-PCL-N$_3$-20, f-PCL-N$_3$-40 and f-PCL-N$_3$-60 fibers, respectively, after 48h with FITC-alkyne in acetonitrile/water solution and with the copper catalysts; scale bar 20 µm.

In Figure III.17, a gradual increase of color intensity, clearly visible to the naked eye, from f-PCL-N$_3$-20 to f-PCL-N$_3$-60 corresponds to a degree of FITC fluorophore implemented onto the fibers.

Figure III.17. The image (from left to right) of f-PCL$_{80}$, f-PCL-N$_3$-20, f-PCL-N$_3$-40 and f-PCL-N$_3$-60 fibers after 48h incubation with FITC-alkyne fluorophore, with (top line) and without catalysts (bottom line)

Figure III.17 clearly demonstrates the successful attachment of the FITC-propargyl fluorophore by click chemistry and macroscopically visible differences in the grafting ratio. This macroscopic observation (Figure III.17) correlates accurately with the results obtained using confocal microscopy (Figure III.15 and III.16). The fluorescent labeling confirmed that surface-azides could be easily accessed and coupled by heterogeneous click chemistry.

4.2 Surface-Functionalization of f-PCL-N_3 Fibers with Carbohydrates

Surface functionalization by click coupling took place at the interface between the aqueous medium containing carbohydrates and catalysts and a solid fibrous surface. Fu *et al.*[164] used click chemistry to covalently bond thermo-sensitive polymer with solvent-resistant nanofibers. Mandal *et al.*[248] and Shi *et al.*[205] adopted click coupling to obtain protein-decorated micro-patterned fibrous scaffolds. Herein, f-PCL-N_3 -20, -40, and -60 fibers were functionalized through heterogeneous click chemistry with propargyl-α-D-mannoside and propargyl-β-D-galactoside and f-PCL_{20}-Man_S, f-PCL_{40}-Man_S and f-PCL_{60}-Man_S, and f-PCL_{20}-Gal_S, f-PCL_{40}-Gal_S and f-PCL_{60}-Gal_S were obtained, respectively.

Figure III.18 shows an example of ATR-FTIR spectra of click-conjugated propargyl-β-D-galactoside on the surface of f-PCL-N_3-20 fibers. Therefrom, we evidence grafting of the sugars onto the fibers from a large peak at 3300 cm^{-1} assigned to stretching vibrations of hydroxyl groups as well as vibrations of N-H at 3744 cm^{-1}. A peak at ~1642 cm^{-1}, corresponding to C-O stretching groups of monosaccharide, absent in native PCL_{80}, was also noted. The characteristic peak of azide –N=N=N groups, noticed at 2100 cm^{-1}, indicates some remaining azido groups on the surface as well as inside the fibers.

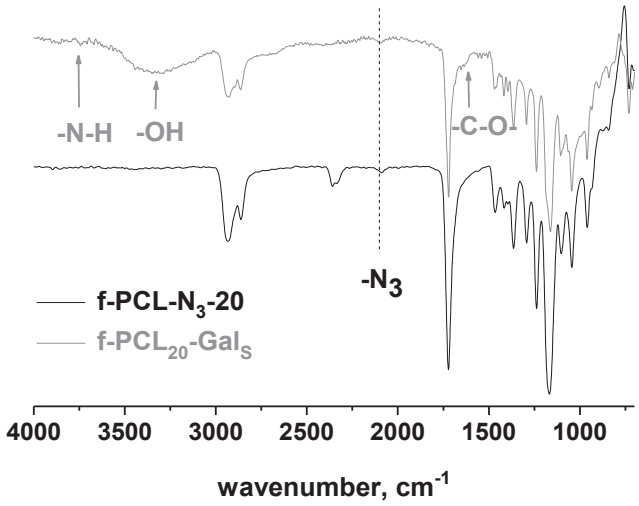

Figure III.18. ATR-FTIR spectra of f-PCL-N_3-20 (black line) and f-PCL_{20}-Gal_S (grey line) fibers

Quantification of total sugar content of the f-PCL-Gal_S and f-PCL-Man_S fibers, was carried out using standard phenol-sulfuric acid method (Dubois).[245] Dubois method has showed equally successful in carbohydrate quantification conjugated on polystyrene copolymer[249] and on poly(ethylene terephthalate) (PET) electrospun fibers.[200]

By using Dubois method we were able to quantify total amount of mannose and galactose coupled onto the fibers. For each fibrous mat, 3 samples were taken, and the average coupling rate onto the f-PCL-N_3 fibers was determined. Table III.3 summarizes experimental and theoretical weights of f-PCL_X-Gal_S and f-PCL_X-Man_S (X = 20, 40 and 60) obtained. The coupling ratio is expressed as weight percentage of experimentally obtained and theoretically calculated mass of sugar at the surface of the fibers: $\frac{m_{exp}}{m_{th}} \cdot 100\%$.

Electrospun fibers	m_{exp} [mg]	m_{theo} [mg]	$m_{exp}/m_{th} \cdot 100\%$
f-PCL_{20}-Gal_S	0,00312	0,0153	20%
f-PCL_{40}-Gal_S	0,00812	0,0305	27%
f-PCL_{60}-Gal_S	0,0112	0,0458	25%
f-PCL_{20}-Man_S	0,00175	0,0153	11%
f-PCL_{40}-Man_S	0,00697	0,0305	23%
f-PCL_{60}-Man_S	0,0146	0,58	32%

Table III.3. Dubois colorimetric method results: defining experimentally found (m_{exp}) and theoretically calculated (m_{theo}) mass of the galactose/mannose as well as their ratio ($\frac{m_{exp}}{m_{theory}} \cdot 100\%$) at the surface of the fibers

In the case of surface functionalization, the overall sugar content of each functionalized fibrous mat is the one at the fiber's surface. Herein, it was represented as a ratio of experimentally found and theoretically calculated mass of the monosaccharide at the surface. Colorimetric results revealed that the carbohydrate concentration at the surface increased with the concentration of azide groups in the f-PCL-N_3 fibers. Interestingly, it was however observed that the overall coupling rate remained constant, about 20 wt. %, for both galactose- and mannose- surface-functionalized fibers. When compared with f-PCL-Gal_B nonwovens, the sugar content available at the surface of the fibers significantly increased.

4.2.1 Water Contact Angle Measurements on Electrospun f-PCL-Gals and f-PCL-Mans Fibers

Wettability and hydrophilicity of the surface-functionalized f-PCL-Gal_S and f-PCL-Man_S fibers was investigated using dynamic water-contact-angle measurement. Figure III.19

assembles the dynamic contact angle measurements of f-PCL-Gal$_S$ (Figure III.19A) and f-PCL-Man$_S$ fibers (Figure III.19B).

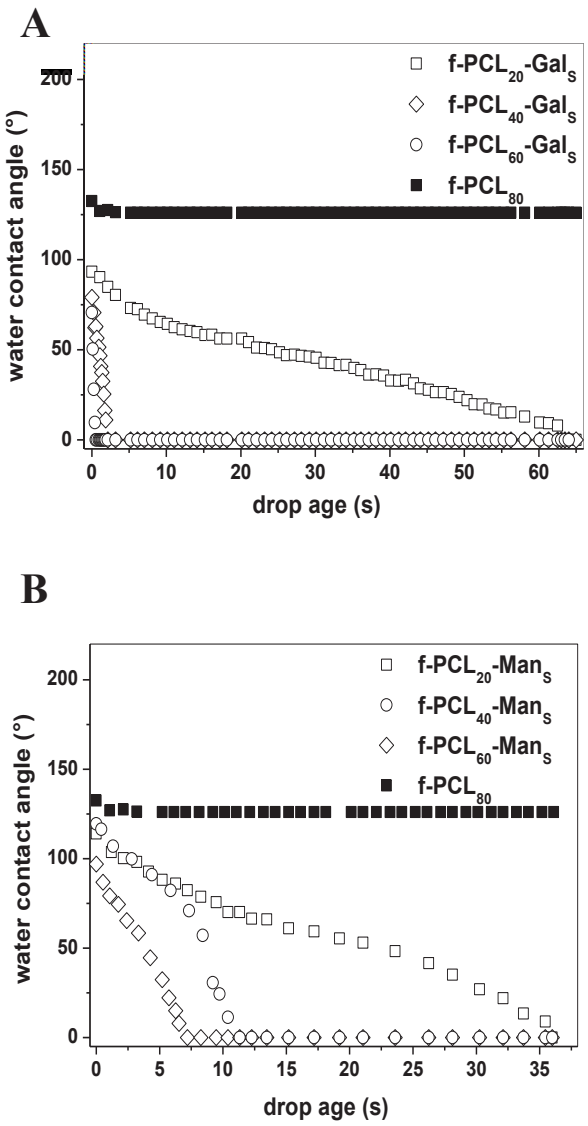

Figure III.19. Dynamic water contact angles of (A): (□) f-PCL$_{20}$-Gal$_S$, (◊) f-PCL$_{40}$-Gal$_S$, and (○) f-PCL$_{60}$-Gal$_S$ and (B): (□) f-PCL$_{20}$-Man$_S$, (◊) f-PCL$_{40}$-Man$_S$, and (○) f-PCL$_{60}$-Man$_S$ surface-functionalized fibers together with (■) f-PCL$_{80}$ as a reference

As it could be observed from the Figure III.19A, the contact angle of f-PCL-Gal$_S$ fibers is decreasing over time. In addition, the soaking rate of f-PCL-Gal$_S$ fibrous membranes accelerated with the increase of galactose content at their surface. While for the f-PCL$_{20}$-Gal$_S$

WCA reached zero in about 60s, f-PCL_{60}-Gal_S fibers' WCA attained 0° value in less than 3s. Furthermore, a gradual difference in the soaking rate was more accentuated for f-PCL-Man_S samples (Figure III.19B) where complete wettability was reached in 40, 12 and 7s for f-PCL_{20}-Man_S, f-PCL_{40}-Man_S and f-PCL_{60}-Man_S fibers, respectively.

Grafahrend *et al.*[196] observed similar trend of complete hydrophilicity after surface-grafting of star-shaped PEO amphiphile onto polyester scaffolds. Across several studies, Grafahrend *et al.*[195,197,199,250] highlighted the potential of surface molecules to completely change fibrous surface from hydrophobic to completely hydrophilic. This study gives a confirmation of that point.

4.2.2 Enzyme-Linked Lectin Assays on f-PCL-Gal_S and f-PCL-Man_S Fibers

Ability of carbohydrates to interact specifically with carbohydrate-binding proteins, i.e. lectins, was investigated through the enzyme linked lectin assay (ELLA). ELLA is a sensitive assay that uses a peroxidase enzyme linked to a lectin as a marker for the detection of a specific carbohydrate. For this study, we exposed f-PCL_X-Gal_S, and f-PCL_X-Man_S fibers as well as their appropriate f-PCL-N_3-X fibers as a control (where X = 20, 40 and 60) to a Concanavalin A-peroxidase conjugate (HRP-ConA) and *Arachis hypogaea*-peroxidase conjugate (HRP-PNA) for detection of mannose and galactose residues, respectively. Otman *et al.*[251] described a specific recognition of α-D-mannose at the surface of polymeric nanoparticles by ConA, demonstrating that mannose groups, conjugated with the poly(ε-caprolactone), could covalently bind the lectin. In this study, upon staining with the AEC substrate, both f-PCL-Gal_S and f-PCL-Man_S fibrous mats exhibited a positive coloration in presence of HPR-PNA and HRP-ConA lectins respectively. Figure III.20 is an image of f-PCL_X-Man_S (Figure III.20A), and f-PCL_X-Gal_S (Figure III.20B) fibers showing positive probes (top line) and their corresponding f-PCL-N_3-X fibers (bottom line) as control samples (X = 20, 40 and 60).

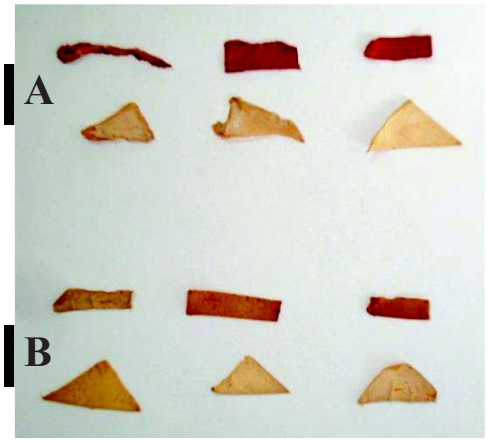

Figure III.20. Image (from left to right) of ELLA assays on: (A) f-PCL$_{20}$-Man$_S$, f-PCL$_{40}$-Man$_S$, and f-PCL$_{60}$-Man$_S$ (B) f-PCL$_{20}$-Gal$_S$, f-PCL$_{40}$-Gal$_S$ and f-PCL$_{60}$-Gal$_S$ fibers. For each sample, top line corresponds to the positive test samples while bottom line matches the control samples

f-PCL-Man$_S$ fibers showed a very intense red color while f-PCL-Gal$_S$ and f-PCL-Gal$_B$ staining was less pronounced (Figure III.20). Such difference between ConA and PNA binding efficiency is not unexpected and Wu *et al.*[252] previously observed that a PNA lectin binds rather weakly to the galactose units, while in the case of lactose a strong conjugation PNA-lactose was observed, suggesting that PNA lectin needs a longer arm-spacer for a better carbohydrate recognition. Nonetheless, the control samples of non-functionalized f-PCL-N_3 fibers showed no significant coloration under the same treatment, demonstrating that ELLA labeling is highly specific to the carbohydrate-functionalized moieties.

Specific recognition of carbohydrates on the fibrous surface as well as their enhanced protein affinity underlines a considerable potential of these scaffolds as advanced bio-active materials.

5. Conclusions

Results presented in this chapter show that it is possible to obtain surface-decorated clickable nanofibers by electrospinning commercially available native PCL$_{80}$ and end-

functionalized PCL_2-N_3 polymers. Additionally, these fibers offer a possibility of using both classical CuAAc copper-catalyzed and alkyl-strained copper-free click chemistry. As copper affects strongly the life quality of living cells, employing copper-free click chemistry could make use of these scaffolds in tissue engineering more comfortable.

We also demonstrated that azides suffer no change during the electrospinning and could be easily accessed for click conjugation. It is interesting to notice that a chemical reduction of azides to amines using PPh_3 could serve as a simple route for obtaining highly amine-functionalized PCL fibers. Amino-fibers of biocompatible PCL could further react by means of peptide coupling with versatile proteins, thus serve as an important precursor to advanced biomaterials for biological and cell culture applications.

In the end, carbohydrate activation of electrospun nonwovens proved to be highly specific for protein adhesion. Carbohydrate functionalization from the bulk showed regular surface and bulk enrichment of the fibers with sugar moieties and could find use as a scaffold where accelerated polymer degradation is needed. On the other hand, surface functionalization of f-PCL-N_3 fibers with the carbohydrates was proved advantageous as the quantity of the introduced functional moiety could be tuned. Furthermore, as diverse chemical groups could be introduced at the fibrous surface by click coupling, final physicochemical properties could be precisely modulated for a targeting purpose.

General Conclusions and Perspectives

General Conclusions and Perspectives

The structure of a material is of outmost importance in the designing process of artificial scaffolds for medical applications. It has been demonstrated that nano-structured scaffolds represent an advantageous material for tissue engineering in terms of size, cost, high porosity, lightness, and organization similar to the one in extracellular matrix (ECM). Among various techniques for nano-fiber fabrication, electrospinning is known for the variety of both materials that can be processed and the final fibrous structures and 3D architectures that can be obtained. The combination of nano-fibrous structure and biologically activated surface has been shown as the most rewarding for positive cell-material interactions. Chemical versatility of carbohydrates, present at the surface of the cells, enables cell communication with different molecular structures (proteins and antibodies) and living organisms (other cells, viruses and bacteria). The use of carbohydrates as bioactive receptors at the surface of the scaffolds has been demonstrated as efficient for improved cell adhesion, proliferation, growth, and further, scaffold degradation. However, their weak mechanical properties and high water-sensitivity have turned the use of carbohydrates simultaneously with mechanically superior synthetic polymers. Poly(ε-caprolactone) is a synthetic polyester, often employed for biomedical applications due to its notable biocompatible and biodegradable properties. Particularly in the electrospinning process, the use of PCL records a constant progress. Nevertheless, hydrophobicity and absence of functional groups necessitate PCL modification for beneficial cell-material interactions.

The objective of this thesis project was to obtain biocompatible nano-fibrous structures, and design their surface with biologically recognized moieties for tissue engineering applications. By using the electrospinning process for fabrication of PCL-based scaffolds and their consequent functionalization with carbohydrates, we aimed toward tissue

engineering application of these nonwovens. Herein, chemical modifications of low-molecular-weight PCL were investigated in both bulk- and surface-functionalization aspects through azide-alkyne cycloaddition reactions (click chemistry). The bulk functionalization consisted of chemical transformations at the PCL chain-ends. Through several modifications, β-D-galactose was finally bonded to PCL and an amphiphilic-like structure was obtained. Due to the chain length of the PCL-Gal polymer and consequently absence of chain entanglements, fiber fabrication was initiated from a blend of bulk-modified PCL-Gal and native high-molecular-weight PCL. Resulting electrospun fibers had galactoside-PCL equally dispersed within the fibers of micron-size diameters with only small amount at the fiber's surface. However, these carbohydrate-functionalized fibrous scaffolds might be used for implants, or in wound healing and for bandages, where accelerated degradation is demanded.

The surface functionalization approach was based on chemical modification of the surface of already electrospun PCL scaffolds. For employing the click chemistry approach, low-molecular weight PCL was end-functionalized with azide groups and then blended with a native PCL to obtain azide-decorated fibrous surface. This multi-step fiber functionalization was rewarded with a predominant concentration of azides at the fibers' surface. By using a fluorescent dye to mark the active azides, confocal microscopy revealed an even and a continuously-spread active places at the surface of the fibers. Click coupling of propargyl-galactose and propargyl-mannose with surface azides gave highly hydrophilic matrices with protein-specific adhesion characteristics. Azide-decorated PCL nonwovens offer fiber's surface coupling with various cell-recognized molecules – carbohydrates or proteins – either through click chemistry or peptide coupling.

Working with biodegradable polymers for medical applications necessitates a significant knowledge about the stability of a polymer composing a biomaterial. Polymer

stability can be analyzed through characteristic relaxation time of the polymeric chains. Herein, we investigated the conformation of polymer chains in electrospun aligned fibers of polystyrene (PS) and their chain relaxation kinetics after thermal annealing by small angle neutron scattering technique (SANS). SANS is a very valuable technique for qualitative and quantitative evaluation of polymer chain conformation and dynamics within a sample of interest (solid, liquid, gel, etc.). The size-dependent behavior and modified chain conformations within the confined structures of materials are well known. However, a very few is published about the chain conformation within the electrospun fibers. In this study, the SANS experiment on polystyrene fibers in as-spun state showed a notable anisotropy of polymeric chains in the direction of the fiber's alignment axis. The elongation ratio in the axial direction of as-spun fibers was found to be 1.22 while the corresponding ratio of the radius of gyration parallel and perpendicular to the fiber alignment axis was 1.34.

Furthermore, it is reported for the first time polymer chain and surface relaxation dynamics after consequent thermal annealing at different temperatures and different time intervals. Fast relaxation of the surface of electrospun fibers and rather slow chain relaxation within the fiber bulk were observed. The thermal annealing experiments enabled us to estimate the characteristic relaxation time of the polymeric chains within the electrospun fibers.

We also investigated the influence of molecular weight distribution on final fiber diameter. The research of solution properties and their impact on the fiber morphology was studied from polymers of the same molecular weight but with different molecular weight distributions. While fibers obtained from polydisperse PS were of micron-size diameters and significantly porous and voided, fibers obtained from monodisperse PS had nano-diameters with narrow diameter size distribution and without the presence of pores at the surface or inside the fiber's bulk. We have demonstrated that molecular weight distribution, an often neglected

parameter in electrospinning process, remarkably influences the fiber's size and morphology and it should be taken into account in further research studies in this field.

This work has opened the gate for many *perspectives*.

During the SANS experiment, we encountered many difficulties in sample preparation and later in data analysis. Regarding the sample preparation, it would be interesting to investigate the possibility in forming a stack of thin films made of electrospun fibers for obtaining stronger signal from scattered neutrons while analyzing highly aligned electrospun fibers. When it comes to the data analysis, attention should be paid to overcoming the strong scattering signal from the fiber's surface by replacing the air with a non-solvent having similar scattering length density as polystyrene.

Regarding the theoretical aspects of the electrospinning process, pioneering SANS experiments done previously and during this PhD research could serve as a basis for more complex studies on electrospun fibers made from:

- crystalline polymers – investigating the orientation of the crystalline zones of the polymer fibers as well as the chain conformation of the amorphous parts of the fibers;
- polymeric blends – studying the phase separation process between two polymers, their respective polymeric chain conformations and influence of the presence of another macromolecule on characteristic relaxation time – acceleration and retardation factors
- polymers containing additives – there are many debates about the surface-segregation of additives during the electrospinning process, and it would be interesting to investigate what causes this phenomenon – electrically induced or

spontaneous – through simultaneous studies of neutron scattering and neutron reflectometry analysis;

- core/shell structures – structural investigation of the core/shell organization and the polymer chain size within, as well as the polymer conformation at the interface core-shell and shell-air; also, it would be interesting to compare the core/shell formation from two different processing techniques – coaxial- and emulsion-electrospinning.

The practical aspects of this thesis were to use the electrospinning setup to fabricate novel biomaterials for tissue engineering applications that are based on commercially-available sources, versatile and with bioactive and cell-friendly surface. We wanted to create *one* material that would preferentially suit *several* applications by simply changing its physicochemical surface structure.

By using click chemistry, galactose and mannose monosaccharides were successfully coupled to the fibers' surface. Nevertheless, surface-functionalized azido-PCL fibers offer the possibility to attach various chemical structures at the surface via click chemistry. Next step in surface functionalization would therefore be the use of complex carbohydrates or proteins and verification of the coupling efficacy. Also, our first approach was to use copper catalysts with end-alkyl molecules. However, it would be interesting to test these fibers by using copper-free click chemistry and strained alkynes, and compare the product yields.

Additionally, azide groups could be easily converted into amine groups and enable peptide coupling of proteins. Plasma treatment is the simplest way to create the amine groups at the surface of PCL fibers. However, amine formation obtained from macromolecular chain breakage may further trigger the fiber degradation and contribute to the weakening of the mechanical properties of these fibers. By simple conversion of azides to amines with

triphenylphosphine, desired amino-groups could be formed at the time needed, without deterioration of the fiber's structure and mechanical properties. Subsequently, it would be intriguing to test the method of peptide coupling with various cell-stimulating proteins on PCL fibers to obtain bioactive scaffolds that meet the high demands for tissue engineering applications.

Materials and Methods

Chapter IV – Materials and Methods

1. Materials

Protonated polystyrene (hPS), M_w 392000 g mol^{-1} and perdeuterated polystyrene (dPS), M_w 385000 g mol^{-1} with narrow molecular-weight distributions (MWD ≤ 1.1) were atactic and purchased from Polymer Source, USA. Poly(ε-caprolactone) (PCL_{80}) M_n 70000-90000 g mol^{-1}, polystyrene (PS) M_w 350000 g mol^{-1} (MWD=2.06), β-D-galactopyranose pentaacetate, α-D-mannopyranose pentaacetate, and all other organic compounds mentioned in this study were purchased from Sigma Aldrich and used without further purification. β-galactosidase (*Aspergillus oryzae*) was dissolved in phosphate-buffer saline (PBS) solution (1:10) in order to make 200 units mL^{-1} concentration. Horseradish peroxidase-labeled lectin (HRP) from *Canavalia ensiformis* (HRP-ConA, mannose-binding lectin) was dissolved in PBS (1:10 dilution) in order to obtain 250 mg mL^{-1} solution. Horseradish peroxidase-labeled lectin (HRP) from *Arachis hypogaea* (HRP-PNA, galactoside-binding lectin) was dissolved in PBS (1:10) to obtain 200 mg mL^{-1} solution. α,ω-Poly(ε-caprolactone)-diol (PCL_2), M_n 2000 g mol^{-1} (Sigma), was recrystallized from diethyl ether prior to use. Aluminium foil (99% purity) was purchased from Goodfellow, England. Certain trade names and company products are identified in order to specify experimental procedures adequately. In no case does such identification imply recommendation or endorsement, nor does it imply that the products are necessarily the best available for the purpose.

2. Syntheses and Preparation Protocols

Synthesis of *α,ω-p*-Toluenesulfonyl-poly(*ε*-caprolactone) (PCL-OTs)

Synthesis of *α,ω-p*-toluenesulfonyl-poly(*ε*-caprolactone), illustrated in the Scheme IV.1, was carried out following the protocol reported elsewhere.[224]

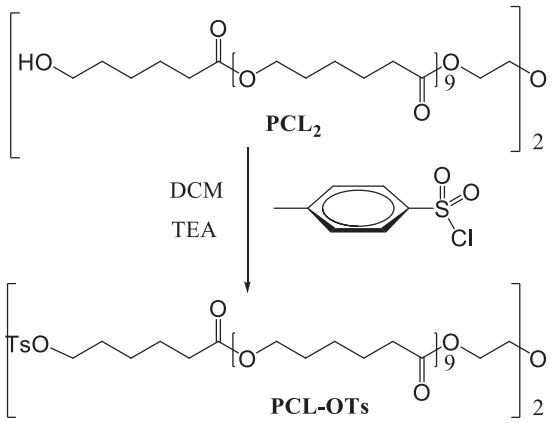

Scheme IV.1. Synthesis of α,ω-p-toluenesulfonyl-poly(ε-caprolactone) (PCL-OTs) polymer

PCL_2 (2 g, 1 mmol) was dissolved in 30 mL of dichloromethane in a 100 mL round-bottom-flask and stirred until dissolution. Then, triethylamine (TEA) (6 equiv., 0.607 g) and TsCl (6 equiv., 1.14 g) dissolved in 20 mL of DCM were added drop-wise into the polymer solution. After 28 h at room temperature, the reaction mixture was then washed with saturated NaCl, 1 M HCl and H_2O. The organic phase was dried over Na_2SO_4 and concentrated. The crude product was dissolved in the minimum of CH_2Cl_2 and then precipitated in cold (4 °C) diethyl ether (10 mL) to give *α,ω-p*-toluenesulfonyl-poly(*ε*-caprolactone) (PCL-OTs) (1.21 g, 54 % yield).

^{1}H NMR (400 MHz, $CDCl_3$,δ): 7.77 (d, 4H, J=8.22 Hz, CH_3-$C_6H_2H_2$-SO_2-), 7.34 (d, 4H, J=8.05 Hz, CH_3-$C_6H_2H_2$-SO_2-), 4.22 (t, 4H, J=4.72 Hz, COO-CH_2-CH_2-O-), 4.05 (t, 84H,

J=6.66 Hz, COO-C*H*$_2$-(CH$_2$)$_4$-), 3.68 (t, 4H, J=4.76 Hz, COO-CH$_2$-C*H*$_2$-O-), 2.44 (s, 6H, C*H*$_3$-C$_6$H$_4$-SO$_2$-), 2.30 (t, 84H, J=7.50 Hz, -(CH$_2$)$_4$-C*H*$_2$-COO-), 1.64 (m, 172H, COO-CH$_2$- C*H*$_2$-CH$_2$- C*H*$_2$- CH$_2$-COO-), 1.37 (dt, 84H, J=1.65, 14.77 Hz, COO-(CH$_2$)$_2$- C*H*$_2$-(CH$_2$)$_2$-COO-).

^{13}C NMR (400 MHz, CDCl$_3$, δ): 173.5, 130.5, 129.8, 129.1, 127.9, 70.2, 69.1, 64.1, 63.3, 34.1, 30, 27.5, 25.5, 24.5.

MALDI-TOF MS: calcd for C$_{138}$H$_{222}$O$_{47}$S$_2$ m/z=2695.42; found m/z= 2718.50 [*M*+Na]$^+$.

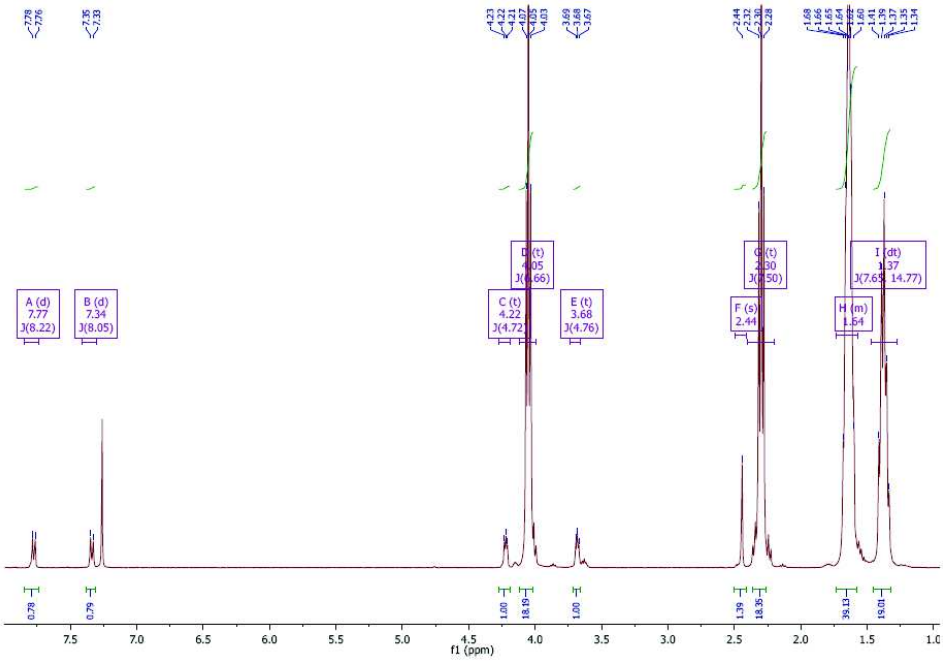

Figure IV.1.^{1}H NMR spectrum of α,ω-p-toluenesulfonyl-poly(ε-caprolactone) (PCL-OTs) in CDCl$_3$

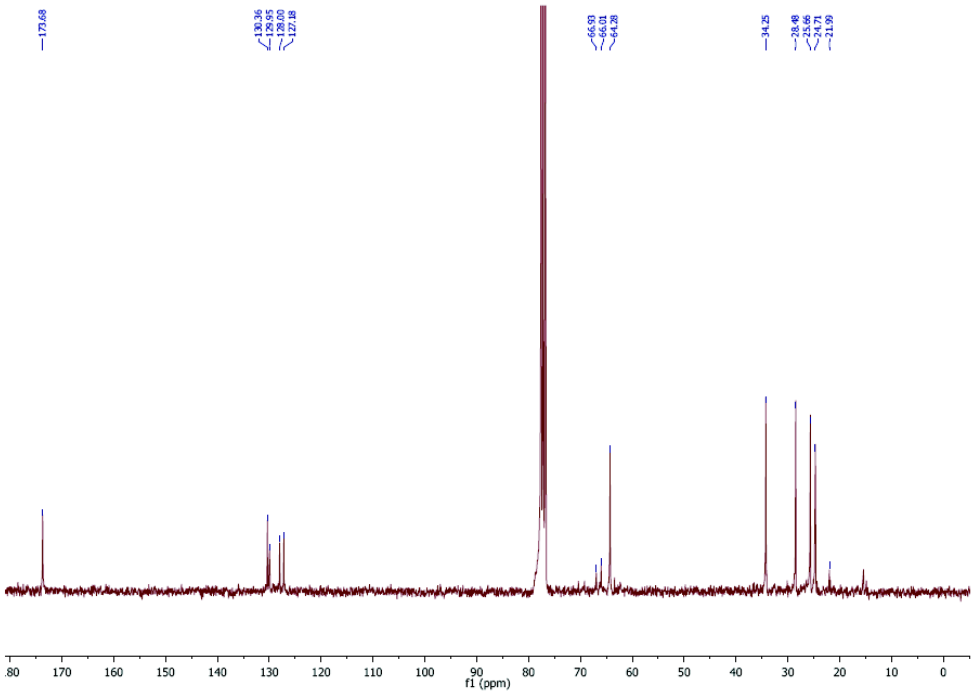

Figure IV.2.[13]C NMR spectrum of α,ω-p-toluenesulfonylpoly(ε-caprolactone) (PCL-OTs) in $CDCl_3$

Synthesis of α,ω-Azide-poly(ε-caprolactone) (PCL-N_3)

α,ω-Azide-poly(ε-caprolactone) synthesis was carried out from the PCL-OTs polymer obtained previously as illustrated in the Scheme IV.2.

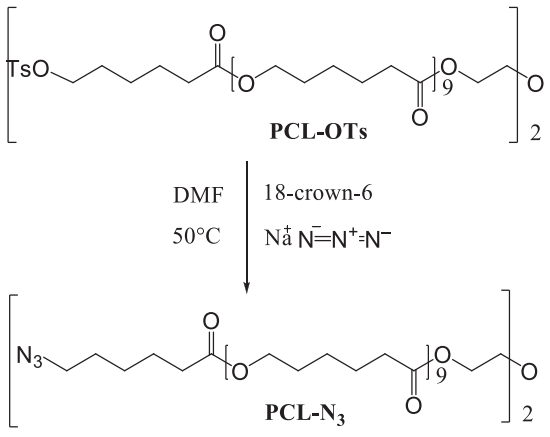

Scheme IV.2. Synthesis of α,ω-azide-poly(ε-caprolactone) (PCL-N_3) polymer

PCL-OTs (1 g, 0.4332 mmol) was dissolved in the minimum of DMF (5 mL) under the flux of Argon. When the polymer was dissolved, NaN_3 (6 equiv., 0.169 g) was added with 1-2

crystals of 18-crown-6 and the reaction was stirred for 24 h at 50 °C. After precipitation in cold water (20 mL), 0.875 g of the final product α,ω-azido-poly(ε-caprolactone) (PCL-N_3) was isolated (98% yield).

^{1}H NMR (400 MHz, $CDCl_3$, δ): 4.22 (t, 4H, J=4.79 Hz, COO-C*H*$_2$-CH_2-O-), 4.05 (t, 84H, J=6.69 Hz, COO-C*H*$_2$-$(CH_2)_4$-), 3.68 (t, 4H, J=4.86 Hz, COO-CH_2-C*H*$_2$-O-), 3.27 (t, 4H, J=6.87 Hz, N_3-C*H*$_2$-), 2.30 (t, 84H, J=7.51 Hz, -$(CH_2)_4$-C*H*$_2$-COO-), 1.63 (m, 172H, COO-CH_2- C*H*$_2$-CH_2- C*H*$_2$- CH_2-COO-), 1.38 (m, 84H, COO-$(CH_2)_2$- C*H*$_2$-$(CH_2)_2$-COO-).

^{13}C NMR (400 MHz, $CDCl_3$, δ): 173.5, 69, 64.1, 63, 55.2, 38.7, 34.1, 28.3, 25.5, 24.6

MALDI-TOF MS: calcd for $C_{112}H_{188}O_{37}N_6$ m/z=2385.49 (for azide-terminated PCL); found m/z=2409.43 [M+Na^+] (N_3→NH_2).[226]

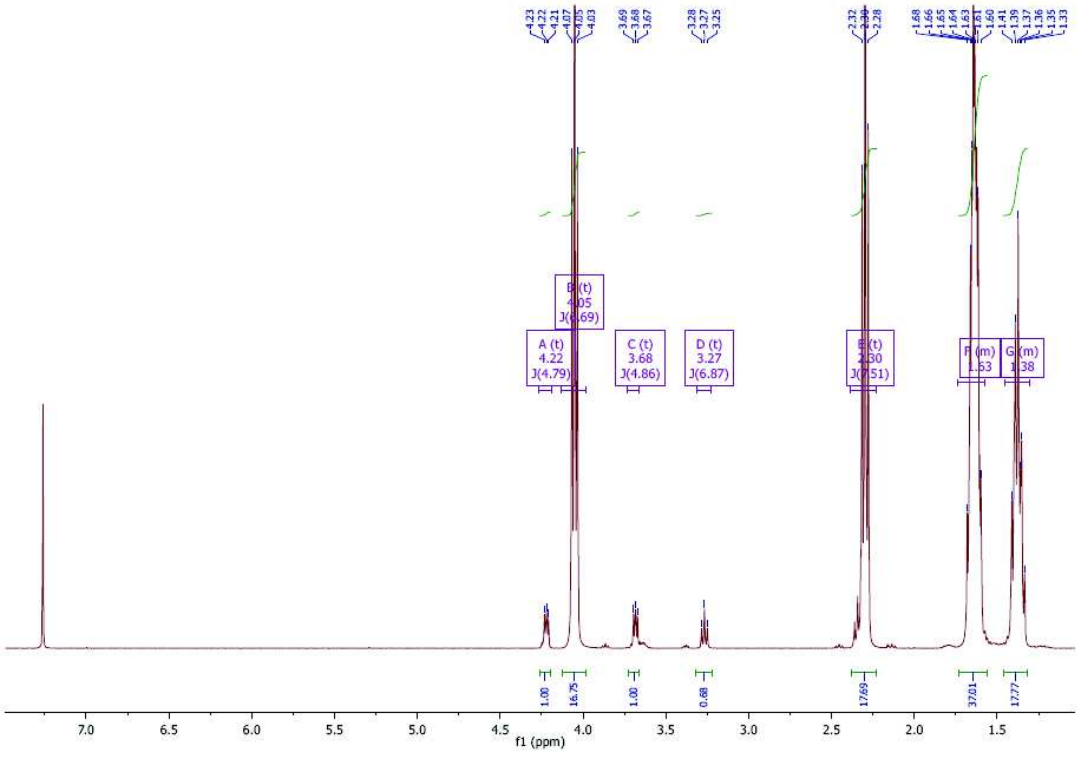

Figure IV.3.^{1}H NMR spectrum of α,ω-azido-poly(ε-caprolactone) (PCL-N_3) in $CDCl_3$

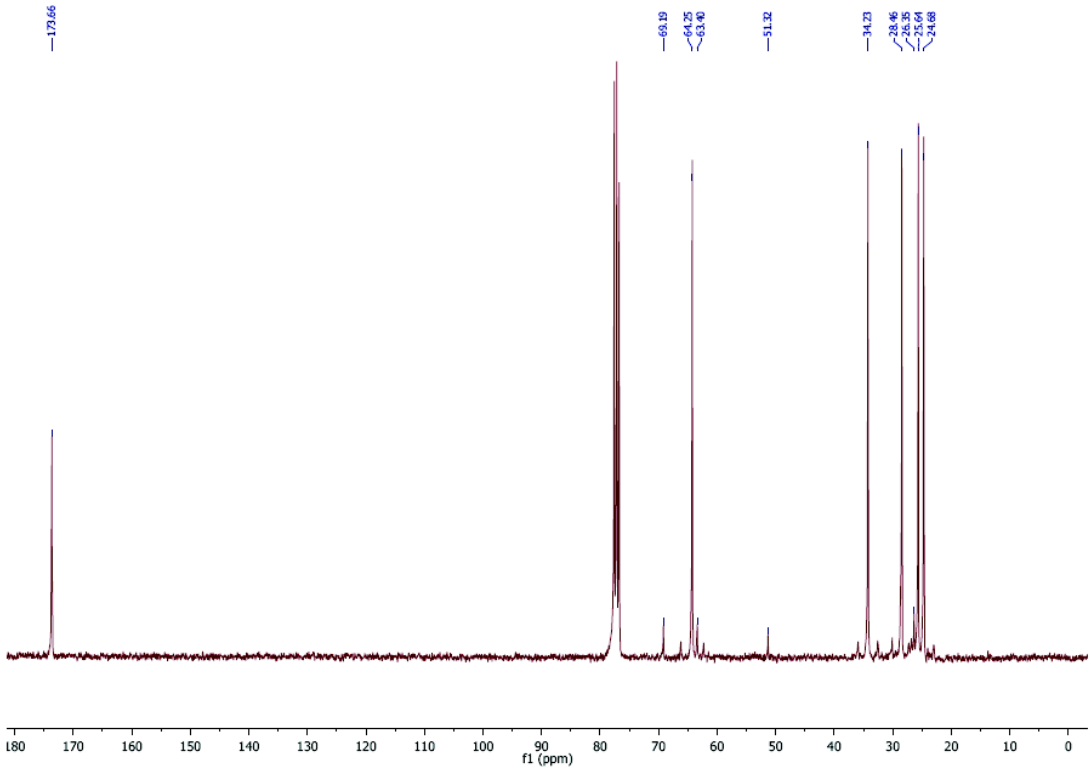

Figure IV.4.[13]C NMR spectrum of α,ω-azido-poly(ε-caprolactone) (PCL-N_3) in $CDCl_3$

Synthesis of α,ω-Propargyl galactoside-poly(ε-caprolactone) (PCL$_2$-Gal) Polymer

Synthesis of α,ω-propargyl galactoside-poly(ε-caprolactone) was carried out from PCL-N_3 polymer as illustrated in Scheme IV.3.

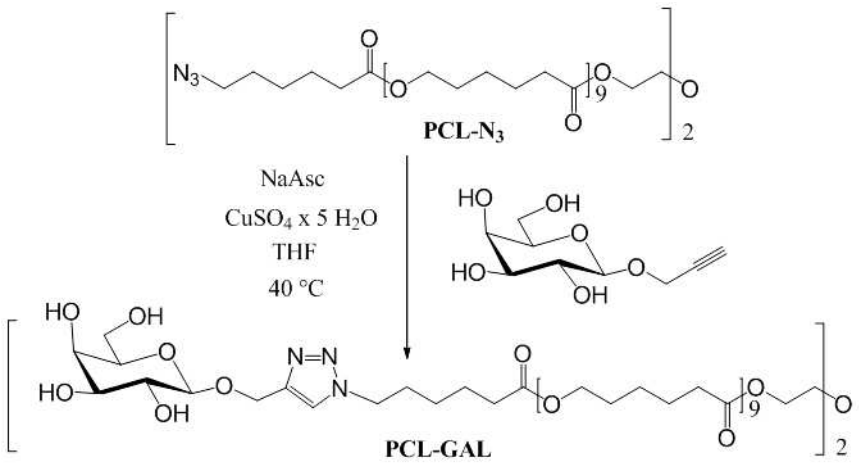

Scheme IV.3. Synthesis of α,ω-propargyl galactoside-poly(ε-caprolactone) (PCL-Gal) polymer

PCL_2-N_3 polymer (1.5 g, 0.72 mmol) was involved into click reaction with propargyl-*β*-D-galactose (see chapters 2.5 and 2.6 detailed syntheses) (1.57 g, 10 equiv.) in THF/water 1/1 solvent mixture (100 mL), at 40 °C for 48h and in the presence of $CuSO_4 \cdot 5H_2O$ (0.36 g, 2 equiv.) and sodium ascorbate (0.28 g, 2 equiv.) catalysts. Reaction mixture was concentrated in rotavapor, dissolved in 2 mL of N,N-dimethylformamide (DMF) and precipitated in 40 mL of toluene. The solid was filtrated and dried under vacuum to provide PCL_2-Gal (1.6 g) in 94% yield.

^{1}H NMR (DMSO-*d*$_6$, 400 MHz) δ: 8.03 (s, 2H,-C=C*H*-N-), 4.81 (d, 2H, *J*=12.21 Hz, -C^1*H*-O-), 4.63 (d, 4H, *J*=12.22 Hz, -C^6*H*$_2$-OH), 4.48 (t, 2H, *J*=5.59 Hz, -C^5*H*-OH), 4.32 (t, 4H, *J*=7.07 Hz, -O-C*H*$_2$-C=), 4.22 (d, 2H,*J*=7.20 Hz, -C^2*H*-OH), 4.18 (d, 2H, *J*=5.86 Hz, -C^4*H*-OH), 4.11 (t, 4H, *J*=4.7 Hz, COO-C*H*$_2$-CH$_2$-O-), 3.99 (t, 84H,*J*=6.49 Hz, COO-C*H*$_2$-(CH$_2$)$_4$-), 3.66 (t, 2H, C^3*H*-OH),3.61 (t, 4H, *J*=4.73 Hz, COO-CH$_2$-C*H*$_2$-O-), 3.55 (d, 4H, J=4.34 Hz), 3.37 (t, 4H, J=5.73 Hz), 2.27 (t, 84H, *J*=7.29 Hz, -(CH$_2$)$_4$-C*H*$_2$-COO-), 1.82 (t, 4H, *J*=7.35 Hz, -N-C*H*$_2$-(CH$_2$)$_4$-), 1.55 (m, 168H, COO-CH$_2$- C*H*$_2$- CH$_2$- C*H*$_2$- CH$_2$-COO-), 1.32 (m, 84H, COO-(CH$_2$)$_2$- C*H*$_2$-(CH$_2$)$_2$-COO-).

^{13}C NMR (DMSO-*d*$_6$, 400 MHz) δ: 172.50, 143.76, 124.14, 123.69, 102.61, 75.21, 73.36, 70.41, 68.10, 63.29, 62.75, 61.36, 60.42, 48.96, 33.23, 33.15, 30.29, 29.17, 27.64, 25.21, 24.73, 23.91, 23.68

MALDI-TOF MS: calcd for $C_{130}H_{216}O_{49}N_6$ m/z=2875.25 g/mol, found m/z= 2898.43 g/mol [*M*+Na]$^+$.

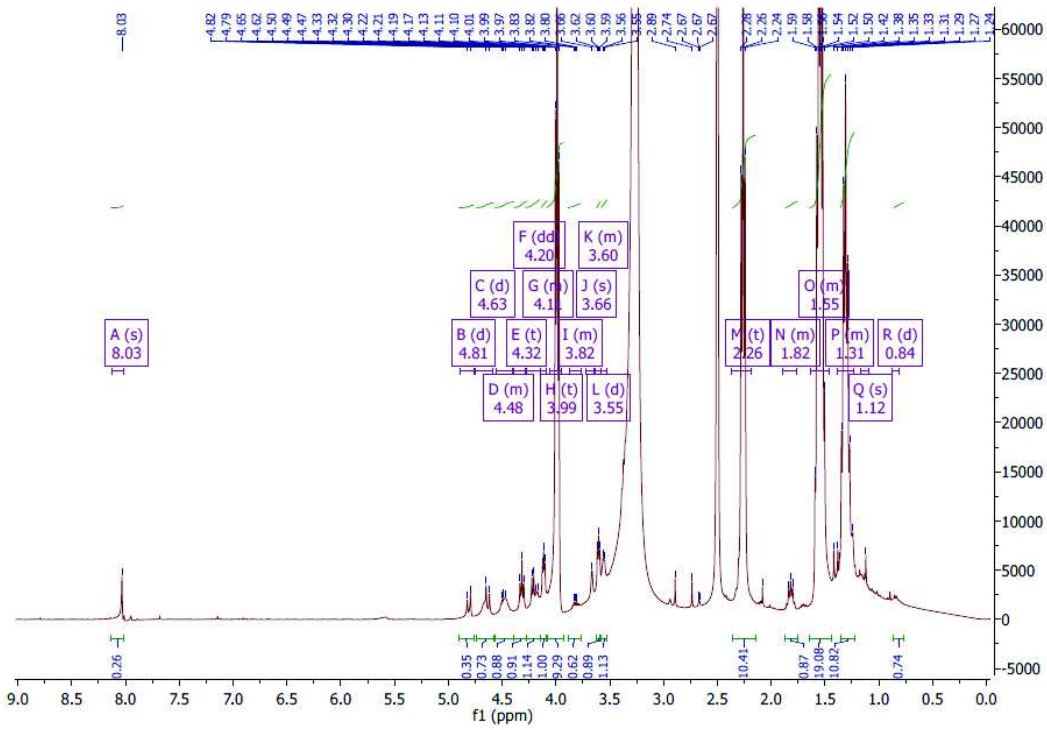

Figure IV.5.[1]H NMR spectrum of α,ω-propargyl galactoside-poly(ε-caprolactone) in DMSO-d_6 at 333 K

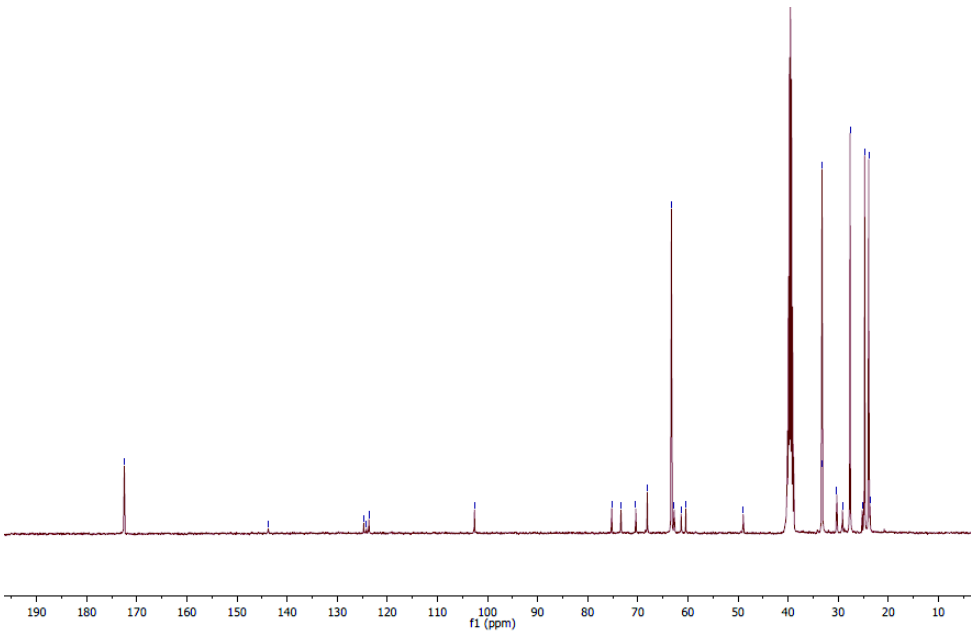

Figure IV.6.[13]C NMR spectrum of α,ω-propargyl galactoside-poly(ε-caprolactone) in DMSO-d_6 at 333 K

Synthesis of Propargyl-Fluorescein Isothiocyanate

Propargyl-fluorescein isothiocyanate was prepared from the fluorescein-isothiocyanate isomer following the procedure reported elsewhere (Scheme IV.4).[253]

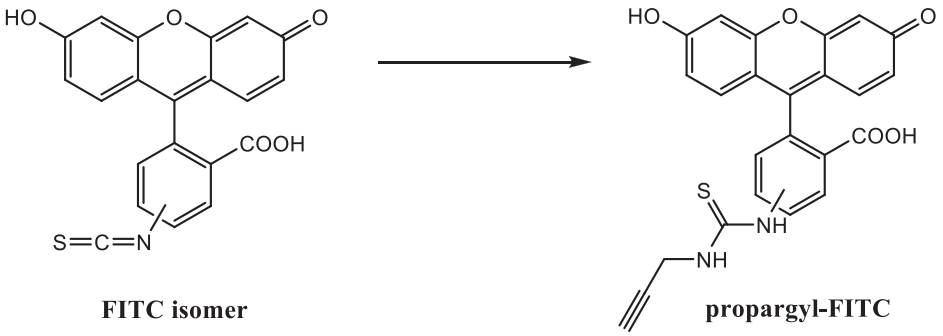

Scheme IV.4. Synthesis of propargyl-fluorescein isothiocyanate

Fluorescein isothiocyanate (FITC) (10 mg, 0.0128 mmol) and propargyl amine (90 µL, 0.703 mmol) were dissolved in 110 µL of DMF in a microcentrifuge tube and stirred in dark for 24 h at room temperature. DMF and excess of propargyl amine were then evaporated and crude product was dissolved in stock solution mixture of acetonitrile/water (1/1).

Synthesis of Propargyl-*β*-D-galactopyranoside

Propargyl-*β*-D-galactopyranoside was obtained from a two-step synthesis protocol illustrated in Scheme IV.5.

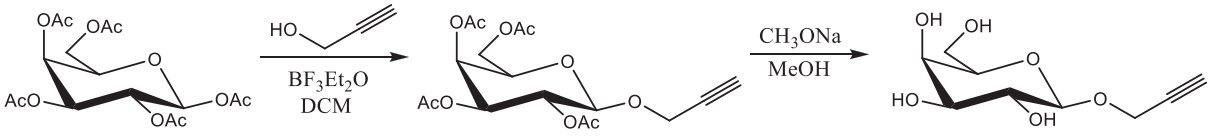

Scheme IV.5.two-step synthesis of propargyl-α-D-galactopyranoside

Boron trifluoridediethylether (9.6 mL, 1.5 equiv.) was added dropwise to a stirred solution of β-D-galactopyranose pentaacetate (20 g, 51.2 mmol) and propargyl alcohol (3.6 mL, 1.2 equiv.) in anhydrous DCM (200 mL) at 0 °C. After 2.5 hours, the reaction mixture was washed with ice-cold water (water and ice), saturated $NaHCO_3$ and saturated NaCl. Organic phase was then dried under Na_2SO_4 and concentrated in the rotavapor. Propargyl-2,3,4,6-tetra-

O-acetyl-*β*-D-galactopyranoside was isolated with 89% yield after purification by flash chromatography on silica gel using ethylacetate and petroleum ether (1:1 v/v) as eluent (3 L).

To a stirred solution of acetylated propargyl galactoside (17.6 g, 45.6 mmol) in MeOH (100 mL) was added sodium methylate (1 M, 1 mL). After completion of the reaction by TLC, the solution was neutralized with the acid resin Amberlite IR 120 H^+, filtered and the filtrate was concentrated. 91% (9.1 g) of pure propargyl-*β*-D-galactopyranoside was isolated after recrystallization in 200 mL of 1-propanol. Purified propargyl-*β*-D-galactopyranoside was either used in the azide-alkyne copper catalyzed cycloaddition reactions with f-PCL-N_3 fibrous mats in a heterogeneus phase or with PCL_2-N_3 polymer in a solution.

^{1}H NMR (D_2O, 400 MHz) δ: 4.58 (d, 1H, *J*=7.87 Hz), 4.49 (m, 2H), 3.94 (d, 1H, *J*=3.40 Hz), 3.72 (m, 4H), 3.54 (dd, 1H, *J*=7.93, 9.85 Hz), 2.07 (s, 1H).

^{13}C NMR (D_2O, 400 MHz) δ: 98.60, 95.86, 72.84, 70.27, 68.19, 66.14, 58.50, 54.04.

MALDI-TOF MS: calcd for $C_9H_{14}O_6$ m/z=218.08, found m/z= 241.0 $[M+Na]^+$.

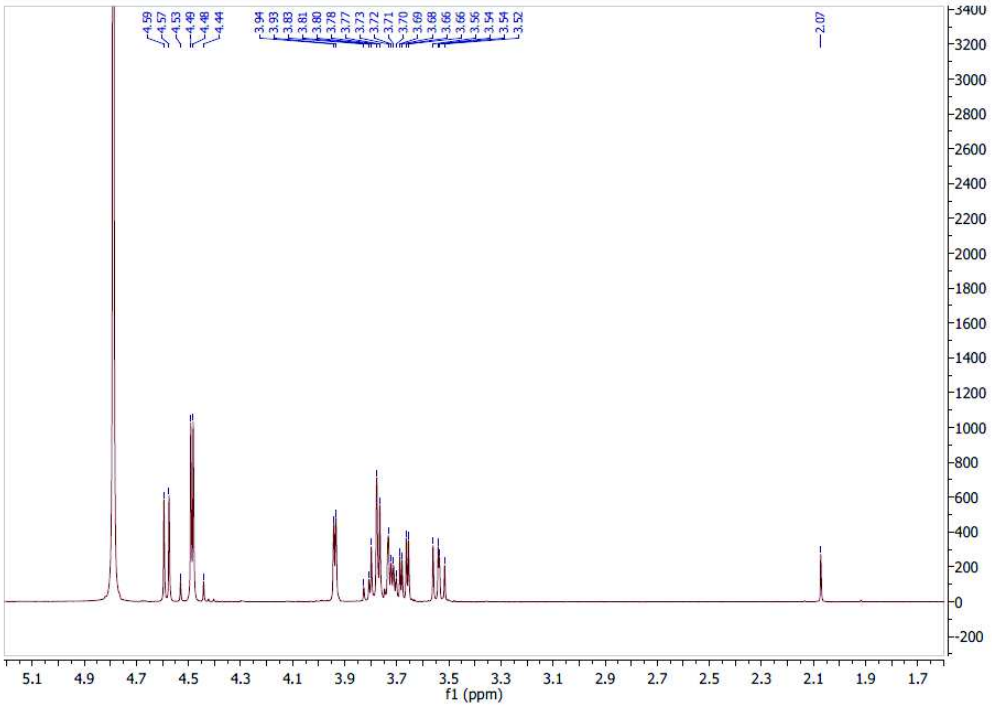

Figure IV.7. ^{1}H NMR spectrum of propargyl-β-D-galactopyranoside in D_2O

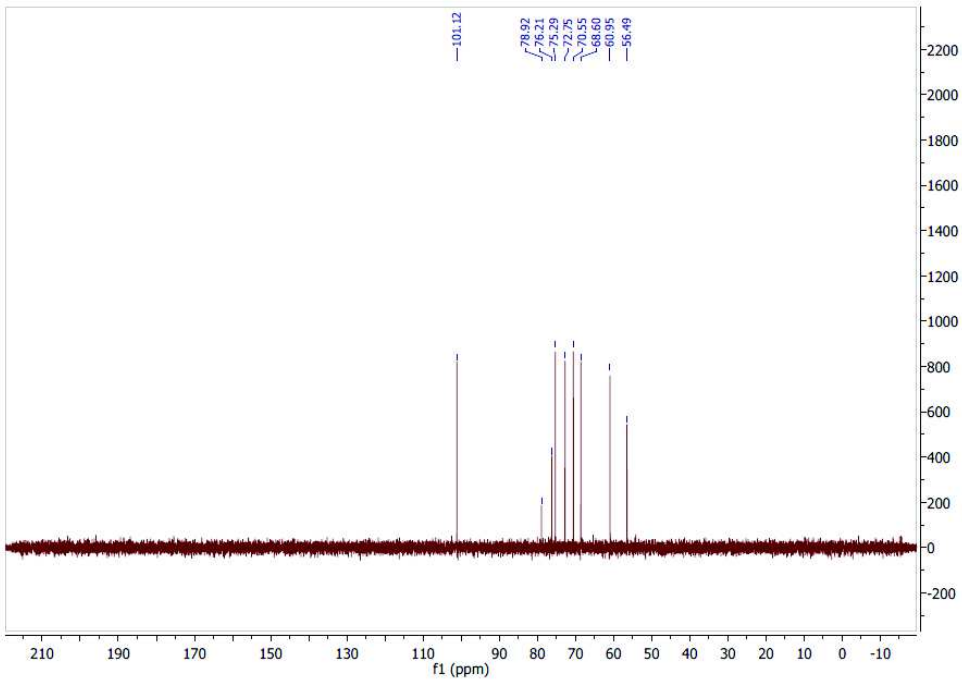

Figure IV.8. ^{13}C NMR spectrum of propargyl-β-D-galactopyranoside in D_2O

Synthesis of Propargyl-α-D-mannopyranoside

Propargyl-α-D-mannopyranoside was obtained from a two-step synthesis as illustrated in Scheme IV.6.

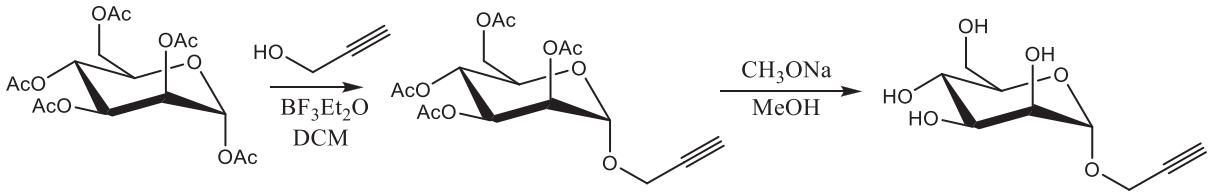

Scheme IV.6. Two-step synthesis of propargyl-α-D-mannopyranoside

To a stirred solution of α-D-mannopyranose pentaacetate (3 g, 7.69 mmol) and propargyl alcohol (0.54 mL, 1.2 equiv.) in anhydrous DCM (30 mL) at 0 °C was added dropwise boron trifluoridediethylether (1.44 mL, 1.5 equiv.). After 2.5 hours, the reaction mixture was washed with ice-cold water (water and ice), saturated $NaHCO_3$ and saturated NaCl. Organic

phase was then dried under Na_2SO_4 and concentrated in the rotavapor. The by-product (propargyl-2,3,4,6-tetra-*O*-acetyl-α-D-mannopyranoside, 0.821 g) was then deacetylated in 20 mL of methanol containing sodium methylate (1M, 200 µL). After 3 h, when the deacetylation was finished, the solution was neutralized with the acid resin Amberlite IR 120 H^+, filtered through cotton and concentrated. Propargyl-α-D-mannopyranoside was isolated (61% yield) after purification by flash chromatography on silica gel using acetonitrile and distilled water (0.95:0.5 v/v) as eluent (2 L). Purified propargyl-α-D-mannopyranoside was then used in the azide-alkyne copper catalyzed cycloaddition reaction with f-PCL-N_3 fibrous mats in a heterogeneous phase, at the interface between water and fiber's surface.

^{1}H NMR (D_2O, 400 MHz) δ: 5.06 (d, 1H, *J*= 1.57 Hz), 4.36 (qd, 2H, *J*= 2.38, 2.36 Hz), 3.90-3.99 (m, 2H), 3.69-3.84 (m, 4H), 2.94-2.95 (m, 2H).

^{13}C NMR (D_2O, 400 MHz) δ: 98.74, 78.81, 76.15, 73.11, 70.43, 69.92, 66.60, 60.80, 54.54.

MALDI-TOF MS: calcd for $C_9H_{14}O_6$ m/z=218.08; found m/z= 241 $[M+Na]^+$.

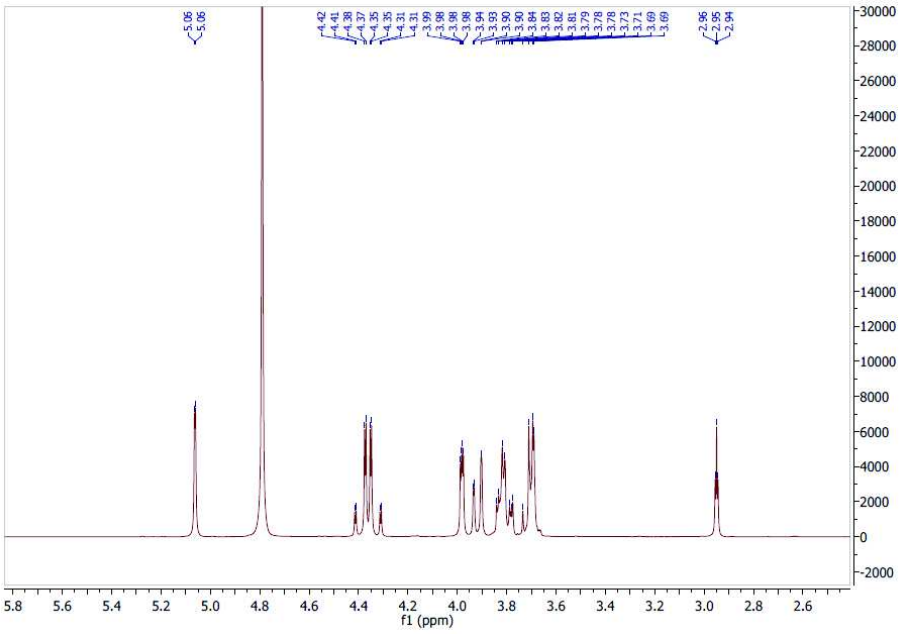

Figure IV.9. ^{1}H NMR spectrum of propargyl-α-D-mannopyranoside in D_2O

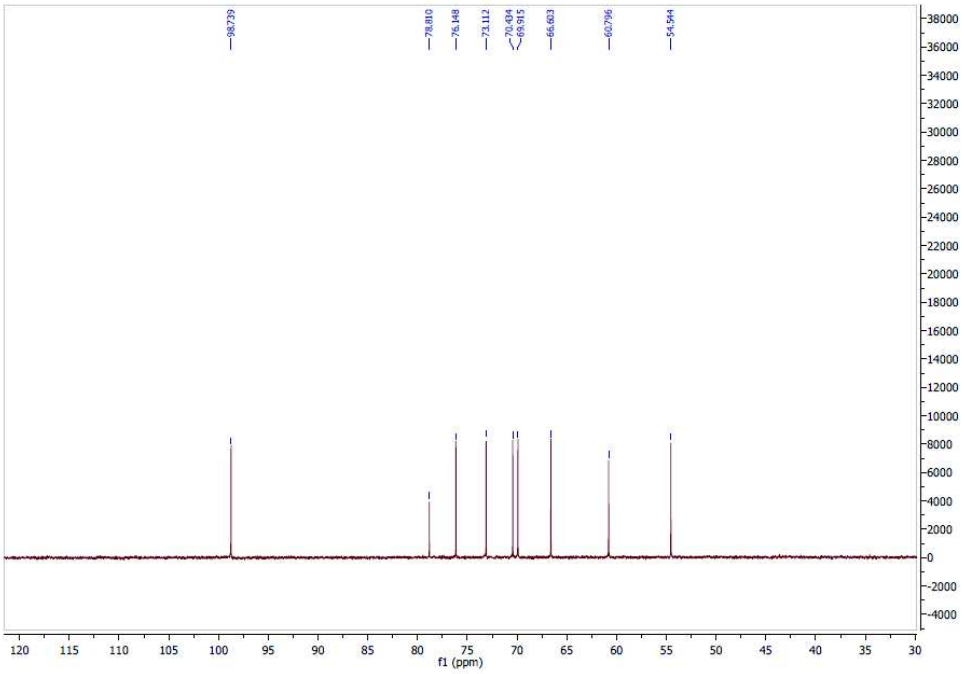

Figure IV.10. ^{13}C NMR spectrum of propargyl-α-D-galactopyranoside in D_2O

3. Electrospinning

Electrospinning setup was designed and manufactured in our laboratory and it is composed of three main units:

- The feeding unit is a syringe pump (KD Scientific series 200, USA) containing a syringe pump filled with electrospinning solution with the blunt 21-gauge needle. Solution flow rate was ranging from 0.01 to 0.03 mL/min.
- The high tension unit is a dual high voltage supply (iseq GMBH Germany, with a ±30 kV range) and was used in experiments in the range between 11 and 15 kV. As the distance between the needle tip and collector was 15 cm, the electric field exerted on the solution in flow was from 0.7 to 1 kV/cm.
- The collecting unit used in the experiments was either static (10 cm^2 aluminium foil) for collecting randomly deposited electrospun fibers, or dynamic and it

consisted of a rotating disc (having 6.5 cm radius and 1.5 cm large) for collecting aligned fibrous mats. Rotating disc was connected to a DC motor (~ 70 W) having the upper speed limit of 1800 rpm.

- All experiments were done at room temperature. The relative humidity noted was between 20 and 55%. For decreasing the relative humidity of the electrospinning box, a dry air was purged at 8 bars (Dew point 4°C) until the humidity was decreased to a desired level.

Preparation of Electrospinning Solutions

Fibrous membranes based on different polymers and polymer blends, were electrospun from a polymer solution. Each solution preparation is detailed below.

f-PCL-N_3 fibers: polymer solutions were prepared in dichoromethane/methanol (DCM/MeOH 4/1) solvent mixture at room temperature. A high molecular weight PCL_{80} and PCL-N_3 were blended in different ratios (20, 40 and 60 wt. % of PCL-N_3) to give a final concentration of 10, 16 and 23 wt. % of polymer in DCM/MeOH solvent mixture, respectively. Polymer content in electrospinning solution is calculated as a mass of the polymer divided by the total mass of both polymer and solvent mixture using the following equation:

$$wt\% = \frac{(mass\ of\ polymer)}{(mass\ of\ polymer + mass\ of\ solvent)} \times 100\% \qquad \text{(IV.1)}$$

f-PCL-Gal_B fibers: PCL_2-Gal was blended with PCL_{80} in ratio 20:80 and 40:60 w/w in DCM/MeOH 4/1 solvent mixture and electrospun. Resulting fibers: f-PCL_{20}-Gal_B and f-PCL_{40}-Gal_B stand for a blend of bulk-functionalized PCL_2-Gal and PCL_{80} polymers in ratios 20/80 and 40/60, respectively.

Polystyrene fibers: Electrospinning solutions of a blend containing hydrogenated (hPS) and perdeuterated (dPS) polystyrene in 1:1 ratio and PS homopolymer solution were prepared

in DMF with a final concentration of 27 w/v %. In order to minimize the possibility of pore formation at the surface of the fibers, humidity was kept below 20%.

Preparation of Polymer Film

PCL_{80} and PCL-N_3 (60 wt. % of PCL-N_3 in the blend) were dissolved in DCM/MeOH (volume ratio 4/1) solvent mixture to a final concentration of 23 wt. %. Polymer cast film was obtained from the solution deposited onto a glass slide that was kept in a vacuum oven at 60 °C for 20 minutes.

4. Heterogeneous Click Chemistry on Solid Nanofibers

Surface Modification of f-PCL-N_3Fibrous Scaffolds with FITC Fluorophore

Reaction click between propargyl-FITC and azido-fibers in heterogeneous phase is described on the f-PCL-N_3-60 fibers as example. Prior use, 0.1 M solutions of $CuSO_4 \cdot 5H_2O$ and of sodium ascorbate, as well as FITC solution in acetonitrile/water, were filtered through PTFE (0.2 µm) filter in order to eliminate possible undissolved crystals that could aggregate on the fibers. f-PCL-N_3-60 fibers (2 mg) were put in the microcentrifuge tube containing 500 µL of acetonitrile, and then 56 µL (10 equiv. per azide group on the surface, as estimated by the ninhydrin assay) solution (6.42 mmol L^{-1}) of FITC-alkyne in acetonitrile/water (1:1) along with 500 µL of distilled water, 7 µL $CuSO_4 \cdot 5H_2O$ in distilled water (0.1 M, 6 equiv.) and 7 µL of sodium ascorbate in distilled water (0.1 M, 6 equiv.) were added. Reaction mixture was stirred in dark for 24 h at room temperature and then fibers were thoroughly washed with acetonitrile/water (1/1). f-PCL-N_3-20 and f-PCL-N_3-40 were prepared using same procedure by keeping the same molar ratio. Resulting f-PCL-N_3-20-FITC, f-PCL-N_3-40-FITC and f-PCL-N_3-60-FITC fibers were kept in acetonitrile/water (1/1) stock solution until observation.

Grafting of Monosaccharides onto the f-PCL-N_3 Fibers

Monosaccharides, propargyl-α-D-mannose and propargyl-β-D-galactose were conjugated onto the surface of f-PCL-N_3 -20, -40, and -60 nanofibers using click chemistry coupling. Resulting fibers were marked as f-PCL_{20}-Gal_S, f-PCL_{40}-Gal_S, and f-PCL_{60}-Gal_S for galactose surface-functionalized, while f-PCL_{20}-Man_S, f-PCL_{40}-Man_S, and f-PCL_{60}-Man_S correspond to the mannose surface-functionalized fibers from f-PCL-N_3 -20, -40, and -60 fibrous mats, respectively. Click reaction between propargyl-monosaccharides and azido-fibers in a heterogeneous phase will be described on example of the f-PCL_{20}-Gal_S fibers. f-PCL-N_3-20 fibers (20 mg) were put in a microcentrifuge tube containing 4 mL of distilled water. Then, 54.7 µL (10 equiv. per azide group on the surface, as estimated by the ninhydrin assay) of 0.1 M aqueous solution of propargyl-β-D-galactose, 21.9 µL $CuSO_4 \cdot 5H_2O$ in distilled water (0.1 M, 4 equiv.) and 21.9 µL of sodium ascorbate in distilled water (0.1 M, 4 equiv.) were added into the microcentrifuge tube. Reaction mixture was stirred for 24 h at room temperature and then fibers were thoroughly washed with distilled water. f-PCL_{40}-Gal_S and f-PCL_{60}-Gal_S were prepared from f-PCL-N_3-40 and f-PCL-N_3-60, respectively, following the same procedure while keeping the same molar ratio. f-PCL_{20}-Man_S, f-PCL_{40}-Man_S and f-PCL_{60}-Man_S functionalized fibers were prepared similarly as f-PCL-Gal_S fibers by replacing propargyl-β-D-galactose with propargyl-α-D-mannose.

5. Characterization Techniques

Fourier-Transformation Infra-Red (FTIR) Spectroscopy

FTIR spectra were recorded in the transmission mode using a Perkin-Elmer 1720X FTIR instrument. Depending of the sample tested, it was used CaF_2 optic plates for powder

compounds and attenuated transmission reflection, using single reflection diamond ATR, for electrospun scaffolds.

Nuclear-Magnetic Resonance (NMR) Spectroscopy

^{1}H and ^{13}C NMR spectra were obtained with a Bruker AVANCE 400 MHz with 5 mm QNP probe at 298 and 333 K.

Mass Spectrometry

Matrix-Assisted Laser Desorption Ionization – Time of Flight Mass Spectroscopy (MALDI-TOF MS) analyses were done in the ionization mode with Autoflex Bruker instrument.

Scanning-Electron Microscopy (SEM)

Field Emission gun Scanning Electron Microscope (FESEM ZEISS ULTRA55) was used for observing the morphology of the fibers at 1 kV accelerating voltage, 5 mm of working distance and at magnifications of 500, 1000 and 2000 times using In-Lens detection system. All samples were sputter coated with Pt of 1 nm thickness. Average fiber diameters of the electrospun fibers, were obtained as a mean value of 150 different diameters measured by ImageJ software.

Transmission Electron Microscopy (TEM)

Fibrous scaffolds were previously entrapped inside the epoxy resin and left some time for resin to solidify. An ultra-thin slice of fiber-containing resin was cut by microtome and observed under TEM microscope under 3000 and 6000 X magnifications.

Fluorescence Confocal Microscopy

Fluorescence intensity of the fibers was monitored using Leica TCS SP2 AOBS (Acoustico Optical Beam Splitter) confocal laser scanning system and an inverted fluorescence microscope equipped with an oil-immersion objective lens 40×. Fibrous samples were put in between two lamellae and covered with 4 µL of stock solution (acetonitrile/water). FITC-labeled fibers were visualized by excitation of the fluorophore with a 488 nm Ar/Kr laser and the emitted fluorescence was collected between 508 and 533 nm, precisely defined by the AOBS.

Viscosity Measurements

Viscosity measurements were done using MCR301 and MARS III controlled-stress rheometers equipped with cone-plate geometry: 60 mm titan cone, having 1° angle and 29 µm and 53 µm gap, respectively.

Dynamic Light Scattering

DLS measurements were performed using an ALV/CGS-8F goniometer, equipped with a linearly polarized He/Ne laser (λ = 632.8 nm, P = 35 mW) and an ALV multiple τ correlator with a 125 ns initial sampling time. The unfiltered mixtures were measured at 25 °C for a typical counting time of 200 s at a scattering angle of 90°. The size distributions were obtained with the CONTIN analysis of the autocorrelation functions and particularly with the Stokes-Einstein equation as detailed elsewhere.[254,255] The viscosity and refractive index of the DCM/MeOH 4/1 solvent mixture alone are calculated to be 0.466 cP and 1.398, respectively.[4]

Number-weighted distribution can be deduced from mass-weighted distribution as reported in Travelet *et al.*[246] Since ~350 nm and ~50 µm objects are present, and since the surface area under the peak of the polymer aggregates represent ~29% of the total surface area then:

$$\frac{N_{Polymer}}{N_{Solvent}} = \left(\frac{50.10^{-6}}{350.10^{-9}}\right)^3 * \left(\frac{0.29}{1-0.29}\right) = 1190818 \quad \text{(IV.2)}$$

$N_{Polymer}$ and $N_{Solvent}$ designate the number of PCL_2-Gal and solvent aggregates respectively.

Small-Angle Neutron Scattering

SANS measurements were performed at Laboratoire Léon Brillouin (LLB), CEA, Saclay, using PAXY beam line. The wavelength (λ) range used lies between 3.5 Å and 12 Å. Detector used is bi-dimentional, able to detect the anisotropy of analyzed sample.

Prior SANS analysis, fibers were removed from aluminium foil, placed between two flat quartz-optic cells, sealed, and put inside the sample holder rack.

Data sets were taken from 2D data, regrouped by sectors of 30 degrees in the direction of the fiber aligning axis, and 10 degrees for the direction perpendicular to the fiber alignment. The signal was substracted from the incoherent part due to hydrogen nuclei and detector noise and normalized by transmission of the sample using PAsiNET.MAT program. The collected results were fitted using standard Debye Gaussian Coil and Porod plots.

Water Contact Angle Measurements

Water Contact Angle (WCA) measurements were done in the sessile-drop mode at 20 °C using Dataphysics Intruments Gmb goniometer. Nonwoven fibrous meshes were fixed onto an object slide using adhesive tapes at the sides of the sample. The volume of the applied droplet is 1 µL. The resulting value of each measurement represents the average value of the left and the right contact angle. The images of the water droplet on electrospun fiber meshes and the corresponding contact angle were recorded from droplet deposition onto the fibers until its stabilization.

Ninhydrin Test on Solid Electrospun Nonwovens

Ninhydrin test was adapted for the detection and quantification of the azide groups (-$N=N^+=N^-$) on PCL fibers. f-PCL-N_3 fibers (10 mg) were dropped in 10 g L^{-1} PPh_3 solution in ethanol (2 mL) for 15 minutes in order to reduce the azide to amine groups. Reduced f-PCL-N_3 fibers were washed in ethanol and then dissolved in 1,4-dioxane (500 µL). Solution mixture of ninhydrin (2 g) and hydrindantin (0.3 g) in 75 mL DMSO and sodium acetate buffer (25 mL) was prepared under argon. It is important that this solution is always fresh and prepared the day when the measurement is taken. The solution mixture was then added (500 µL) to the solution of fibers in 1,4-dioxane (1/1 v/v) in the screw-capped test tubes, heated at 100 °C for 15 minutes and finally cooled in an ice bath. At the end, 3 mL of 1,4-dioxane was added into each tube, thoroughly mixed with a Vortex mixer and absorbance at 570 nm was measured with UVIKON 810 UV-vis spectrophotometer.

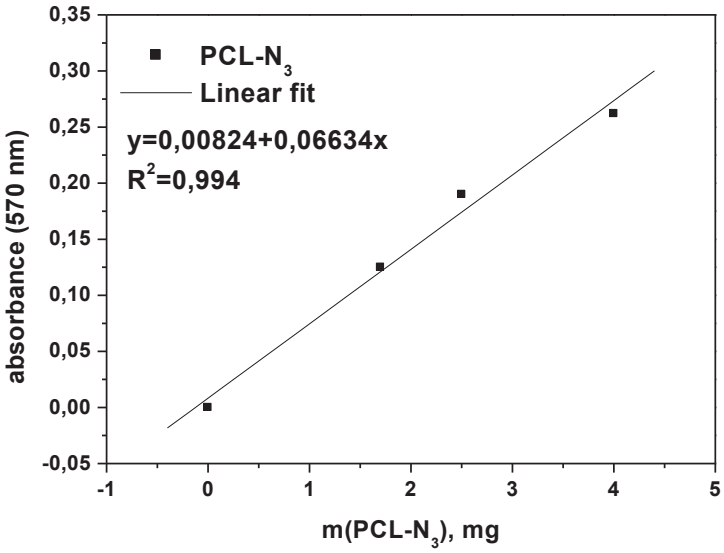

Figure IV.11. Calibration curve as a correlation between the mass of reduced PCL-N_3 to PCL-NH_2, dissolved in 500 µL 1,4-dioxane and absorbance at 570 nm

Figure IV.11 represents the calibration curve of PCL-N_3 polymer powder, used for quantification of azides on the surface of f-PCL-N_3 fibers. PCL-N_3 polymer was reduced to PCL-NH_2 in solution of PPh_3 in ethanol at room temperature. Ninhydrin test was performed following the same procedure as described for f-PCL-N_3 fibers.

Phenol-Sulphuric Acid Assay (Dubois Method)

Sugar-decorated fibers (2 mg) were dispersed in 100 µL of distilled water and 100 µL of phenol solution (5 w/v %) was added followed by addition of 1 mL of 96% of sulfuric acid. The solution was vigorously agitated for 15 min at room temperature and absorbance at 490 nm was measured with UVIKON 810 UV-Vis spectrophotometer. The concentration of sugar was determined by reference to a calibration curve with galactose as a standard for f-PCL-Gal_S fibers and mannose as a standard for f-PCL-Man_S fibers.

Enzymatic Hydrolysis

f-PCL-Gal_B fibers (4 mg) were put in microcentrifuge tube containing 500 µL acetate buffer (0.2 M, pH=4.50) and 25 µL of *β*-galactosidase from *Aspergillus oryzae* (Sigma) (200 units/mL in PBS 1:10 dilution), at 30 °C with gentle stirring. The sample (50 µL) was taken after 4, 24, 48 and 72 h reaction time for the standard phenol-sulfuric acid colorimetric titration in aqueous medium.

Enzyme-Linked Lectin Assay (ELLA)

ELLA test was done to determine the presence and bioavailability of the carbohydrates on the fiber surface. Prepared solutions of horseradish peroxidase-labeled lectin (HRP) from *Canavalia ensiformis* (HRP-ConA, mannose-binding lectin) and horseradish peroxidase-labeled lectin (HRP) from *Arachis hypogaea* (HRP-PNA, galactoside-binding lectin) were used. Carbohydrate bulk- and surface-functionalized fibers, f-PCL-Gal_B and f-PCL-Gal_S as well

as native fibers, PCL_{80}, were placed separately in screw-capped test tubes and left for 5 min at room temperature in PBS (1:10 dilution, pH=7.2-7.6) containing 2 vol. % of TWEEN 20 for blocking extra binding sites. The fibers were washed in PBS (1:10 dilution) and then put in a 1 mL of fresh PBS (1:10 dilution) containing 25 μL of HRP-PNA solution (200 μg mL^{-1}), with 1 mM $MnCl_2$, 1 mM $MgCl_2$ and 1 mM $CaCl_2$ for 16 h at 20 °C. Fibers were then thoroughly washed with PBS (1:10 dilution) and then put in 4 mL of deionized water where 2 drops of (2.5 M, pH=5.0) acetate buffer, 1 drop of AEC Chromogen (Sigma) and 1 drop of 3% hydrogen peroxide were added. After 10-15 minutes, the reddish coloration of the f-PCL-Gal_B and f-PCL-Gal_S fibers was observed. Similar procedure was followed for f-PCL-Man_S fibers with the difference of the lectin used. For α-mannose recognition, 25 μL of HRP-ConA solution (200 μg/mL) was used.

References

References

(1) Taylor, G. F. *Physical Review* **1924**, *23*, 655–660.
(2) Ondarçuhu, T.; Joachim, C. *Europhysics Letters (EPL)* **1998**, *42*, 215–220.
(3) Cao, G.; Liu, D. *Advances in Colloid and Interface Science* **2008**, *136*, 45–64.
(4) Yang, Z.; Niu, Z.; Cao, X.; Yang, Z.; Lu, Y.; Hu, Z.; Han, C. C. *Angewandte Chemie International Edition* **2003**, *42*, 4201–4203.
(5) Thurn-Albrecht, T.; Schotter, J.; Kästle, G. A.; Emley, N.; Shibauchi, T.; Krusin-Elbaum, L.; Guarini, K.; Black, C. T.; Tuominen, M. T.; Russell, T. P. *Science* **2000**, *290*, 2126–2129.
(6) Lakshmi, B. B.; Dorhout, P. K.; Martin, C. R. *Chemistry of Materials* **1997**, *9*, 857–862.
(7) Lei, B.; Shin, K.-H.; Noh, D.-Y.; Jo, I.-H.; Koh, Y.-H.; Kim, H.-E.; Kim, S. E. *Materials Science and Engineering: C* **2013**, *33*, 1102–1108.
(8) Sharma, M. K.; Ambolikar, A. S.; Aggarwal, S. K. *Journal of Nanoparticle Research* **2012**, *14*, 1–10.
(9) Hulteen, J. C.; Chen, H. X.; Chambliss, C. K.; Martin, C. R. *Nanostructured Materials* **1997**, *9*, 133–136.
(10) Porter, J. R.; Henson, A.; Popat, K. C. *Biomaterials* **2009**, *30*, 780–788.
(11) Hoa, N. D.; Van Quy, N.; Cho, Y.; Kim, D. *Sensors and Actuators B* **2007**, *127*, 447–454.
(12) Grimm, S.; Martín, J.; Rodriguez, G.; Fernández-Gutierrez, M.; Mathwig, K.; Wehrspohn, R. B.; Gösele, U.; Roman, J. S.; Mijangos, C.; Steinhart, M. *Journal of Materials Chemistry* **2010**, *20*, 3171–3177.
(13) Smith, L. A.; Liu, X.; Ma, P. X. *Soft Matter* **2008**, *4*, 2144–2149.
(14) Diban, N.; Haimi, S.; Bolhuis-Versteeg, L.; Teixeira, S.; Miettinen, S.; Poot, A.; Grijpma, D.; Stamatialis, D. *Journal of Membrane Science* **2013**, *438*, 29–37.
(15) Chung, T.-W.; Yang, M.-C.; Tseng, C.-C.; Sheu, S.-H.; Wang, S.-S.; Huang, Y.-Y.; Chen, S.-D. *Biomaterials* **2011**, *32*, 734–743.
(16) Asefnejad, A.; Khorasani, M. T.; Behnamghader, A.; Farsadzadeh B.; Bonakdar S. *International Journal of Nanomedicine* **2011**, 2375.
(17) Dobry, A; Boyer-Kawenoki, F. J. *Journal of Polymer Science Part A: Polymer Chemistry* **1947**, *2*, 90-100.
(18) Huie, J. C. *Smart Materials and Structures* **2003**, *12*, 264–271.
(19) Zhang, S. *Biotechnology Advances* **2002**, *20*, 321–339.
(20) Polarz, S.; Smarsly, B.; Antonietti, M. *ChemPhysChem* **2001**, *2*, 457–461.
(21) Kadler, K. E.; Holmes, D. F.; Trotter, J, A.; Chapman, J A. *Biochemical Journal* **1996**, *316*, 1–11.
(22) Shibata, M.; Teramoto, N.; Kaneko, K. *Journal of Polymer Science Part B: Polymer Physics* **2010**, *48*, 1281–1289.
(23) Vauthey, S.; Santoso, S.; Gong, H.; Watson, N.; Zhang, S. *Proceedings of National Academy of Science of the U.S.A* **2002**, *99*, 5355–5360.
(24) Cooley, J. F. *Apparatus for Electrically Dispersing Fluids* 692631, February 4, **1902**.
(25) Cooley, J. F. *Electrical Method of Dispersing Fluids* 745276, November 24, **1903**.
(26) Formhals, A. *Process and Apparatus for Preparing Artificial Threads* 1975504, October 2, **1934**.
(27) Formhals, A. *Method and apparatus for spinning* 2349950, May 30, **1944**.
(28) Formhals, A. *Artificial Thread and Method of Producing Same* 2187306, January 16, **1940**.

(29) Taylor, G. *Proceedings of the Royal Society: A* **1964**, *280*, 383–397.
(30) Doshi, J.; Reneker, D. H. *Journal of Electrostatics* **1995**, *35*, 151–160.
(31) Reneker, D. H.; Chun, I. *Nanotechnology* **1996**, *7*, 216–223.
(32) Yarin, A. L.; Koombhongse, S.; Reneker, D. H. *Journal of Applied Physics* **2001**, *90*, 4836–4846.
(33) Koombhongse, S.; Liu, W.; Reneker, D. H. *Journal of Polymer Science Part B: Polymer Physics* **2001**, *39*, 2598–2606.
(34) Badgley, W. J.; Mark, H. *Journal of Physical and Colloid Chemistry* **1947**, *51*, 58–70.
(35) Daoud, M.; Cotton, J. P.; Farnoux, B.; Jannink, G.; Sarma, G.; Benoit, H.; Duplessix, C.; Picot, C.; de Gennes, P. G. *Macromolecules* **1975**, *8*, 804–818.
(36) de Gennes, G.; Scaling Concepts in Polymer Physics, *Cornell University Press*, Ithaca, N. Y. **1979**
(37) Gupta, P.; Elkins, C.; Long, T. E.; Wilkes, G. L. *Polymer* **2005**, *46*, 4799–4810.
(38) Shenoy, S. L.; Bates, W. D.; Frisch, H. L.; Wnek, G. E. *Polymer* **2005**, *46*, 3372–3384.
(39) Munir, M. M.; Suryamas, A. B.; Iskandar, F.; Okuyama, K. *Polymer* **2009**, *50*, 4935–4943.
(40) Wang, C.; Cheng, Y.-W.; Hsu, C.-H.; Chien, H.-S.; Tsou, S.-Y. *Journal of Polymer Research* **2011**, *18*, 111–123.
(41) Lindner, A.; Wagner, C. *Comptes Rendus Physique* **2009**, *10*, 712–727.
(42) Schoenmaker, B. D.; Goethals, A.; Schueren, L. V. der; Rahier, H.; Clerck, K. D. *Journal of Materials Science* **2012**, *47*, 4118–4126.
(43) Jia, L.; Qin, X. *Journal of Thermal Analysis and Calorimetry* **2013**, *112*, 595–605.
(44) Luo, C. J.; Stride, E.; Edirisinghe, M. *Macromolecules* **2012**, *45*, 4669–4680.
(45) Guarino, V.; Cirillo, V.; Taddei, P.; Alvarez-Perez, M. A.; Ambrosio, L. *Macromolecular Bioscience* **2011**, *11*, 1694–1705.
(46) Pattamaprom, C.; Hongrojjanawiwat, W.; Koombhongse, P.; Supaphol, P.; Jarusuwannapoo, T.; Rangkupan, R. *Macromolecular Materials and Engineering* **2006**, *291*, 840–847.
(47) Jarusuwannapoom, T.; Hongrojjanawiwat, W.; Jitjaicham, S.; Wannatong, L.; Nithitanakul, M.; Pattamaprom, C.; Koombhongse, P.; Rangkupan, R.; Supaphol, P. *European Polymer Journal* **2005**, *41*, 409–421.
(48) Son, W. K.; Youk, J. H.; Lee, T. S.; Park, W. H. *Polymer* **2004**, *45*, 2959–2966.
(49) Zong, X.; Kim, K.; Fang, D.; Ran, S.; Hsiao, B. S.; Chu, B. *Polymer* **2002**, *43*, 4403–4412.
(50) Abdelmegeid, M. A.; Soliman, M. J.; Anke Klingner, A. *Journal of Genetic Engineering and Biotechnology*, **2010**, *8*, 29–32.
(51) Sundaray, B.; Bossard, F.; Latil, P.; Orgéas, L.; Sanchez, J. Y.; Lepretre, J. C. *Polymer* **2013**, *54*, 4588–4593.
(52) Medeiros, E. S.; Mattoso, L. H. C.; Offeman, R. D.; Wood, D. F.; Orts, W. J. *Canadian Journal of Chemistry* **2008**, *86*, 590–599.
(53) Demir, M. M. *eXPRESS Polymer Letters*, **2010**, *4*, 2–8.
(54) Teo, W. E.; Ramakrishna, S. *Nanotechnology* **2006**, *17*, R89–R106.
(55) Cooper, A.; Bhattarai, N.; Zhang, M. *Carbohydrate Polymers* **2011**, *85*, 149–156.
(56) Li, D.; Wang, Y.; Xia, Y. *Nano Letters* **2003**, *3*, 1167–1171.
(57) Teo, W. E.; Ramakrishna, S. *Nanotechnology* **2005**, *16*, 1878.
(58) Beachley, V.; Wen, X. *Materials Science and Engineering: C* **2009**, *29*, 663–668.
(59) Theron, A.; Zussman, E.; Yarin, A. L. *Nanotechnology* **2001**, *12*, 384.
(60) Sundaray, B.; Subramanian, V.; Natarajan, T. S.; Xiang, R.-Z.; Chang, C.-C.; Fann, W.-S. *Applied Physics Letters* **2004**, *84*, 1222–1224.

(61) Kim, K. W.; Lee, K. H.; Khil, M. S.; Ho, Y. S.; Kim, H. Y. *Fibers and Polymers* **2004**, *5*, 122–127.
(62) Zussman, E.; Theron, A.; Yarin, A. L. *Applied Physics Letters* **2003**, *82*, 973–975.
(63) Lavielle, N.; Hébraud, A.; Mendoza-Palomares, C.; Ferrand, A.; Benkirane-Jessel, N.; Schlatter, G. *Macromolecular Materials and Engineering* **2012**, *297*, 958–968.
(64) Dalton, P. D.; Klinkhammer, K.; Salber, J.; Klee, D.; Möller, M. *Biomacromolecules* **2006**, *7*, 686–690.
(65) Li, X.; Su, Y.; Liu, S.; Tan, L.; Mo, X.; Ramakrishna, S. *Colloids and Surfaces B: Biointerfaces* **2010**, *75*, 418–424.
(66) Sun, Z.; Zussman, E.; Yarin, A. l.; Wendorff, J. h.; Greiner, A. *Advanced Materials* **2003**, *15*, 1929–1932.
(67) Larsen, G.; Spretz, R.; Velarde-Ortiz, R. *Advanced Materials* **2004**, *16*, 166–169.
(68) Xu, X.; Yang, L.; Xu, X.; Wang, X.; Chen, X.; Liang, Q.; Zeng, J.; Jing, X. *Journal of Controlled Release* **2005**, *108*, 33–42.
(69) Xu, X.; Zhuang, X.; Chen, X.; Wang, X.; Yang, L.; Jing, X. *Macromolecular Rapid Communications* **2006**, *27*, 1637–1642.
(70) Yang, D.; Lu, B.; Zhao, Y.; Jiang, X. *Advanced Materials* **2007**, *19*, 3702–3706.
(71) Jirsak, O.; Petrik, S. *International Journal of Nanotechnology* **2012**, *9*, 836–845.
(72) Yarin, A. L.; Zussman, E. *Polymer* **2004**, *45*, 2977–2980.
(73) Hammouda, B. *NIST Tutorial*, Part II, SANS Nuts and Bolts
(74) Bates, F. S. *Macromolecules* **1985**, *18*, 525–528.
(75) Hammouda, B.; Ho, D. L. *Journal of Polymer Science Part B: Polymer Physics* **2007**, *45*, 2196–2200.
(76) Norman, A. I.; Fei, Y.; Ho, D. L.; Greer, S. C. *Macromolecules* **2007**, *40*, 2559–2567.
(77) Wu, L.; Lodge, T. P.; Bates, F. S. *Macromolecules* **2006**, *39*, 294–299.
(78) Zeroni, I.; Lodge, T. P. *Macromolecules* **2008**, *41*, 1050–1052.
(79) Jones, R. L.; Kumar, S. K.; Ho, D. L.; Briber, R. M.; Russell, T. P. *Nature* **1999**, *400*, 146–149.
(80) Millon, L. E.; Nieh, M.-P.; Hutter, J. L.; Wan, W. *Macromolecules* **2007**, *40*, 3655–3662.
(81) Burford, R. P.; Markotsis, M. G.; Knott, R. B. *Physica B: Condensed Matter* **2006**, *385–386, Part 1*, 766–769.
(82) Gerber, M. J.; Walker, L. M. *Langmuir* **2006**, *22*, 941–948.
(83) Castelletto, V.; Newby, G. E.; Zhu, Z.; Hamley, I. W.; Noirez, L. *Langmuir* **2010**, *26*, 9986–9996.
(84) Hammouda, B. *Journal of Polymer Science Part B: Polymer Physics* **2006**, *44*, 3195–3199.
(85) Hadjiantoniou, N. A.; Triftaridou, A. I.; Kafouris, D.; Gradzielski, M.; Patrickios, C. S. *Macromolecules* **2009**, *42*, 5492–5498.
(86) Boué, F.; Bastide, J.; Buzier, M.; Lapp, A.; Herz, J.; Vilgis, T. A. *Colloid and Polymer Science* **1991**, *269*, 195–216.
(87) Hudson, S. D.; Hutter, J. L.; Nieh, M.-P.; Pencer, J.; Millon, L. E.; Wan, W. *The Journal of Chemical Physics* **2009**, *130*, 034903–034903–9.
(88) Mohan, S. D.; Davis, F., J.; Olley, R. H.; Mitchell, G. R. *Journal of Physics: Conference Series* **2010**, *247*, 012042.
(89) Williams, D. F. *Biomaterials* **2008**, *29*, 2941–2953.
(90) Holzapfel, B. M.; Reichert, J. C.; Schantz, J.-T.; Gbureck, U.; Rackwitz, L.; Nöth, U.; Jakob, F.; Rudert, M.; Groll, J.; Hutmacher, D. W. *Advanced Drug Delivery Reviews*.
(91) Hench, L. L.; Wilson, J. *Science* **1984**, *226*, 630–636.
(92) Hench, L. L. *Science* **1980**, *208*, 826–831.

(93) Hench, L. L.; Polak, J. M. *Science* **2002**, *295*, 1014–1017.
(94) Williams, D. F. *Biomaterials* **2009**, *30*, 5897–5909.
(95) Stevens, M. M.; George, J. H. *Science* **2005**, *310*, 1135–1138.
(96) Chakraborty, S.; Liao, I.-C.; Adler, A.; Leong, K. W. *Advanced Drug Delivery Reviews* **2009**, *61*, 1043–1054.
(97) Hu, J.; Wei, J.; Liu, W.; Chen, Y. *Journal of Biomaterials Science, Polymer Edition* **2013**, *24*, 972–985.
(98) Mickova, A.; Buzgo, M.; Benada, O.; Rampichova, M.; Fisar, Z.; Filova, E.; Tesarova, M.; Lukas, D.; Amler, E. *Biomacromolecules* **2012**, *13*, 952–962.
(99) Dasaratha Dhanaraju, M.; Vema, K.; Jayakumar, R.; Vamsadhara, C. *International Journal of Pharmaceutics* **2003**, *268*, 23–29.
(100) Dasaratha Dhanaraju, M.; Gopinath, D.; Rafiuddin Ahmed, M.; Jayakumar, R.; Vamsadhara, C. *Journal of Biomedical Materials Research Part A* **2006**, *76A*, 63–72.
(101) Lalani, R.; Liu, L. *Biomacromolecules* **2012**, *13*, 1853–1863.
(102) Merrell, J. G.; McLaughlin, S. W.; Tie, L.; Laurencin, C. T.; Chen, A. F.; Nair, L. S. *Clinical and Experimental Pharmacology and Physiology* **2009**, *36*, 1149–1156.
(103) Francis, M. P.; Sachs, P. C.; Madurantakam, P. A.; Sell, S. A.; Elmore, L. W.; Bowlin, G. L.; Holt, S. E. *Journal of Biomedical Materials Research Part A* **2012**, *100A*, 1716–1724.
(104) Ghasemi-Mobarakeh, L.; Prabhakaran, M. P.; Morshed, M.; Nasr-Esfahani, M. H.; Ramakrishna, S. *Materials Science and Engineering: C* **2010**, *30*, 1129–1136.
(105) Schiffman, J. D.; Schauer, C. L. *Polymer Reviews* **2008**, *48*, 317–352.
(106) Pashkuleva, I.; Reis, R. L. *Journal of Materials Chemistry* **2010**, *20*, 8803–8818.
(107) Sharon, N.; Lis, H. *Scientific American* **1993**, *268*, 82–89.
(108) Bastide, L.; Priem, B.; Fort, S. *Carbohydrate Research* **2011**, *346*, 348–351.
(109) Gentsch, R.; Pippig, F.; Nilles, K.; Theato, P.; Kikkeri, R.; Maglinao, M.; Lepenies, B.; Seeberger, P. H.; Börner, H. G. *Macromolecules* **2010**, *43*, 9239–9247.
(110) Pillai, C. K. S.; Paul, W.; Sharma, C. P. *Progress in Polymer Science* **2009**, *34*, 641–678.
(111) Yang, Y.; Wu, J.; Wang, X.; Liu, J.; Ding, F.; Gu, X. *Advanced Engineering Materials* **2009**, *11*, B209–B218.
(112) Hussain, A.; Collins, G.; Yip, D.; Cho, C. H. *Biotechnology and Bioengineering* **2013**, *110*, 637–647.
(113) Hirano, S.; Zhang, M.; Nakagawa, M.; Miyata, T. *Biomaterials* **2000**, *21*, 997–1003.
(114) Ohkawa, K.; Cha, D.; Kim, H.; Nishida, A.; Yamamoto, H. *Macromolecular Rapid Communications* **2004**, *25*, 1600–1605.
(115) Ohkawa, K.; Minato, K.-I.; Kumagai, G.; Hayashi, S.; Yamamoto, H. *Biomacromolecules* **2006**, *7*, 3291–3294.
(116) Nguyen, T. T. T.; Chung, O. H.; Park, J. S. *Carbohydrate Polymers* **2011**, *86*, 1799–1806.
(117) Sell, S. A.; McClure, M. J.; Barnes, C. P.; Knapp, D. C.; Walpoth, B. H.; Simpson, D. G.; Bowlin, G. L. *Biomedical Materials* **2006**, *1*, 72.
(118) Sell, S. A.; Wolfe, P. S.; Garg, K.; McCool, J. M.; Rodriguez, I. A.; Bowlin, G. L. *Polymers* **2010**, *2*, 522–553.
(119) Zhang, Y.; Ouyang, H.; Lim, C. T.; Ramakrishna, S.; Huang, Z.-M. *Journal of Biomedical Materials Research Part B: Applied Biomaterials* **2005**, *72B*, 156–165.
(120) Chen, Z.; Cao, L.; Wang, L.; Zhu, H.; Jiang, H. *Journal of Applied Polymer Science* **2013**, *127*, 4225–4232.
(121) Yang, X.; Xu, Q.; Yan, N.; Sui, G.; Cai, Q.; Deng, X. *Polymers for Advanced Technologies* **2011**, *22*, 2222–2230.

(122) Khadka, D. B.; Haynie, D. T. *Nanomedicine: Nanotechnology, Biology and Medicine* **2012**, *8*, 1242–1262.
(123) Khadka, D. B.; Haynie, D. T. *ACS Applied Materials and Interfaces* **2010**, *2*, 2728–2732.
(124) Khadka, D. B.; Cross, M. C.; Haynie, D. T. *ACS Applied Materials and Interfaces* **2011**, *3*, 2994–3001.
(125) Tinschert, J.; Natt, G.; Mohrbotter, N.; Spiekermann, H.; Schulze, K. A. *Journal of Biomedical Materials Research Part B: Applied Biomaterials* **2007**, *80B*, 317–321.
(126) Vega-Lugo, A.-C.; Lim, L.-T. *Journal of Polymer Science Part B: Polymer Physics* **2012**, *50*, 1188–1197.
(127) Pakravan, M.; Heuzey, M.-C.; Ajji, A. *Biomacromolecules* **2012**, *13*, 412–421.
(128) Rieger, J.; Dubois, P.; Jérôme, R.; Jérôme, C. *Langmuir* **2006**, *22*, 7471–7479.
(129) Torchilin, V. P. *Journal of Microencapsulation* **1998**, *15*, 1–19.
(130) Sharma, S.; Johnson, R. W.; Desai, T. A. *Langmuir* **2004**, *20*, 348–356.
(131) Grafahrend, D.; Calvet, J. L.; Salber, J.; Dalton, P. D.; Moeller, M.; Klee, D. *Journal of Materials Science: Materials in Medicine* **2008**, *19*, 1479–1484.
(132) Grafahrend, D.; Calvet, J. L.; Klinkhammer, K.; Salber, J.; Dalton, P. D.; Möller, M.; Klee, D. *Biotechnology and Bioengineering* **2008**, *101*, 609–621.
(133) Wang, N.; Burugapalli, K.; Song, W.; Halls, J.; Moussy, F.; Zheng, Y.; Ma, Y.; Wu, Z.; Li, K. *Journal of Membrane Science* **2013**, *427*, 207–217.
(134) Wang, N.; Burugapalli, K.; Song, W.; Halls, J.; Moussy, F.; Ray, A.; Zheng, Y. *Biomaterials* **2013**, *34*, 888–901.
(135) Wang, H. B.; Mullins, M. E.; Cregg, J. M.; Hurtado, A.; Oudega, M.; Trombley, M. T.; Gilbert, R. J. *Journal Neural Engineering* **2009**, *6*, 016001.
(136) Yang, F.; Murugan, R.; Ramakrishna, S.; Wang, X.; Ma, Y.-X.; Wang, S. *Biomaterials* **2004**, *25*, 1891–1900.
(137) Yang, F.; Murugan, R.; Wang, S.; Ramakrishna, S. *Biomaterials* **2005**, *26*, 2603–2610.
(138) Cui, W.; Cheng, L.; Li, H.; Zhou, Y.; Zhang, Y.; Chang, J. *Polymer* **2012**, *53*, 2298–2305.
(139) Xing, Z.-C.; Han, S.-J.; Shin, Y.-S.; Kang, I.-K. *Journal of Nanomaterials* **2011**, *2011*.
(140) Hutmacher, D. W. *Journal of Biomaterials Science, Polymer Edition* **2001**, *12*, 107–124.
(141) Labet, M.; Thielemans, W. *Chemical Society Reviews* **2009**, *38*, 3484–3504.
(142) Vert, M.; Li, S. M.; Spenlehauer, G.; Guerin, P. *Journal of Materials Science Materials in Medicine* **1992**, *3*, 432–446.
(143) Woodruff, M. A.; Hutmacher, D. W. *Progress in Polymer Science* **2010**, *35*, 1217–1256.
(144) Lam, C. X. F.; Savalani, M. M.; Teoh, S.-H.; Hutmacher, D. W. *Biomedical Materials* **2008**, *3*, 034108.
(145) Namboodiri, A. G.; Parameswaran, R. *Journal of Applied Polymer Science* **2013**, *129*, 2280–2286.
(146) Luong-Van, E.; Grøndahl, L.; Chua, K. N.; Leong, K. W.; Nurcombe, V.; Cool, S. M. *Biomaterials* **2006**, *27*, 2042–2050.
(147) Schnell, E.; Klinkhammer, K.; Balzer, S.; Brook, G.; Klee, D.; Dalton, P.; Mey, J. *Biomaterials* **2007**, *28*, 3012–3025.
(148) Malheiro, V. N.; Caridade, S. G.; Alves, N. M.; Mano, J. F. *Acta Biomaterialia* **2010**, *6*, 418–428.
(149) Liu, X.; Chu, P. K.; Ding, C. *Materials Science and Engineering: R: Reports* **2010**, *70*, 275–302.
(150) Agarwal, S.; Wendorff, J. H.; Greiner, A. *Advanced Materials* **2009**, *21*, 3343–3351.
(151) Steyaert, I.; Van der Schueren, L.; Rahier, H.; de Clerck, K. *Macromolecular Symposia* **2012**, *321-322*, 71–75.

(152) Van der Schueren, L.; De Schoenmaker, B.; Kalaoglu, Ö. I.; De Clerck, K. *European Polymer Journal* **2011**, *47*, 1256–1263.
(153) Van der Schueren, L.; Steyaert, I.; De Schoenmaker, B.; De Clerck, K. *Carbohydrate Polymers* **2012**, *88*, 1221–1226.
(154) Van der Schueren, L.; De Meyer, T.; Steyaert, I.; Ceylan, Ö.; Hemelsoet, K.; Van Speybroeck, V.; De Clerck, K. *Carbohydrate Polymers* **2013**, *91*, 284–293.
(155) Wulf, K.; Teske, M.; Löbler, M.; Luderer, F.; Schmitz, K.; Sternberg, K. *Journal of Biomedical Materials Research Part B: Applied Biomaterials* **2011**, *98B*, 89–100.
(156) Croll, T. I.; O'Connor, A. J.; Stevens, G. W.; Cooper-White, J. J. *Biomacromolecules* **2004**, *5*, 463–473.
(157) Huisgen, R. *Angewandte Chemie International Edition in English* **1963**, *2*, 565–598.
(158) Huisgen, R. *Angewandte Chemie International Edition in English* **1963**, *2*, 633–645.
(159) Kolb, H. C.; Finn, M. G.; Sharpless, K. B. *Angewandte Chemie International Edition* **2001**, *40*, 2004–2021.
(160) Tornøe, C. W.; Christensen, C.; Meldal, M. *Journal of Organic Chemistry* **2002**, *67*, 3057–3064.
(161) Whittaker, M. R.; Urbani, C. N.; Monteiro, M. J. *Journal of American Chemical Society* **2006**, *128*, 11360–11361.
(162) Wang, Q.; Chan, T. R.; Hilgraf, R.; Fokin, V. V.; Sharpless, K. B.; Finn, M. G. *Journal of American Chemical Society* **2003**, *125*, 3192–3193.
(163) Fleischmann, S.; Hinrichs, K.; Oertel, U.; Reichelt, S.; Eichhorn, K.-J.; Voit, B. *Macromolecular Rapid Communications* **2008**, *29*, 1177–1185.
(164) Fu, G. D.; Xu, L. Q.; Yao, F.; Zhang, K.; Wang, X. F.; Zhu, M. F.; Nie, S. Z. *ACS Applied Materials and Interfaces* **2009**, *1*, 239–243.
(165) Chang, Z.; Xu, Y.; Zhao, X.; Zhang, Q.; Chen, D. *ACS Applied Materials and Interfaces* **2009**, *1*, 2804–2811.
(166) Shi, Q.; Chen, X.; Lu, T.; Jing, X. *Biomaterials* **2008**, *29*, 1118–1126.
(167) Xu, N.; Lu, F.-Z.; Du, F.-S.; Li, Z.-C. *Macromolecular Chemistry and Physics* **2007**, *208*, 730–738.
(168) Hammouda, B. *Polymer Reviews* **2010**, *50*, 14–39.
(169) Arinstein, A.; Zussman, E. *Journal of Polymer Science Part B: Polymer Physics* **2011**, *49*, 691–707.
(170) Kim, G. H.; Yoon, H. *Applied Physics Letters* **2008**, *93*, 023127–023127–3.
(171) Mitchell, G. R.; Belal, M.; Davis, F. J.; Elliott, D. E.; Kariduraganavar, M.; Mohan, S. D.; Olley, R. H.; Sen, S. *Advanced Materials Research* **2008**, *55-57*, 33–36.
(172) Mohan, S. D.; Mitchell, G. R.; Davis, F. J. *Soft Matter* **2011**, *7*, 4397–4404.
(173) Mohan, S.; Sen, S.; Mitchell, G. R.; Olley, R. H.; Davis, F. J. *Journal of Physics: Conference Series* **2009**, *183*, 012019.
(174) Wannatong, L.; Sirivat, A.; Supaphol, P. *Polymer International* **2004**, *53*, 1851–1859.
(175) Chanunpanich, N.; Byun, H. *Journal of Applied Polymer Science* **2007**, *106*, 3648–3652.
(176) Lee, K. H.; Kim, H. Y.; Bang, H. J.; Jung, Y. H.; Lee, S. G. *Polymer* **2003**, *44*, 4029–4034.
(177) Eda, G.; Shivkumar, S. *Journal of Applied Polymer Science* **2007**, *106*, 475–487.
(178) Effects of Solvent Properties, Solvent System http://www.docstoc.com/docs/34974145/Effects-of-Solvent-Properties-Solvent-System
(179) Manee-in, J.; Nithitanakul M.; Supaphol P. *Iranian Polymer Journal*, **2006**, *15*, 341–354.
(180) Fashandi, H.; Karimi, M. *Thermochimica Acta* **2012**, *547*, 38–46.
(181) Eda, G.; Liu, J.; Shivkumar, S. *European Polymer Journal* **2007**, *43*, 1154–1167.
(182) Arinstein, A.; Burman, M.; Gendelman, O.; Zussman, E. *Nature Nanotechnology* **2007**, *2*, 59–62.

(183) Arinstein, A. *Journal of Polymer Science Part B: Polymer Physics* **2013**, *51*, 756–763.
(184) Ji, Y.; Li, C.; Wang, G.; Koo, J.; Ge, S.; Li, B.; Jiang, J.; Herzberg, B.; Klein, T.; Chen, S.; Sokolov, J. C.; Rafailovich, M. H. *EPL Europhysics Letters* **2008**, *84*, 56002.
(185) Boué, F.; Nierlich, M.; Jannink, G.; Ball, R. *Journal de Physique* **1982**, *43*, 137–148.
(186) Brûlet, A.; Boué; Menelle, A.; Cotton, J. P. *Macromolecules* **2000**, *33*, 997–1001.
(187) Jones, R. L.; Kumar, S. K.; Ho, D. L.; Briber, R. M.; Russell, T. P. *Macromolecules* **2001**, *34*, 559–567.
(188) Boué, F. In *Polymer Physics*; Advances in Polymer Science; Springer Berlin Heidelberg, **1987**, 47–101.
(189) Han, T.; Yarin, A. L.; Reneker, D. H. *Polymer* **2008**, *49*, 1651–1658.
(190) Cassagnau, P. *Dynamique moléculaire: Mécanisme de renouvellement du tube, comportement rhéologique des polymères polymoléculaires*, PhD thesis, Pau, **1988**.
(191) Ojha, S. S.; Afshari, M.; Kotek, R.; Gorga, R. E. *Journal of Applied Polymer Science* **2008**, *108*, 308–319.
(192) Cipitria, A.; Skelton, A.; Dargaville, T. R.; Dalton, P. D.; Hutmacher, D. W. *Journal of Materials Chemistry* **2011**, *21*, 9419–9453.
(193) Mattanavee, W.; Suwantong, O.; Puthong, S.; Bunaprasert, T.; Hoven, V. P.; Supaphol, P. *ACS Applied Materials and Interfaces* **2009**, *1*, 1076–1085.
(194) Zander, N. E.; Orlicki, J. A.; Rawlett, A. M.; Beebe, T. P. *ACS Applied Materials and Interfaces* **2012**, *4*, 2074–2081.
(195) Grafahrend, D.; Calvet, J. L.; Klinkhammer, K.; Salber, J.; Dalton, P. D.; Möller, M.; Klee, D. *Biotechnology and Bioengineering* **2008**, *101*, 609–621.
(196) Grafahrend, D.; Heffels, K.-H.; Beer, M. V.; Gasteier, P.; Möller, M.; Boehm, G.; Dalton, P. D.; Groll, J. *Nature Materials* **2011**, *10*, 67–73.
(197) Klinkhammer, K.; Bockelmann, J.; Simitzis, C.; Brook, G. A.; Grafahrend, D.; Groll, J.; Möller, M.; Mey, J.; Klee, D. *Journal of Materials Science Materials in Medicine* **2010**, *21*, 2637–2651.
(198) Grafahrend, D.; Heffels, K.-H.; Möller, M.; Klee, D.; Groll, J. *Macromolecular Bioscience* **2010**, *10*, 1022–1027.
(199) Lösel, R.; Grafahrend, D.; Möller, M.; Klee, D. *Macromolecular Bioscience* **2010**, *10*, 1177–1183.
(200) Galgali, P.; Puntambekar, U. .; Gokhale, D. .; Varma, A. . *Carbohydrate Polymers* **2004**, *55*, 393–399.
(201) Chua, K.-N.; Lim, W.-S.; Zhang, P.; Lu, H.; Wen, J.; Ramakrishna, S.; Leong, K. W.; Mao, H.-Q. *Biomaterials* **2005**, *26*, 2537–2547.
(202) Kim, T. G.; Park, T. G. *Biotechnology Progress* **2006**, *22*, 1108–1113.
(203) Fraser, C.; Grubbs, R. H. *Macromolecules* **1995**, *28*, 7248–7255.
(204) Shukla, R. K.; Tiwari, A. *Carbohydrate Polymers* **2012**, *88*, 399–416.
(205) Shi, Q.; Chen, X.; Lu, T.; Jing, X. *Biomaterials* **2008**, *29*, 1118–1126.
(206) Reneker, D. .; Kataphinan, W.; Theron, A.; Zussman, E.; Yarin, A. *Polymer* **2002**, *43*, 6785–6794.
(207) Edwards, M. D.; Mitchell, G. R.; Mohan, S. D.; Olley, R. H. *European Polymer Journal* **2010**, *46*, 1175–1183.
(208) Nottelet, B.; Pektok, E.; Mandracchia, D.; Tille, J.-C.; Walpoth, B.; Gurny, R.; Möller, M. *Journal of Biomedical Materials Research Part A* **2009**, *89A*, 865–875.
(209) Gholipour Kanani, A.; Bahrami, S. H. *Journal of Nanomaterials* **2011**, *2011*.
(210) Lavielle, N.; Popa, A.-M.; de Geus, M.; Hébraud, A.; Schlatter, G.; Thöny-Meyer, L.; Rossi, R. M. *European Polymer Journal* **2013**, *49*, 1331–1336.

(211) Lee, K. H.; Kim, H. Y.; Khil, M. S.; Ra, Y. M.; Lee, D. R. *Polymer* **2003**, *44*, 1287–1294.
(212) Croisier, F.; Duwez, A.-S.; Jérôme, C.; Léonard, A. F.; van der Werf, K. O.; Dijkstra, P. J.; Bennink, M. L. *Acta Biomaterialia* **2012**, *8*, 218–224.
(213) Li, W.-J. W.-J.; Tuli, R.; Okafor, C.; Derfoul, A.; Danielson, K. G. K. G.; Hall, D. J. D. J.; Tuan, R. S. R. S. *Biomaterials* **2005**, *26*, 599–609.
(214) Li, W.-J.; Tuli, R.; Huang, X.; Laquerriere, P.; Tuan, R. S. *Biomaterials* **2005**, *26*, 5158–5166.
(215) Li, W.-J.; Danielson, K. G.; Alexander, P. G.; Tuan, R. S. *Journal of Biomedical Materials Research: A* **2003**, *67*, 1105–1114.
(216) Pham, Q. P.; Sharma, U.; Mikos, A. G. *Biomacromolecules* **2006**, *7*, 2796–2805.
(217) Luong-Van, E.; Grøndahl, L.; Chua, K. N.; Leong, K. W.; Nurcombe, V.; Cool, S. M. *Biomaterials* **2006**, *27*, 2042–2050.
(218) Venugopal, J.; Zhang, Y. Z.; Ramakrishna, S. *Nanotechnology* **2005**, *16*, 2138.
(219) Rutlegde, G. C.; Lowery, J. L.; Pai, C.-L. *Journal of Engineered Fibers and Fabrics*, **2009**, *4*, 1–13.
(220) Kong, L.; Ziegler, G. R. *Biomacromolecules* **2012**, *13*, 2247–2253.
(221) McKee, M. G.; Wilkes, G. L.; Colby, R. H.; Long, T. E. *Macromolecules* **2004**, *37*, 1760–1767.
(222) McKee, M. G.; Hunley, M. T.; Layman, J. M.; Long, T. E. *Macromolecules* **2006**, *39*, 575–583.
(223) Codelli, J. A.; Baskin, J. M.; Agard, N. J.; Bertozzi, C. R. *Journal of American Chemical Society* **2008**, *130*, 11486–11493.
(224) Krouit, M.; Bras, J.; Belgacem, M. N. *European Polymer Journal* **2008**, *44*, 4074–4081.
(225) Li, Y.; Hoskins, J. N.; Sreerama, S. G.; Grayson, S. M. *Macromolecules* **2010**, *43*, 6225–6228.
(226) Peltier, J. M.; Smith, R. W.; MacLean, D. B.; Szarek, W. A. *Carbohydrate Research* **1990**, *207*, 1–10.
(227) Varma, A. .; Kennedy, J. .; Galgali, P. *Carbohydrate Polymers* **2004**, *56*, 429–445.
(228) Persson, P. V.; Schröder, J.; Wickholm, K.; Hedenström, E.; Iversen, T. *Macromolecules* **2004**, *37*, 5889–5893.
(229) Neves, S. C.; Moreira Teixeira, L. S.; Moroni, L.; Reis, R. L.; Van Blitterswijk, C. A.; Alves, N. M.; Karperien, M.; Mano, J. F. *Biomaterials* **2011**, *32*, 1068–1079.
(230) Haamann, D.; Bispinghoff, M.; Hönders, D.; Suschek, C.; Möller, M.; Klee, D. *Journal of Applied Polymer Science* **2012**, *125*, 3638–3647.
(231) Yu, W.; Zhao, W.; Zhu, C.; Zhang, X.; Ye, D.; Zhang, W.; Zhou, Y.; Jiang, X.; Zhang, Z. *BMC Neuroscience* **2011**, *12*, 68.
(232) Thomas, V.; Jose, M. V.; Chowdhury, S.; Sullivan, J. F.; Dean, D. R.; Vohra, Y. K. *Journal of Biomaterials Science, Polymer Edition* **2006**, *17*, 969–984.
(233) Punna, S.; Finn, M. G. *Synlett* **2004**, 99–100.
(234) Sun, S.-W.; Lin, Y.-C.; Weng, Y.-M.; Chen, M.-J. *Journal of Food Composition and Analysis* **2006**, *19*, 112–117.
(235) Lamothe, P. J.; McCormick, P. G. *Analytical Chemistry* **1973**, *45*, 1906–1911.
(236) Hardman, S. J.; Muhamad-Sarih, N.; Riggs, H. J.; Thompson, R. L.; Rigby, J.; Bergius, W. N. A.; Hutchings, L. R. *Macromolecules* **2011**, *44*, 6461–6470.
(237) Ansari, I. A.; Clarke, N.; Hutchings, L. R.; Pillay-Narrainen, A.; Terry, A. E.; Thompson, R. L.; Webster, J. R. P. *Langmuir* **2007**, *23*, 4405–4413.
(238) Stachewicz, U.; Barber, A. H. *Langmuir* **2011**, *27*, 3024–3029.
(239) Stachewicz, U.; Li, S.; Bilotti, E.; Barber, A. H. *Applied Physics Letters* **2012**, *100*, 094104–094104–4.

(240) Fu, G. D.; Lei, J. Y.; Yao, C.; Li, X. S.; Yao, F.; Nie, S. Z.; Kang, E. T.; Neoh, K. G. *Macromolecules* **2008**, *41*, 6854–6858.
(241) Sun, X.-Y.; Shankar, R.; Börner, H. G.; Ghosh, T. K.; Spontak, R. J. *Advanced Materials* **2007**, *19*, 87–91.
(242) Gentsch, R.; Pippig, F.; Schmidt, S.; Cernoch, P.; Polleux, J.; Börner, H. G. *Macromolecules* **2011**, *44*, 453–461.
(243) Chen, F.-F.; Wang, F. *Molecules* **2009**, *14*, 2656–2668.
(244) Gao, S. H.; Zhang, G. X.; Zhang, F. X. *Advanced Materials Research* **2011**, *331*, 133–138.
(245) DuBois, M.; Gilles, K. A.; Hamilton, J. K.; Rebers, P. A.; Smith, F. *Analytical Chemistry* **1956**, *28*, 350–356.
(246) Travelet, C.; Stemmelen, M.; Lapinte, V.; Dubreuil, F.; Robin, J.-J.; Borsali, R. *Journal of Nanoparticle Research* **2013**, *15*, 1–16.
(247) Yu, D.-G.; Branford-White, C.; Williams, G. R.; Bligh, S. W. A.; White, K.; Zhu, L.-M.; Chatterton, N. P. *Soft Matter* **2011**, *7*, 8239.
(248) Mandal, S.; Bhaskar, S.; Lahann, J. *Macromolecular Rapid Communications* **2009**, *30*, 1638–1644.
(249) Bech, L.; Lepoittevin, B.; El Achhab, A.; Lepleux, E.; Teulé-Gay, L.; Boisse-Laporte, C.; Roger, P. *Langmuir* **2007**, *23*, 10348–10352.
(250) Grafahrend, D.; Heffels, K.-H.; Möller, M.; Klee, D.; Groll, J. *Macromolecular Bioscience* **2010**, *10*, 1022–1027.
(251) Otman, O.; Boullanger, P.; Drockenmuller, E.; Hamaide, T. *Beilstein Journal of Organic Chemistry* **2010**, *6*.
(252) Wu, P.; Chen, X.; Hu, N.; Tam, U. C.; Blixt, O.; Zettl, A.; Bertozzi, C. R. *Angewandte Chemie International Edition* **2008**, *47*, 5022–5025.
(253) Xu, C.; Ye, L. *Chemical Communications* **2011**, *47*, 6096–6098.
(254) Provencher, S. W. *Die Makromolekulare Chemie* **1979**, *180*, 201–209.
(255) Dal Bó, A. G.; Soldi, V.; Giacomelli, F. C.; Travelet, C.; Jean, B.; Pignot-Paintrand, I.; Borsali, R.; Fort, S. *Langmuir* **2012**, *28*, 1418–1426.

Abstract

Electrospinning process has become a leading technique for producing nano-fibrous scaffolds that are highly porous, lighter, and with superior mechanical properties than their bulk equivalents. Structural properties of electrospun fibers closely resemble to the connective cell tissue, making these nonwovens readily employed in medicine and pharmacy. The research study of this thesis focused on bridging the commercially available biopolymers with the tissue engineering applications through multifunctional aspects of carbohydrates and click chemistry coupling. Biocompatible fibers were electrospun from poly(ε-caprolactone) and further optimized into clickable azido-PCL scaffolds. Their surface-activity was visualized after click coupling of a fluorescent dye onto PCL-based electrospun fibers, while hydrophilicity and bioactivity were achieved by covalent bonding of carbohydrates, enabling specific cell adhesion possibilities of these nonwovens. Selective lectin surface-immobilization revealed the potential of these scaffolds for specific protein adhesion and therefore controlled cell-material interactions. Polymer stability is an important factor for controlled degradation in tissue engineering applications. Small angle neutron scattering studies were carried out to estimate the stability of polystyrene as a model-polymer, its chain conformation in as-spun and thermally annealed electrospun fibers. Notable anisotropy of polymeric chains within the fibers was observed. The terminal relaxation time of the polystyrene was estimated and compared to the theoretical value.

Résumé

Le procédé d'électro-filage est devenu une technique privilégiée pour la préparation des matériaux nano-fibreux, grâce à sa simplicité de mise en œuvre, la polyvalence des matières premières utilisées, ainsi que la diversité des structures obtenues. Sa capacité à produire des réseaux fibrillaires, proches de ceux du vivant ont ouvert la voie à d'importantes applications en ingénierie tissulaire. Cette étude a porté sur i) l'élaboration de nano-fibres à base de biopolymères commerciaux par un procédé d'électro-filage, pour des applications en ingénierie tissulaire, ii) leur fonctionnalisation et, iii) l'étude par SANS de la stabilité des chaînes de polymères constituant ces fibres. La stabilité d'un polymère est un facteur important pour la dégradation contrôlée dans les systèmes biologiques. Des études de la stabilité de polystyrène, utilisé ici comme un modèle simple, dans le milieu confiné des nanofibres, ont été élaborés avec la technique de diffusion de neutrons aux petits angles. L'investigation de la conformation des chaînes de polymère dans les nanofibres montre une anisotropie remarquable, en suggérant une forte déformation des chaînes dans la direction axiale des fibres d'au cours de procédé d'électro-filage. La dynamique de relaxation des chaînes a permis d'évaluer leur stabilité et vieillissement dans le milieu confiné des nanofibres. Des fibres biocompatibles à base de poly(ε-caprolactone) (PCL) ont été électro-filées et optimisées pour obtenir des matériaux nano-structurés et fonctionnalisés en vue d'applications biomédicales. L'introduction par chimie click azide-alcyne de groupes saccharidiques dans le cœur ou en surface des fibres de PCL a été réalisée très efficacement selon deux approches distinctes avant ou après électro-filage. Les caractérisations physico-chimiques et biologiques réalisées sur les différents systèmes ont notamment permis de mettre en évidence la biodisponibilité des sucres à la surface des fibres ainsi que leur capacité à rendre la PCL hydrophile. Ces résultats attestent du potentiel de la chimie click à permettre la fonctionnalisation de fibres de polyesters sans altération de leur structure ouvrant ainsi d'importantes perspectives dans le domaine de l'ingénierie tissulaire.